ACOUSTICALLY INDUCED STRESS ANALYSIS OF CENTER FUSELAGE SKIN PANELS OF A BASIC TRAINING AIRCRAFT USING STATISTICAL ENERGY ANALYSIS

A THESIS SUBMITTED TO
THE GRADUATE SCHOOL OF NATURAL AND APPLIED SCIENCES
OF
MIDDLE EAST TECHNICAL UNIVERSITY

BY

İLKER KURTOĞLU

IN PARTIAL FULFILLMENT OF THE REQUIREMENTS
FOR
THE DEGREE OF MASTER OF SCIENCE
IN
MECHANICAL ENGINEERING

JUNE 2009

Approval of the thesis;

ACOUSTICALLY INDUCED STRESS ANALYSIS OF CENTER FUSELAGE SKIN PANELS OF A BASIC TRAINING AIRCRAFT USING STATISTICAL ENERGY ANALYSIS

submitted by **İLKER KURTOĞLU** in partial fulfillment of the requirements for the degree of **Master of Science in Mechanical Engineering Department, Middle East Technical University by**,

Prof. Dr. Canan Özgen _____
Dean, Graduate School of **Natural and Applied Sciences**

Prof. Dr. Süha Oral _____
Head of Department, **Mechanical Engineering**

Prof. Dr. Mehmet Çalışkan _____
Supervisor, **Mechanical Engineering Dept., METU**

Examining Committee Members:

Prof. Dr. Y. Samim Ünlüsoy _____
Mechanical Engineering Dept., METU

Prof. Dr. Mehmet Çalışkan _____
Mechanical Engineering Dept., METU

Asst. Prof. Dr. Yiğit Yazıcıoğlu _____
Mechanical Engineering Dept., METU

Inst. Dr. Gökhan O. Özgen _____
Mechanical Engineering Dept., METU

Prof. Dr. Yavuz Yaman _____
Aerospace Engineering Dept., METU

Date: _____

I hereby declare that all information in this document has been obtained and presented in accordance with academic rules and ethical conduct. I also declare that, as required by these rules and conduct, I have fully cited and referenced all material and results that are not original to this work.

Name, Last name :

Signature :

ABSTRACT

ACOUSTICALLY INDUCED STRESS ANALYSIS OF CENTER FUSELAGE SKIN PANELS OF A BASIC TRAINING AIRCRAFT USING STATISTICAL ENERGY ANALYSIS

Kurtoğlu, İlker

M.Sc., Department of Mechanical Engineering

Supervisor: Prof. Dr. Mehmet Çalışkan

June 2009, 103 pages

Two sample statistical energy analysis (SEA) models are generated for a section of the fuselage panel of an aircraft, namely the uniform panel model which includes the frames and stringers, and the ribbed panel model in which the frames and stringers are smeared into the skin. Turbulent boundary layer (TBL) excitation is used as the primary acoustic excitation source. Stress levels are estimated from the average velocity data of the panels. The stress results are found comply with those obtained by the AGARD method. Effect of radiation from panels to exterior and interior of the sample skin panel as well as the pressurization of the skin panels are investigated separately to analyze their effects on the stress levels. The method is then used in the analysis of center fuselage skin panels on a basic training aircraft. Two models are generated for the aircraft analysis, namely the complete aircraft model and the simplified model which excludes the wings and the empennage. In addition to TBL, propeller noise is used as the primary acoustic excitation source. The effects of the wings and the empennage on the stress levels in the center fuselage skin panels are also investigated along with the radiation from panels to the exterior and interior of the aircraft and pressurization of the pilot cabin.

Keywords: Statistical Energy Analysis, Acoustic Fatigue, Acoustically Induced Stress Analysis

ÖZ

BAŞLANGIÇ TEMEL EĞİTİM UÇAĞI ORTA GÖVDE PANELLERİNİN AKUSTİK GERİLME ANALİZLERİNİN İSTATİSTİKSEL ENERJİ ANALİZİ METODU İLE İNCELENMESİ

Kurtoğlu, İlker

Yüksek Lisans, Makina Mühendisliği Bölümü

Tez Yöneticisi: Prof. Dr. Mehmet Çalışkan

Haziran 2009, 103 sayfa

Örnek bir uçak gövde paneli için iki farklı istatistiksel enerji analizi (İEA) modeli geliştirilmiştir. Birinci model kabuk, çerçeve ve çıtalar ayrı ayrı modellenerek, ikincisi ise takviyeli panel modeli kullanılarak (çerçeve ve çıta özellikleri kabuğa yedirilerek) hazırlanmıştır. Türbülanslı sınır katmanı temel akustik tetikleme kaynakları olarak kullanılmıştır. Kabuklardan alınan ortalama hız verileri gerilme değerlerini elde etmek için kullanılmış ve AGARD metodu ile elde edilen sonuçlarla uyum sağladığı görülmüştür. Panellerden uçak kabinine ve dış ortama olan akustik radyasyon ile kabin basınçlandırmasının gerilme düzeyleri üzerindeki etkileri ayrıca incelenmiştir. Aynı yöntem başlangıç temel eğitim uçağı orta gövde panellerinin analizinde kullanılmıştır. Birincisi tüm uçak, ikincisi ise kanat ve kuyruk yapıları ihmal edilmiş olmak üzere iki farklı model hazırlanmıştır. Türbülanslı sınır katmanına ek olarak pervane gürültüsü de akustik tetikleme olarak kullanılmıştır. Panellerden iç ve dış ortama radyasyon ve kabin basınçlandırmasına ek olarak kanat ve kuyruk elemanlarının orta gövde panellerindeki gerilme düzeylerine etkisi incelenmiştir.

Anahtar Sözcükler: İstatistiksel Enerji Analizi, Akustik Yorulma, Akustik Kaynaklı Gerilme Analizi.

To my parents and friends…

ACKNOWLEDGEMENTS

I give my appreciation to my supervisor Prof. Dr. Mehmet Çalışkan for his suggestions throughout this study. I must also thank to my chief Dr. Muvaffak Hasan for his suggestions in the model development period.

For their great effort in supporting me with their technical knowledge, I must thank Anders Wilson from ESI Software and Onur Öztürk from Infotron. They really worked hard for answering my questions about SEA and VA One™.

I must thank to my friends and family for their patience because of my nervous behavior during the preparation of this study.

I also thank to TÜBİTAK for the scholarship they give my in the first two years of my study.

TABLE OF CONTENTS

LIST OF TABLES

TABLES

LIST OF FIGURES

FIGURES

LIST OF SYMBOLS AND ABBREVIATIONS

A	Area (m^2)
$<a^2>$	Mean Square Acceleration ($(m/s^2)^2$)
c_0	Speed of Sound In Air (m/s)
c_B	Bending Wave Speed (m/s)
c_θ	Phase Speed
c_g	Energy Group Speed
c_L	Longitudinal Wave Speed (m/s)
c_p	Plate Bending Phase Speed (m/s)
c_T	Torsinal Wave Speed (rad/s)
$<d^2>$	Mean Square Displacement (m^2)
δ_{BC}	Boundary Condition Constant
δf	Average Frequency Spacing Between Resonances (Hz)
$\Delta\omega$	Band Width (rad/s)
E	Elastic (Young's) Modulus (MPa)
E_i	Subsystem Energy (Joule)
$<\varepsilon^2>$	Mean Square Strain
η_i	Damping Loss Factor
η_{ij}	Coupling Loss Factor
f	Center Frequency of the Band (Hz)
F	Force (N)
h	Thickness (mm)
J	Mass Weighted Polar Moment of Inertia
I_p	Polar Area Moment of Inertia (mm^4)
K	Frequency parameter
K_{shape}	Non-dimensional Geometry Factor
k	Wave Number
k_L	Wave Number of Longitudinal Waves
k_0	Wave Number of Sound In Air
k_B	Wave Number of Bending Waves

L	Length (mm)
L_a	Acceleration Level (dB, ref =10 m/s^2)
L_d	Displacement Level (dB, ref = 1mm)
L_E	Energy Level (dB, ref = 10^{-12} J)
L_ε	Strain Level (dB, ref = 10^{-6} mm/mm)
L_p	Sound Pressure Level (dB, ref = $2x10^{-5}$ Pa)
L_σ	Stress Level (dB, ref = 1 Pa)
L_W	Sound Power Level (dB, ref = 10^{-12} W)
λ	Wave length (mm)
m	Mass (kg)
M	Number of Subsystems
μ	Poisson's Ratio
N	Number of Modes
ΔN	Number of Modes in frequency band $\Delta\omega$
$n(\omega)$	Modal Density (modes/(rad/s))
$n(f)$	Modal Density (modes/Hz)
Q	Torsional Rigidity
ω	Center Frequency of the Band (rad/s)
P	Power (W)
$P_{i,in}$	Power Input to Subsystem i
$P_{i,diss}$	Power Dissipated Within Subsystem i
P_{ij}	Power Flow From Subsystem i to Subsystem j
$<p^2>$	Mean Square Acoustic Pressure (Pa^2)
RMS	Root Mean Square
S	Surface Area of an Acoustic Volume (m^2)
S_{RMS}	Root Mean Square Stress (MPa)
ρ	Mass Density (kg/m^3)
r	Radius (m)
$<\sigma^2>$	Mean Square Stress (MPa^2)
U	Volume Velocity (m/s)
U_c	Convection Velocity (m/s)
U_∞	Free Stream Velocity (m/s)

V	Volume (mm^3)
V_S	Velocity parameter in AGARD method (mm)
$<v^2>$	Mean Square Velocity ($(m/s)^2$)
AGARD	Advisory Group for Aerospace Research and Development
CLF	Coupling Loss Factor
DAF	Diffuse Acoustic Field
FEA	Finite Element Analysis
FEM	Finite Element Model
SEA	Statistical Energy Analysis
SIF	Semi-infinite Fluid
PSD	Power Spectral Density (g^2/Hz)
TBL	Turbulent Boundary Layer

CHAPTER 1

INTRODUCTION

1.1. GENERAL OVERVIEW

Vibration of mechanical structures has always been a challenging problem for structural engineers. Numerical methods such as finite element method (FEM) and boundary element method (BEM) are theoretically applicable at all frequency ranges. However, in practice, they have some deficiencies at high frequencies where changes in the response at a single frequency are affected by small changes in structure geometry and material property. Another deficiency of FEM and BEM is their need of computational effort. At higher frequencies, excessive amount of degrees of freedom are required in even simple systems causing the computation time to increase significantly.

For analyzing the high frequency behavior of the structures, a new method called Statistical Energy Analysis (SEA) was developed by Lyon [1]. The method uses the principle of energy balance between the subsystems which are assumed to be linearly coupled. These subsystems are geometrical structural parts of the structure or the wave types in the structure, such as longitudinal, bending and torsional waves. The interaction between subsystems is constructed via junctions. These junctions are used to calculate the power flow between subsystems using the parameters such as modal density and coupling loss factor. These parameters are explained in detail in the following sections.

SEA is a powerful tool for high frequency analysis with the advantage of having a small model size for the complete analysis of a complex structure. When the model required for an FEA is compared with the one required for SEA, it is obvious that the model for SEA makes the analyst more comfortable in analyzing complex structures in a short period of time. Also, it allows the analyst to describe

the system simpler. This makes it possible to analyze the system even with simple hand calculations.

Although SEA has important advantages, it has also some disadvantages. One of them is that it gives statistical answers for the response of a system which means that there is some uncertainty in the results. Also, it is not possible to obtain maximum vibration amplitude of a system because the results are the average responses for the system.

SEA is generally used for the prediction of interior noise of aircrafts and automobiles. There are a large number of studies in the industry for reducing the noise in aircraft and automobiles. Especially in the aircraft industry, there exist strict noise regulations leading the companies to improve their design in terms of acoustic insulation. However, in this study, the method is used for estimating the structural response of an aircraft fuselage panel due to the acoustic excitation sources.

Acoustic fatigue (sonic fatigue) is an important problem especially in aircrafts having turbojet engines. The increasing sound levels of the engines require the engineers analyze this phenomenon in detail. In this study, the stress levels are determined by SEA method to analyze the acoustic fatigue behavior of center fuselage skin panels of a basic training aircraft with a turboprop engine.

1.2. SCOPE AND OBJECTIVES

The aim of this thesis is to define a procedure to investigate acoustic fatigue behavior of center fuselage skin panels of a basic single engine turbo propeller aircraft using SEA. This study is done by using the commercial software VA One^{TM}. The primary excitations are given as the turbulent boundary layer (TBL) excitation and the propeller noise. Different modeling methods for TBL are compared with each other, namely diffuse acoustic field (DAF) and point force excitation. For the stress analysis, the most conservative modeling method is found.

The second chapter of the study represents the previous studies on SEA and acoustic fatigue. The SEA studies are divided into two parts. The former represents

the general studies on the theory of SEA. The latter represents the academic and industrial applications for SEA.

In third chapter, the basic theory for SEA is introduced. The important SEA parameters such as modal density, loss factor, coupling loss factor are defined. Necessary information is also given for conversion between the response variables.

Fourth chapter is dedicated to the model development procedure. The aircraft model used in the analyses is introduced. The subsystems developed for the aircraft are given in detail.

Chapter 5 includes the case studies. First, a simple case study is investigated to validate the procedure defined in the beginning of the chapter. In this study, in addition to the validation case, several other conditions are analyzed in order to see their effects on stress levels. Then, the aircraft analyses are performed considering various effects step by step.

In chapter 6, discussions and conclusions are represented for the results obtained in chapter 5. Recommendations for future work are also provided.

CHAPTER 2

LITERATURE SURVEY

2.1. SURVEY ON STATISTICAL ENERGY ANALYSIS

The survey on SEA is divided into two parts. In the first part, the studies related to the basic theory and theoretical applications of SEA are examined. In the second part, the studies including the practical applications of SEA are considered.

2.1.1. THE BASICS OF SEA

The first studies on the concept of SEA were done by Lyon and Smith [1]. Lyon calculated the power flow between two linear resonators which are lightly coupled. He showed that the power was flowing from the oscillator having higher energy to the one having lower energy. On the other hand, Smith calculated the response of a resonator excited by a diffuse, broadband sound field.

Mace has several studies on statistical energy analysis. In one of his studies, he investigated power flow between two continuous one dimensional subsystems using a wave solution approach [2]. In this study, he examined the statistics of power flow for weak and strong coupling. In his later work, he investigated the energy influence coefficients of a built-up structure in terms of the modes of the structure [3]. He found the conditions under which the system can be described as a SEA subsystem in terms of modal parameters. Later, he studied on the indirect coupling of the subsystems [4]. He found the conditions under which the indirect coupling loss factors are zero, leading to a situation that the system can be defined as a proper SEA subsystem. In another study with Wester, Mace studied the statistical energy analysis of two edge coupled rectangular plates using a wave solution technique [5]. They derived the analytical expressions for ensemble

average input and coupling powers resulting from "rain on the roof" excitation on one of the plates. In his another study with Rosenberg, they studied the subsystem irregularities in their work [6]. They used two coupled plates and determine the coupling power and coupling loss factor by various methods. At the end, they found that if the damping is large enough, implying weak coupling, the response of the subsystems are independent of the subsystem shape. On the other hand, if the damping is light, the response depends on the plate geometry.

Langley also has several studies on SEA. He investigated the conditions under which an exact theory concerning the energy power flow relationships for a complex dynamic system can be reduced to standard SEA equations [7]. He showed that the assumption of indirect coupling is zero if the subsystems are not connected directly is invalid even in the presence of weak coupling. Later, he studied the elastic wave transmission properties of a junction where an arbitrary number of curved panels meet using a wave dynamic stiffness matrix approach [8]. Langley, in his study with Smith and Fahy, studied the stiffened panels in their work [9]. They proposed that the panel can be modeled as a damping element between the two structures. The absorption and transmission coefficients are calculated according to the periodic structure theory. The derivation is applied to a structure constructed by two panels including a stiffened panel between them. They compared their results with other various methods.

Xie, Thompson and Jones investigated the effects of boundary conditions on mode count and modal density of one and two dimensional subsystems by using the wave number integration method [10]. They realized that the modal density is largely independent of boundary conditions for one dimensional subsystem, whereas it is dependent of boundary conditions for two dimensional subsystems. They found that the inclusion of the effect of boundary conditions in SEA estimations results in improved agreements with both analytical and numerical results.

Manning in his study derived the formulae for SEA parameters using mobility functions [11]. He presented the simplifications resulting from averaging the parameters and showed that these simplifications make it possible to apply SEA to very complex structural-acoustic systems.

Several authors studied on the investigation of the important SEA parameter coupling loss factor. Cacciolati and Guyader derived the calculation of coupling loss factors for homogenous and non-homogenous structures using point mobility [12]. They made some simplifications to fit basic SEA relations, validated their study with experiments and obtained reasonable results. Another study by Fahy and Ruivo was performed to find the coupling loss factors along with damping loss factor by an input power modulation method [13]. In this method response measurements were done at only one point for each subsystem. They obtained reasonably accurate results when compared with the conventional power injection method. Manik introduced another method to determine the coupling loss factor in his study [14]. He used the power injection method which has no numerical difficulty in the calculation process and independent of the strength of the coupling between the subsystems. A newer study by Thite and Mace was about the estimating the coupling loss factors from finite element analysis [15].

Keane, in his study with Price, studied the methods evolved from the study of wave propagation through geometrically periodic media are used to enhance the probabilistic models used in SEA [16]. They used two parts of a ship structure in their analyses. Their new approach provided worthwhile improvements in energy flow predictions when compared to traditional SEA.

Bremner, in his study, defined a simple formulation for the vibro-acoustic behavior of ribbed panel structures [41]. He used a modal formulation to superimpose the wavefields of plate and ribs. This formulation is used in the commercial software AutoSEA and gave a good agreement with the experimental data.

2.1.2. APPLICATIONS OF SEA

Orrenius and Wareing used coupled FE/SEA analysis to evaluate the effect of constrained damping treatment on curved, rib-stiffened aluminum panels [17]. They used three different models, which are full SEA model, full FEA model and a hybrid model composed of both SEA and FEA elements. They used a point force excitation and diffuse acoustic excitation in their analyses. At the end, they compared the

results with test measurement, leading to a result that hybrid and full SEA models give better results than full FE model.

Kuroda and others investigated the effects of in-plane vibration on building SEA model for flexural vibration [18]. They used a FEM calculation to compare the SEA loss factors concerning flexural vibration between with and without taking the in-plane vibration into consideration. They used two plates with an L-Shaped configuration and compare the results with the analytical solutions. They showed that frequency and space averaged subsystem energy emphasized the influence of in-plane vibrations.

In another study, Kuroda and others studied a structural optimization method which realizes the desired value of coupling loss factors in statistical energy analysis [19]. They used a part of a whole system and considered a junction together with their neighboring SEA subsystems. Moreover, they used finite element method and optimization algorithms to implement the method.

Ragnarsson and others studied a calculation procedure to expand SEA into mid frequency range [20]. They used the idea of enriching the SEA model with FE data, named as hybrid approach. They compare the results obtained from pure FEA, pure SEA and hybrid FE/SEA analysis for an automobile Body-in-White model. They showed that FEA is valid below 200 Hz; however it shows more random results above 200 Hz. They also showed that SEA misses the deterministic peaks in low and mid-frequencies.

Cotoni and others studied modeling methods for vibro-acoustic analysis of commercial aircrafts [21]. In their study, they focused on the noise and vibration transmission in an actual section of a Boeing 737 aircraft including the trimmed sidewalls, stowage bins, and connected floor structure. They used a hybrid FE/SEA approach and general periodic SEA subsystem, and obtained good agreements with the test results.

In another study of Cotoni, with Langley, he investigated a general periodic subsystem based on the periodic structure theory [22]. They used a finite element model of a unit cell and used analytical expressions to obtain SEA parameters of larger structures composed of such unit cells. At the end, they come up with an

efficient and accurate approach to model arbitrarily complex sections in SEA that are difficult to model using traditional formulations.

2.2. SURVEY ON ACOUSTIC FATIGUE

Engineering Sciences Data Unit (ESDU) published several studies on stress distribution and acoustic fatigue of aircraft structures. They investigated the root mean square (RMS) stress distribution in skin panels [23], stiffened skin panels [24] and internal plates of a box structure [25] subjected to random acoustic loading. In all of the studies, it is assumed that the fundamental mode of the skin panel is contributing to the stress level most and effects of other modes are neglected. The calculated stress values were compared with the measured data and reasonable accuracy was obtained.

Climent and Casalengua studied a PSD method for acoustic fatigue evaluation of complex structures [26]. They converted the sound pressure levels (SPL) to acoustic pressures and applied to a finite element model. They found that this model can cover the complex geometries in substructures, the effect of reinforcements and contribution of several modes, which improved the results in ESDU documents explained in previous paragraph.

Blevins studied an approximate method for the sonic fatigue analysis of plates and shells [27]. He based the methods on separating the temporal and spatial aspects of the problem and developing approximations for both. He compared the results with the experimental data directly and saw that the results agreed within the uncertainty of the experimental method.

Choi and Vaicaitis studied the nonlinear response and fatigue of stiffened panels to random pressure and thermal loads [28]. In their study, they simulated the random pressures in time domain and the nonlinear equations of motion are solved with Monte Carlo method. They realized that an analysis based on a linear theory could give overestimated stress values, which results in short fatigue life. They also realized that the stress distributions are non-Gaussian and the stress peaks do not follow Rayleigh distribution.

Benchekchou and White in their study investigated the fatigue properties of lightweight composite structures as they applied to the thin skin panels of aircrafts [29]. In their study, they performed finite element analyses and fatigue tests in order to understand the dynamic behavior of the panels.

Sun and Miles studied the acoustic fatigue life of nonlinear structures [30]. They used an approximate method and a conventional numerical method to estimate the fatigue life of a nonlinear beam under random excitation. They found that the approximate method required considerably lower computational time than the conventional method. Therefore, the approximate method was found to be more practical in estimating the fatigue of complex nonlinear systems.

CHAPTER 3

BASIC THEORY OF SEA

3.1. OVERVIEW

SEA is used to predict the energy levels of a complex system composed of subsystems to an external power input. The subsystems consist of similar resonant modes within a structure or acoustic space. For example, for a flat plate the bending waves, shear waves and longitudinal waves can be treated as separate subsystems. Moreover, the subsystems can also be the physical components of a complex system. These subsystems are coupled via junctions through whom the energy is transferred. The power flow between the subsystems is proportional to the differences of the modal energies of the coupled system. And the energy is dissipated within a subsystem related with the loss factor. According to the basic concepts of SEA, the procedures are formulated by making the following assumptions:

1. The excitation spectrum is broadband and the excitation forces are statistically independent. There are no pure tones in the input spectra.
2. There is no energy generation or dissipation in the couplings between the subsystems.
3. The damping loss factor is the same for each mode within a subsystem and frequency band.
4. Modes within a subsystem do not interact except to share equipartitioned energy.

The above terms are related with the modal approach to SEA. Both modal and wave approaches lead to same equations in SEA, therefore they lead to same predictions. They only represent different physical views of SEA.

3.1.1. TYPES OF AVERAGING

The SEA does not want to predict the detailed spatial pattern of the response of the structure at every single frequency of excitation [31]. The method predicts the average response in three senses: the spatial average, the ensemble average and the frequency average.

1. Spatial average is a consequence of the fact that the method predicts the overall vibration levels of the subsystem instead of the level of the every single point on the subsystem.
2. Ensemble average refers to average taken over a number of identical structures, which have random dynamic properties due to manufacturing tolerances.
3. Frequency average arises from the fact that SEA analysis is performed in frequency bands, which may be constant bandwidth or 1/3 octave bands.

3.2. GENERAL PROCEDURE

The basic idea of SEA states that the power flow between two connected subsystems is related with the uncoupled resonant modes of the subsystems [1]. The power always flows from the subsystem which has a higher energy to the one having lower energy. These arguments are brought down to the basic SEA equation:

$$P_{ij} = \omega \left(\eta_{ij}E_i - \eta_{ji}E_j\right) \tag{3.2.1}$$

In this equation, ω is the analysis band center frequency; η_{ij} and η_{ji} are the coupling loss factors, and E_i and E_j are the uncoupled total subsystem energies. SEA assumes that in narrow frequency bands, all modes have the same energy at steady-state.

Here, an important reciprocity relationship for SEA must be introduced:

$$\eta_{ij} n_i = \eta_{ji} n_j \tag{3.2.2}$$

By using Equation (3.2.1) and Equation (3.2.2), the general SEA power flow equation can be represented as:

$$P_{i,in} = \omega \eta_{ij} n_i \left(\frac{E_1}{n_1} - \frac{E_2}{n_2} \right) \tag{3.2.3}$$

The total energy in each element in a frequency band with a center frequency of ω can be found by the equation:

$$E_i = n_i e_i \tag{3.2.4}$$

In this equation, n_i represents the modal density of the element in the frequency band interested, and e_i represents the element's modal energy.

Moreover, the power dissipated within the system i can be found by using the element's internal loss factor, η_i,, with the equation:

$$P_{i,diss} = \omega E_i \eta_i \tag{3.2.5}$$

By using Equation (3.2.3) and Equation (3.2.5), the power balance for subsystem i can be written as:

$$P_{i,in} = P_{ij} + P_{i,diss} \tag{3.2.6}$$

$$P_{i,in} = \omega E_i \eta_i + \omega \eta_{ij} n_i \left(\frac{E_1}{n_1} - \frac{E_2}{n_2} \right) \tag{3.2.7}$$

In most general form, for a complex system having more than two subsystems connected to each other, for example S subsystems, Equation (3.2.7) can be written as:

$$P_{i,in} = \omega E_i \eta_i + \sum_{j=1}^{S} \omega \eta_{ij} n_i \left(\frac{E_i}{n_i} - \frac{E_j}{n_j} \right) \tag{3.2.8}$$

This summation arises from the fact that the subsystem i can be coupled to any subsystems. If there is no other subsystem, then the coupling loss factor η_{ij} will be equal to zero. The complete set of equations can be written in matrix form [31]

$$\omega \begin{bmatrix} \eta_1 n_1 + \sum_{j=1}^{S} \eta_{1j} n_1 & -\eta_{12} n_1 & .. & -\eta_{1S} n_S \\ -\eta_{21} n_2 & \eta_2 n_2 + \sum_{j=2}^{S} \eta_{2j} n_2 & .. & -\eta_{2S} n_S \\ \vdots & \vdots & \vdots & \vdots \\ -\eta_{S1} n_M & -\eta_{S2} n_S & .. & \eta_S n_S + \sum_{j=S}^{S} \eta_{Sj} n_S \end{bmatrix} \begin{bmatrix} E_1/n_1 \\ E_2/n_2 \\ \vdots \\ E_S/n_S \end{bmatrix} = \begin{bmatrix} P_{1,in} \\ P_{2,in} \\ \vdots \\ P_{S,in} \end{bmatrix} \tag{3.2.9}$$

According to Equation (3.2.9), if the system parameters, which are loss factors (η_i), coupling loss factors (η_{ij}), modal densities (n_i), power inputs and the analysis center frequency are known, the energy distribution of the subsystems can be found.

In summary, the general procedure for SEA calculations is as follows:

1. Specify the frequency bands for the analysis.
2. Define the subsystems.
3. Calculate the subsystem properties, namely modal density, loss factor and the coupling loss factor.
4. Determine the external power input to each subsystem.
5. Formulate the power balance equation, which is the Equation (3.2.8).
6. Solve the equation to obtain the average energy in each subsystem.
7. Convert average subsystem energies into desired response quantities.

3.3. DEFINITION OF SUBSYSTEMS

As mentioned before, an SEA model consists of an assembly of subsystems. These subsystems can be the wave types in a component, as well as the component itself. This leads to a considerable flexibility in identifying the subsystems when creating an SEA model. There are some guidelines for creating the subsystems [31]:

1. For any particular band, each subsystem should contain a minimum number of modes whose natural frequency falls within the band. The "minimum number" can be taken as three to seven; however there is no significant definition for this.
2. The energy should be equipartitioned between the modes of a subsystem, which means that no single mode or a small group of modes will dominate the subsystems.
3. The subsystems should be weakly coupled which means that if only one particular subsystem is subjected to excitation, the response of that subsystem will be significantly greater than that of any other subsystems.

Addition to these, some guidelines can also be given for the wave approach for subsystems [31]:

1. The structural wavelength must be significantly less than the dimensions of the subsystem.
2. The wavefield in a subsystem should be diffuse, so the waves propagate equally in all directions.
3. Wave transmission coefficient should be small at a subsystem boundary, or the damping must be sufficiently high to ensure that most of the energy input to a particular subsystem is dissipated within that subsystem.

Although these guidelines are coming from the assumptions of SEA, the model can still give accurate results when one or two of the assumptions are ignored. The definitions of the subsystems are made according to the following parameters [1]:

1. Modal density (or the average frequency spacing between the modal resonances.
2. The average modal damping loss.
3. Total input power to the modes from external excitations.
4. The average coupling loss factor between mode groups.

There are also some guidelines in the commercial software for creating the subsystems. The VA One™ suggests [40] to choose the subsystems such that the subsystem

1. Captures the correct energy storage capacity of the component, which means that each SEA subsystem should have the same number of modes in band and the same propagating wavelengths, as the physical component being modeled.
2. Has the correct mass density and average section thickness so that the energy of the system can accurately be converted to spatial averaged engineering unit response.
3. Is reverberant, which means that the energy transmission between the subsystems should be with the reverberant field rather than the direct field transmission.
4. Contains several local modes in the frequency band of interest.
5. Correctly describes the overall damping level in a physical component.

3.4. MODE COUNT, MODAL DENSITY AND MODAL OVERLAP

The mode count N_i of a subsystem is the number of modes of that subsystem that resonate in the frequency band Δf under consideration [1]. The mode count of a subsystem is very important because it represents the the number of resonant modes available to receive and store energy. There exists three ways to represent the mode count and modal density:

1. $N = n(\omega)\Delta\omega$ or ΔN represents the number of modes in a frequency band.
2. $n(\omega) = dN/d\omega$ represents the modal density in modes per rad/s.
3. $\delta f = 1 / [2\pi n(\omega)]$ represents the average frequency spacing between modal resonances in Hertz.

There have been many theoretical studies of modal density for both structural and acoustic subsystems [1]. When these calculations are compared with tests, it is seen that they are fairly reliable. The following elements have calculations for modal density [1]:

1. Flat plates with various boundary conditions.
2. Flat plates of complex construction including layered plates.
3. Shells and shell segments, including spheres, cones, and cylinders.
4. Acoustical spaces of most shapes, including rectangular, spherical, and cylindrical; and volumes representing combinations of these.
5. Various beam and girder shapes including flexural and torsional deformations.

The mode count and modal density can also be found by using finite element analysis. However, in order to obtain accurate number of modes at high frequencies, the element size should be adequate leading to very long computation times.

For a one dimensional subsystem, the wavelength of the N^{th} mode is given by [1]

$$\lambda_N = \frac{2L}{N \pm \delta_{BC}} \tag{3.4.1}$$

In Equation (3.4.2), the constant δ_{BC} is a constant depending on the boundary conditions and its magnitude is between 0 and 1. The corresponding wave number per unit length is

$$k_N = (N \pm \delta_{BC}) \frac{\pi}{L} \tag{3.4.2}$$

The mode which has a certain wavenumber or wave length can be found by solving for N in Equation (3.4.2) and define this equation as the mode count function

$$N(k)^{1D} = \frac{kL}{\pi} \pm \delta_{BC} \tag{3.4.3}$$

where 1D indicates that the results is for a one dimensional subsystem.

Neglecting the effect of the boundary conditions, the modal density for a one dimensional structural subsystem is given by

$$n(\omega) = \frac{L}{\pi c_g} \tag{3.4.4}$$

where c_g is the group velocity and is given by

$$c_g = \frac{d\omega}{dk} \tag{3.4.5}$$

For the bending waves of thin beams, the bending wave speed, c_B, depends on the frequency. Therefore, the modal density for the bending of beams is calculated by [34]

$$n(f) = \frac{L}{c_B} = \frac{3^{1/4}}{\sqrt{\pi}} \frac{L}{\sqrt{c_L h f}} \tag{3.4.6}$$

For two and three dimensional subsystem, the derivations of the mode count and modal density formulas are similar to the one dimensional case.

The average frequency spacing between two modal resonances of a two dimensional subsystem with an area A is given by

$$\delta f^{2D} = \frac{1}{2\pi n(\omega)} = \frac{c_\phi c_g}{2\pi f A} \tag{3.4.7}$$

Similarly, the average frequency spacing between two modal resonances of a three dimensional subsystem with a volume V is given by

$$\delta f^{3D} = \frac{c_\phi{}^2 c_g}{4\pi V f^2} \tag{3.4.8}$$

For a special case of *"simply supported isotropic plate"*, the number of modes is given by [34]

$$N(k) = \frac{k^2 A}{4\pi} \tag{3.4.9}$$

Moreover, the modal density can be obtained by

$$n(\omega) = \frac{kA}{2\pi c_g} \tag{3.4.10}$$

If the phase velocity and the group velocity are the same, the modal density in Hertz becomes

$$n(f) = \frac{2\pi f A}{c_0^2} \tag{3.4.11}$$

A special case of *"standard room"* is an important three dimensional subsystem. The modal density for the standard three dimensional rooms is given by [33]

$$n(f) = \frac{4\pi f^2 V}{c_0^3} + \frac{\pi f S}{2c_0^2} + \frac{L}{8c_0} \tag{3.4.12}$$

It is observed that at high frequencies the first term dominates the modal density because it is growing with the square of the frequency. Therefore, at high frequencies, the last two terms can be ignored and the modal density becomes

$$n(f) \cong \frac{4\pi f^2 V}{c_0^3} \tag{3.4.13}$$

Theoretical formulation for the mode count and the modal densities of simple structures are given in Table 3.4.1 [32].

Table 3.4.1. Number of modes and modal densities.

System	Mode Count	Modal Density
Beam, longitudinal	$N=\frac{k_L L}{\pi}=\frac{\omega L}{c_L \pi}$	$\frac{\Delta N}{\Delta \omega}=\frac{L}{c_L \pi}$
Beam, bending	$N=\frac{k_B L}{\pi}=\frac{\sqrt{\omega} L}{1.7\sqrt{c_L h}}$	$\frac{\Delta N}{\Delta \omega}=\frac{k_B L}{2\pi\omega}=\frac{L}{3.4\sqrt{c_L h}\sqrt{\omega}}$
Plate, bending	$N=\frac{k_B{}^2 A}{4\pi}=\frac{\omega A}{3.6 c_L h}$	$\frac{\Delta N}{\Delta \omega}=\frac{k_B{}^2 A}{4\pi\omega}=\frac{A}{3.6 c_L h}$
Volume, airborne sound	$N=\frac{k_o{}^3 V}{6\pi^2}=\frac{\omega^3 V}{6\pi^2 c_0{}^3}$	$\frac{\Delta N}{\Delta \omega}=\frac{k_0{}^2 V}{2\pi^2 c_0{}^3}=\frac{\omega^2 V}{2\pi^2 c_0}$
Ring, radially excited	$N=2k_B R=\frac{3.7\sqrt{\omega} R}{\sqrt{c_L h}}$	$\frac{\Delta N}{\Delta \omega}=\frac{k_B R}{\omega}=\frac{1.9R}{\sqrt{c_L h}\sqrt{\omega}}$
Thin walled tube, for $v<1$	$N\cong\frac{3\sqrt{3}L\left(\omega R/c_L\right)^{3/2}}{2\pi h}$	$\frac{\Delta N}{\Delta \omega}=2\sqrt{\omega}R^{3/2}=\frac{L}{1.6 h c_L{}^{3/2}}$
Thin walled tube, for $v>1$	$N\cong\frac{\sqrt{3}LR\omega}{c_L h}$	$\frac{\Delta N}{\Delta \omega}\cong\frac{\sqrt{3}LR}{c_L h}$

Another important parameter for SEA is the modal overlap. It defined as the ratio of the width of a resonant peak to the average modal spacing [24]. If the factor is in the region of unity or greater, then the frequency response function can be expected to be a fairly smooth function of frequency, since the resonant peaks will tend to merge together. The modal overlap, M(ω), can be found by the equation

$$M(\omega)=\omega\eta n(\omega) \qquad (3.4.14)$$

3.5. LOSS FACTORS

The loss factor for SEA is examined under two subtitles:

1. Damping loss factor referring to the internal energy dissipation of a subsystem.
2. Coupling loss factor referring to the energy transfer between the connected subsystems.

3.5.1. DAMPING LOSS FACTOR

Damping loss factor represents the amount of damping that exists in the subsystem itself. For a simple oscillator, the parameter η_i is defined as:

$$\eta_i = \frac{1}{2\pi} \frac{P_{diss}}{\omega E} \tag{3.5.1}$$

where P_{diss} is the total time averaged power dissipation in the frequency band and E is the total time averaged energy in the frequency band.

3.5.2. COUPLING LOSS FACTOR

Coupling loss factor η_{ij} is related to energy flow from subsystem i to subsystem j. This indicates the efficiency of power transmission by means of vibration from one subsystem to another. The coupling loss factor depends upon the nature and the properties of the subsystems, together with the details of the way in which the subsystems are coupled [31]. The coupling loss factor from subsystem i to subsystem j is generally defined as

$$\eta_{ij} = \left| \frac{\overline{P_{ij}}}{\omega E_i} \right|_{\bar{E}_j=0} \tag{3.5.2}$$

There exist two different approaches for the derivation of coupling loss factors, which are modal approach and wave approach. In modal approach, the coupling between the individual modes is computed and an average is taken for each mode in the frequency band. In wave approach, the coupling loss factor is related with the power transmissibility for semi-infinite structures, which is often easier to estimate the average of coupling between modes of finite subsystems.

It is also possible to relate the coupling loss factor to the power transmission coefficient with the formula

$$\tau_{ij} = \frac{P_{trans}}{P_{inc}} = \frac{\omega \eta_{ij} E_{tot}}{E_{tot}\left(c_g / L_f\right)} = \frac{\omega \eta_{ij} L_f}{c_g} \tag{3.5.3}$$

where P_{trans} is the transmitted power through the junction, P_{inc} is the incident power to the junction and L_f is the mean free path length between the incidences of the junction.

Then, the transmission loss, R, can be calculated by the equation

$$R = 10 \log\left(\frac{1}{\tau_{ij}}\right) \tag{3.5.4}$$

Table 3.5.1 gives the coupling loss factors for basic subsystem and junction types [33].

Table 3.5.1. Coupling loss factors.

Subsystem i	**Subsystem j**	**Type of junction**	**Formula for η_{ij}**
Plate	Plate	Line	$\frac{c_{gi}L_j}{\pi\omega A_i}$
Cantilever Beam	Plate	Point	$(2\rho_i c_i K_i A_{bi})^2(\omega M_i)^{-1} * \mathrm{Re}(z_j)^{-1}\lvert z_j/(z_j+z_i)\rvert^{-2}$
Plate	Plate	Stiff Bridges	$\frac{2Z_iZ_j}{(\pi\omega n_i)}/(Z_i+Z_j)^2$
Plate or cylindrical shell	Acoustic cavity	Acoustic	$\frac{\rho_0 c_0 \sigma}{\omega m_{pi}}$
Acoustic cavity	Acoustic cavity	Aperture or common partition	$\frac{c_0 A_w \tau_{ij}}{8\pi f V_i}$
Plate	Plate	N Points	$\frac{4N}{\sqrt{3}}\frac{h_i c_i}{\omega A_i}\frac{h_i^2 h_j^2}{(h_i^2+h_j^2)^2}$ for $\lambda_b < 1$ $\left(\frac{2}{3}\right)^{1/4}\frac{L_j}{A_i}\left(\frac{h_i c_i}{\omega}\right)^{1/2}\frac{h_i^{3/2}h_j^{3/2}}{(h_i^{3/2}+h_j^{3/2})^2}$ for $\lambda_b > 1$

The detailed derivations of the coupling loss factors are described in [1,39,45] for different coupled structures.

3.6. POWER INPUT

All the response variables in SEA depend on the power input. The power input to a subsystem can be found by experiments or analytical calculations. Moreover, the power input can also be found by the SEA model parameters.

Lyon gives the power input to a point excited structure by the time averaged product of applied force *F* and the velocity *v*

$$P_{in} = \langle Fv \rangle \tag{3.6.1}$$

This relationship shows that for the special case of point force excitation, the power input depends on the motion of the excitation point, which is known as the *"point mobility"*.

Addition to this relation, the power input to a point excited beam or plate can be expressed with the SEA parameters [31].

$$P_{i,in} = \frac{1}{2}\left(\frac{\pi n_i(\omega)}{2m_i}\right)F^2 \tag{3.6.2}$$

It can be seen in the Equation (3.6.2) that the power input to a subsystem i depends of the modal density, $n_i(\omega)$, and the total mass, m_i, of that subsystem.

For an acoustical space, the power input is related to the acoustical volume velocity, *U*, and the acoustical volume pressure, *p.* The input power to an acoustical space can be found by

$$P_{in} = \langle Up \rangle \tag{3.6.3}$$

When the excitation of a system is distributed over space, the input power depends on the matching of the spatial distribution of the input and the mode shapes of the subsystem in the frequency range of interest.

An important type of excitation for the plate subsystems is the turbulent boundary layer (TBL), which is associated with a fluid flowing parallel to the plate

with a free stream velocity of U_∞. The wavenumber spectrum of the TBL pressure distribution in the direction of the flow has a strong peak around a wavenumber equal to $2\pi f/U_c$ where U_c is the convection velocity given by [1]

$$U_c = 0.75U_\infty \tag{3.6.4}$$

The power input depends of the matching of the spatial distribution of the TBL pressure with the mode shapes of the plate, as mentioned before; the degree of matching is equal to the ratio of U_c to the plate bending phase speed c_p.

For high speed gas and thin plate problems where $U_c > c_p$, the power input into the modes matching with the TBL pressure distribution in the direction of flow is given by

$$P_{in} = \frac{A_p \langle p_{TBL}{}^2 \rangle}{\pi^2 f \rho_p h_p} \left(\frac{U_c}{c_p} \right) \tag{3.6.5}$$

where p denotes the plate.

3.7. SOLVING FOR ENERGY DISTRIBUTIONS

The primary response variable is the average modal energy of a subsystem in SEA. The other engineering variables such as velocity, acceleration, power, etc. can be derived from this information.

In order to obtain the modal energies of subsystems, Equation (3.2.9) can be written as:

$$\begin{bmatrix} \eta_1+\sum_{j=1}^{S}\eta_{1j} & -\eta_{12} & .. & -\eta_{1S} \\ -\eta_{21} & \eta_2+\sum_{j=2}^{S}\eta_{2j} & .. & -\eta_{2S} \\ : & : & : & : \\ -\eta_{S1} & -\eta_{S2} & .. & \eta_S+\sum_{j=S}^{S}\eta_{Sj} \end{bmatrix} \begin{bmatrix} E_1\omega \\ E_2\omega \\ : \\ E_S\omega \end{bmatrix} = \begin{bmatrix} P_{1,in} \\ P_{2,in} \\ : \\ P_{S,in} \end{bmatrix} \tag{3.7.1}$$

This equation can be simplified to a simple matrix equation as:

$$\omega[B]\{E\} = \{P_{in}\} \tag{3.7.2}$$

In order to solve for the energy distributions, both sides of this equation are multiplied by $[B]^{-1}$ and divided by ω. The resulting equation is:

$$\{E\}=\frac{1}{\omega}[B]^{-1}\ \{P_{in}\} \tag{3.7.3}$$

Addition to this, the modal power of subsystem i is defined by the equation

$$\Phi_i = \frac{E_i}{n(\omega)_i} \tag{3.7.4}$$

The matrix [B] in Equation (3.7.3) is positive-definite and diagonally dominant which makes the matrix inversion very stable. Also the inverse of the matrix will yield all positive, non-zero elements which mean that all interconnected subsystems will have some positive energy when power is injected into a subsystem. Another property is that for a subsystem with coupling loss factors as large as the damping loss factor, the calculated energy value is insensitive to errors in the CLF's because the diagonal terms are the sum of off-diagonal CLF terms plus a damping term.

3.8. ENERGY TO OTHER ENGINEERING VARIABLES

The relation between vibratory energy and the space-time mean square velocity of the structure or the sound field is defined in [1] as

$$E = M\langle v^2 \rangle = M\, v_{RMS}^2 \tag{3.8.1}$$

where M is the structural mass in kilograms.

By taking the 10 log of this expression, a relation between energy levels and velocity levels can be expressed as

$$L_E = 10\log\left(\frac{E}{E_{ref}}\right) = 10\log M + L_v + 120 \tag{3.8.2}$$

where

$$L_v = 20\log\left(\frac{v_{RMS}}{v_{ref}}\right) \tag{3.8.3}$$

and $v_{ref} = 1$ m/s.

It is known that the displacement, velocity and acceleration are related with each other with the equations [1]

$$<a^2> = 4\pi^2 f^2 <v^2> \tag{3.8.4}$$

$$<d^2> = \frac{<v^2>}{4\pi^2 f^2} \tag{3.8.5}$$

If the reference acceleration is taken as 10 m/s^2 and reference displacement is taken as 1 m, the acceleration and displacement levels can be found in terms of velocity levels by the following equations

$$L_a = L_v + 20\log(f) - 4 \tag{3.8.6}$$

$$L_d = L_v - 20\log(f) - 16 \tag{3.8.7}$$

In addition to these primary response variables, there are some simple relations between velocity and the strain. The relationship is given by [1]

$$\langle \varepsilon^2 \rangle = K \frac{\langle v^2 \rangle}{c_L{}^2} \tag{3.8.8}$$

where K is a constant which depends on the type of motion (flexure, torsion, compression, etc.) and geometry. If the value of K is taken 1 for simplification, and ε_{ref} is taken as 10^{-6} (1 microstrain), then the strain level can be calculated as

$$L_\varepsilon = L_v - 20\log(c_L) - 120 \tag{3.8.9}$$

Taking the modulus of elasticity as E_0, the mean square stress is related to the mean square strain by the formulation

$$\langle \sigma^2 \rangle = E_0{}^2 \langle \varepsilon^2 \rangle \tag{3.8.10}$$

By taking the reference stress, σ_{ref} as 1 MPa, the stress level can be found by the equation.

$$L_\sigma = L_v + 20\log(\rho\, c_L) \tag{3.8.11}$$

Various formulations for estimating the stress and strain data for beams, plates and shells are presented by Karczub and Norton [35-36]. They found the formulation for spatial maximum far field dynamic strain as

$$\langle \varepsilon_{FF}{}^2(x, f) \rangle = \left(\frac{K_{shape}}{c_L} \right)^2 \langle v_{FF}{}^2(x, f) \rangle \tag{3.8.12}$$

for a beam structure. For a plate structure, this equation becomes

$$<\varepsilon_{FF}^2(x, y, f)> = \left(\frac{K_{shape}}{c_L}\right)^2 <v_{FF}^2(x, y, f)> \quad (3.8.13)$$

where K_{shape} is the non-dimensional geometric shape factor which is equal to $\sqrt{3}$ for a rectangular bar and flat plate. The longitudinal wave speed c_L is defined as

$$c_L = \sqrt{\frac{E}{\rho}} \quad (3.8.14)$$

for a beam and

$$c_L = \sqrt{\frac{E}{\rho(1-\mu^2)}} \quad (3.8.15)$$

for a flat plate.

CHAPTER 4

MODEL DEVELOPMENT

4.1. AIRCRAFT MODEL

The aircraft model used in this study is a basic training aircraft model which has a 5 bladed propeller. The aircraft is shown in Figure 4.1.1.

Figure 4.1.1. Basic training aircraft used in the analyses.

The general properties of the aircraft are given in Table 4.1.1.

Table 4.1.1. General properties of the aircraft.

Maximum Take-off Weight	3000 kg
G Limits	+7g/-3.5g
Stall Speed	70 knot
Maximum Cruise Speed	270 knot (sea level)
Climb Rate	0 - 15000ft in 5 min
Service Ceiling	30000ft

The joint master FEM of the aircraft that is used for creating the SEA subsystems is shown in Figure 4.1.2.

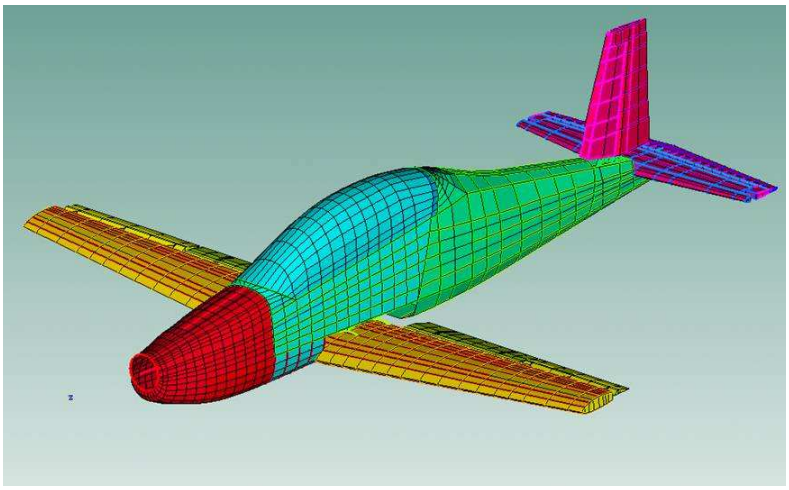

Figure 4.1.2. Joint master FEM of the aircraft.

In the development period, the model is divided into five regions, namely forward, center, rear fuselage, empennage and wings. Depending on the type of the structure, an appropriate subsystem property is chosen. The properties used in the model are uniform plate, ribbed plate and composite layup.

In the uniform plate, the wavefield properties are calculated using the thin plate theory. For the ribbed plate, wavefield properties account for the existence of one or two sets of orthogonally oriented ribs. For the composite layup property, wavefield properties are calculated using composite section theory [40].

The whole model of the aircraft including only the structural subsystems is shown in Figure 4.1.3.

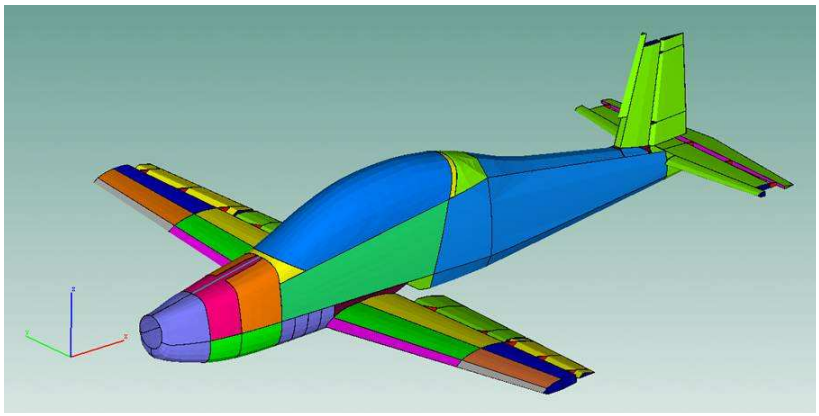

Figure 4.1.3. SEA model of the aircraft.

In order to be consistent within the model, a subsystem naming format is generated. The aircraft is divided into 5 main regions, namely, forward, center, rear fuselages, wings and the empennage.

The forward fuselage subsystems are composed of singly curved shells. Most of the forward fuselage structures are made of composite materials. Therefore, these parts are modeled with composite layup property. The rest of the curved shell parts are modeled as uniform plate. There also exists a beam subsystem in the

forward fuselage. The subsystems composing the forward fuselage are shown in Figure 4.1.4.

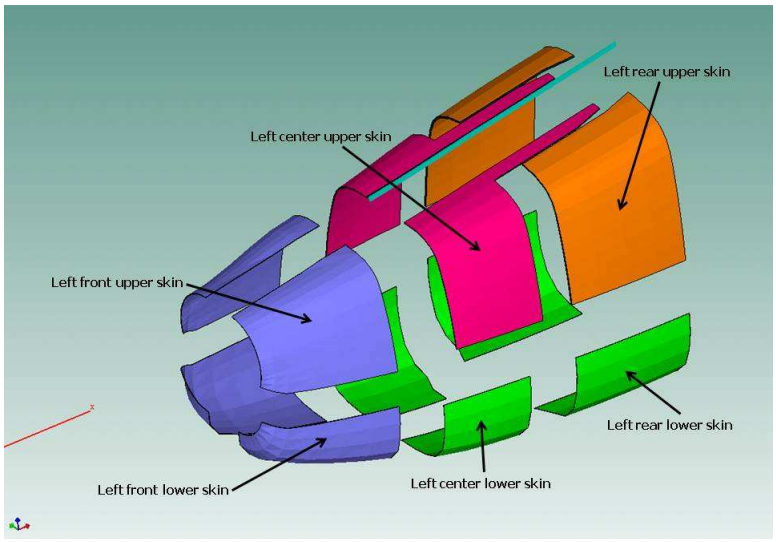

Figure 4.1.4. Subsystems of forward fuselage.

The SEA parameter modal density is evaluated for all subsystems. Since the model is symmetric, only the modal densities of the subsystems existing on one part are given in Figure 4.1.5, Figure 4.1.6 and Figure 4.1.7.

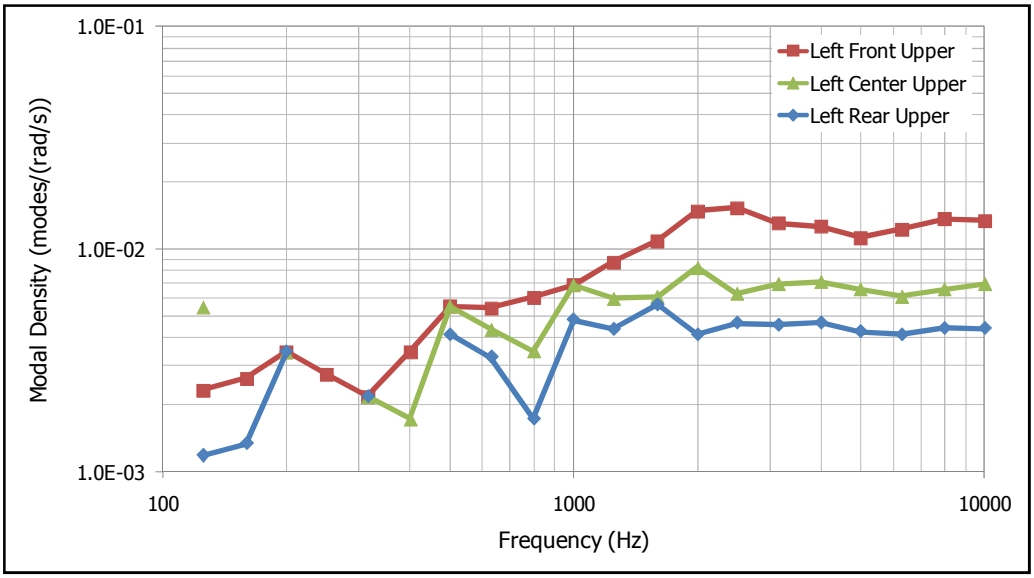

Figure 4.1.5. Modal densities of forward fuselage upper skin subsystems.

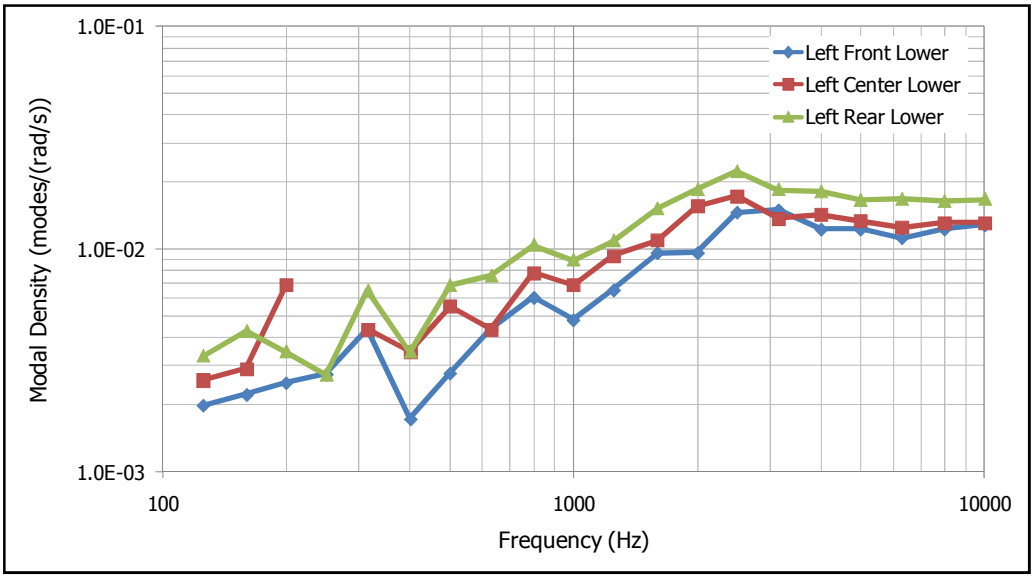

Figure 4.1.6. Modal densities of forward fuselage lower skin subsystems.

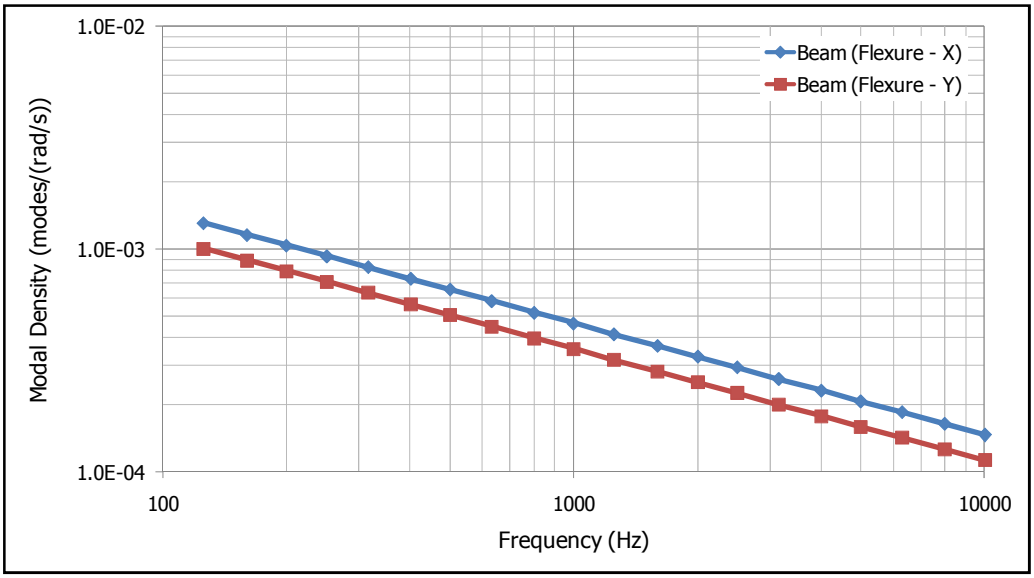

Figure 4.1.7. Modal densities of forward fuselage beam subsystems.

The center fuselage is composed of metallic structures and the canopy. When creating the center fuselage skin panel, ribbed panel property is used. In this case, it is assumed the distances between the frames and the stringers are constant; hence the taper effect in the skin panel is not taken into account. The model of the mid fuselage is shown in Figure 4.1.8.

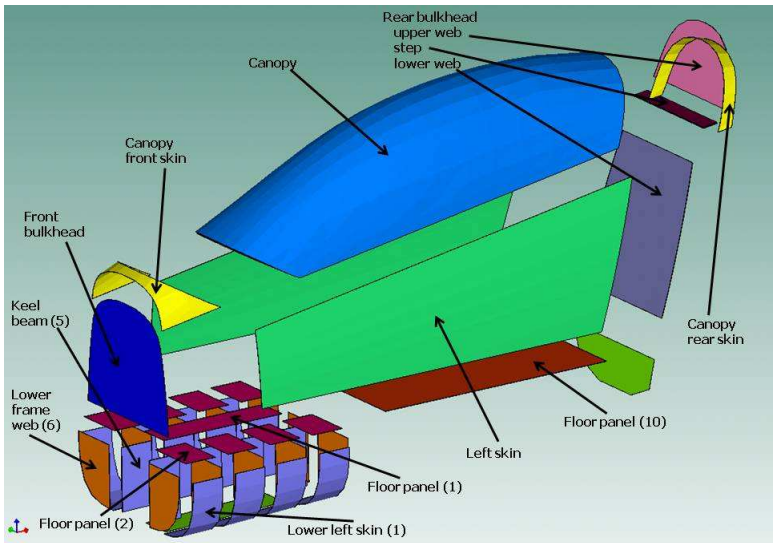

Figure 4.1.8. Subsystems of mid fuselage.

Like the center fuselage skin panel, the floor region is also modeled as ribbed panel. The floor subsystems between the keel beam and the lower skin panels are modeled as flat plate. The frame webs, keel beam and lower skin panels are modeled as flat plate, as well. The modal densities of the center fuselage subsystems are shown in the Figure 4.1.9, Figure 4.1.10 and Figure 4.1.11. Since the center fuselage has the largest number of subsystems, they are separated into groups. These groups are:

1. The bulkheads
2. The floor panel elements
3. The external skin elements

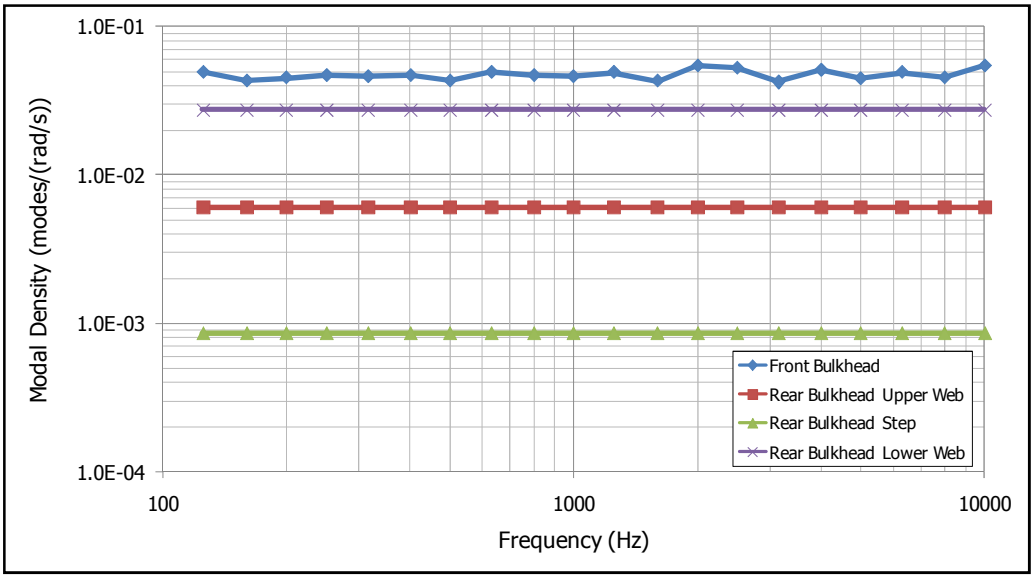

Figure 4.1.9. Modal densities of center fuselage bulkheads.

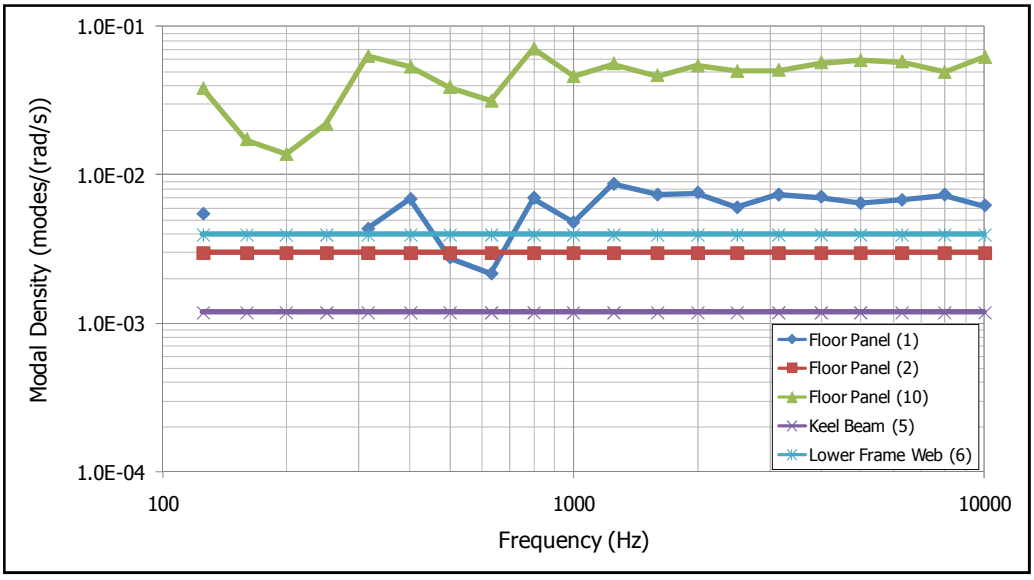

Figure 4.1.10. Modal densities of center fuselage floor elements.

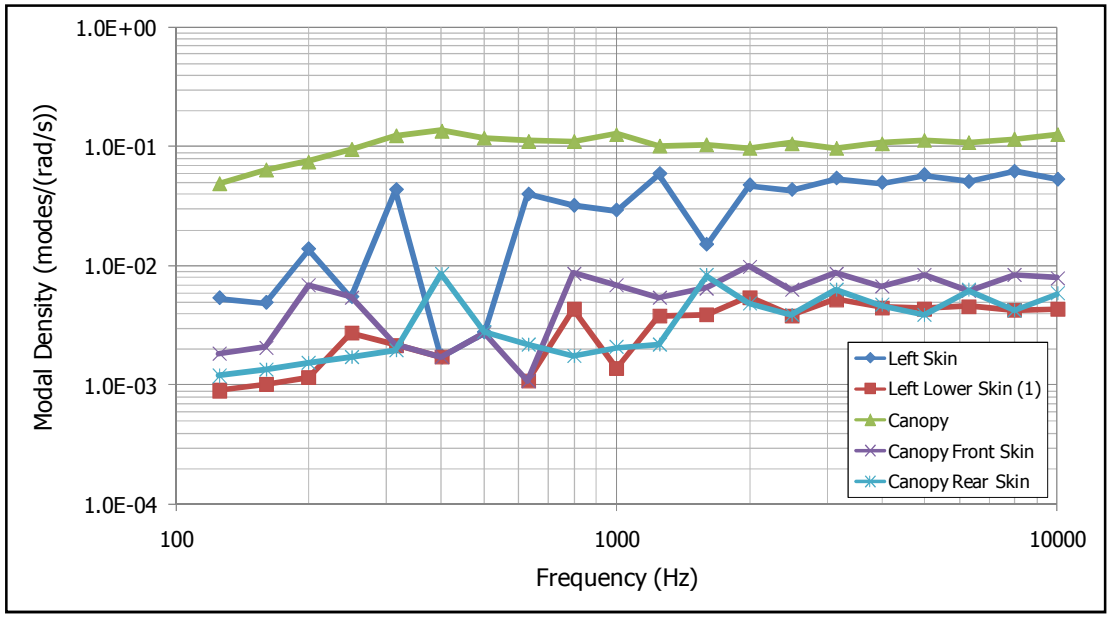

Figure 4.1.11. Modal densities of center fuselage external elements.

Actually there are applied treatments to the center fuselage skin panels for the thermal and acoustic problems. These treatments are also increasing the mass of the system causing vibration levels to decrease. However, in order to make the model simpler and conservative, these treatments are not applied to the model.

The cross section details of the stiffeners used in the floor panel, frames and stringers in the skin panel used in the SEA model are given in Table 4.1.2.

Table 4.1.2. Cross section properties for mid fuselage.

Property	**Value for Stringer**	**Value for Frame**	**Value for Floor Panel Stiffeners**
I_{xx} (mm^4)	3277	204500	42050
I_{yy} (mm^4)	3243	50260	7213
Q (mm^4)	26.9	494.1	134.4
J (mm^4)	6521	254200	49270
Area (mm^2)	57.5	306.2	154.9
Perimeter (mm)	120	282.8	196.8

The rear fuselage is composed of metallic structures only, as well. Like the center fuselage skin panels, the frames and the stringers are smeared into the skin panels of the rear fuselage by means of ribbed panel model. The taper of the generated subsystems is not taken into account. Moreover, the frames close to the empennage are not positioned vertically. This is also not taken into consideration in order to create a simple ribbed panel subsystem. The subsystems of the rear fuselage are shown in Figure 4.1.12.

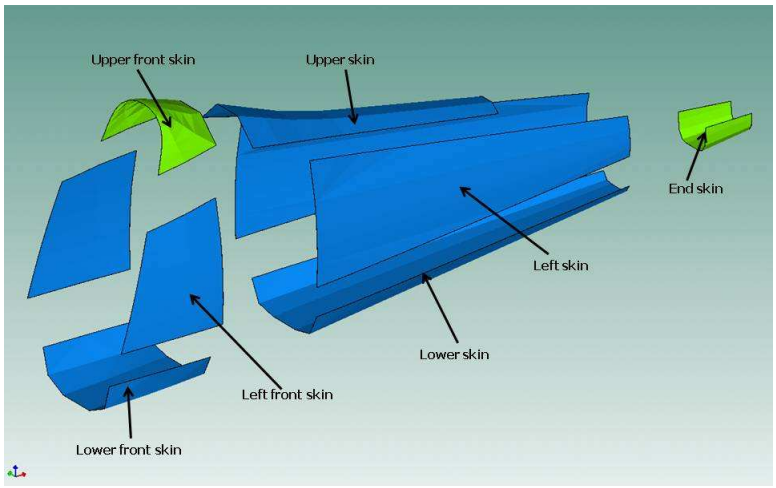

Figure 4.1.12. Subsystems of rear fuselage.

The modal densities of the rear fuselage subsystems are shown in Figure 4.1.13 and Figure 4.1.14. For the symmetric subsystems only modal density of one of them is given.

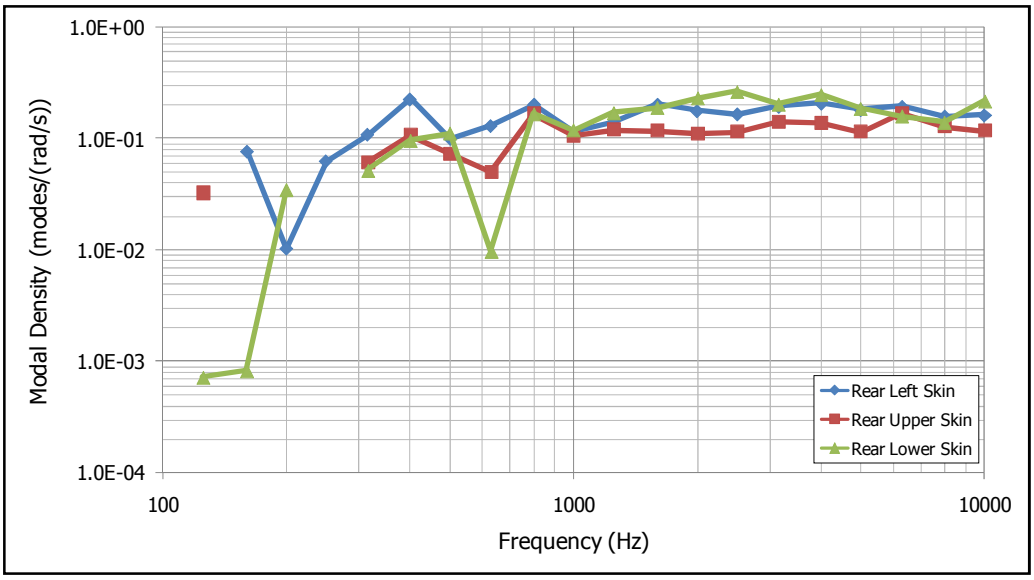

Figure 4.1.13. Modal densities of rear fuselage subsystems (1).

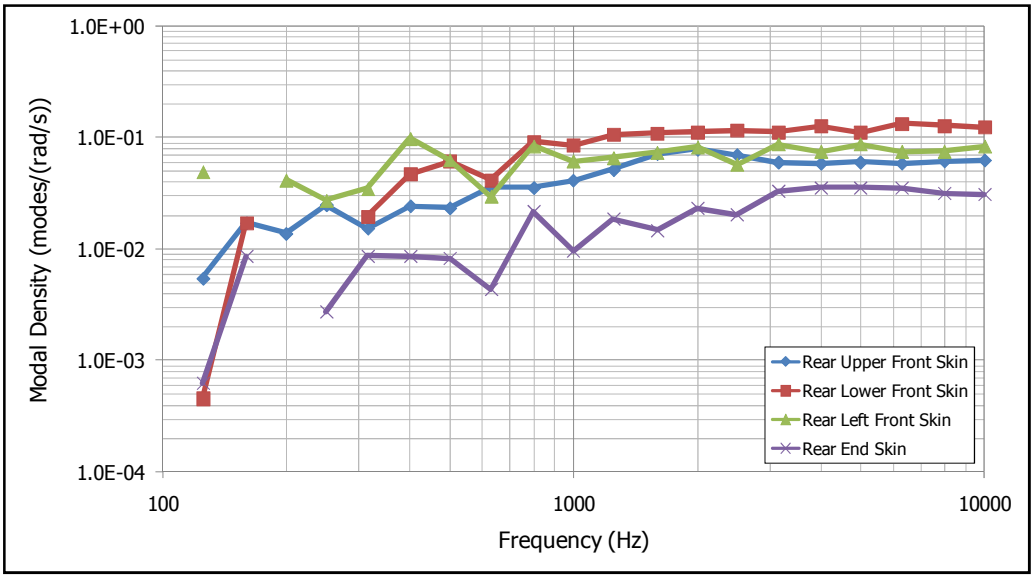

Figure 4.1.14. Modal densities of rear fuselage subsystems (2).

Like the stiffeners, stringers and frames used in the mid fuselage, the cross section details of the frames of the rear fuselage are not given. Instead of the dimensions, the cross sectional properties used in the SEA model are given in Table 4.1.3.

Table 4.1.3. Frame cross sectional properties of rear fuselage.

Property	**Value for Frames**
I_{xx} (mm^4)	211000
I_{yy} (mm^4)	18120
Q (mm^4)	187.5
J (mm^4)	229100
Area (mm^2)	219.7
Perimeter (mm)	277.8

The wings are composed of ribbed panels (wing skins and wing box), and uniform plates (spars). Actually the wing skins are connected to each other via ribs. However, in order to create an SEA model, these ribs are assumed to be separated into two and half of them are smeared to the upper skin and half of them are smeared to the lower skin. The front and main (mid) spars are modeled in two pieces. The rear spar is modeled in several pieces in order to be consistent with the connection locations of the control surfaces. The model view of the left wing is shown in Figure 4.1.15.

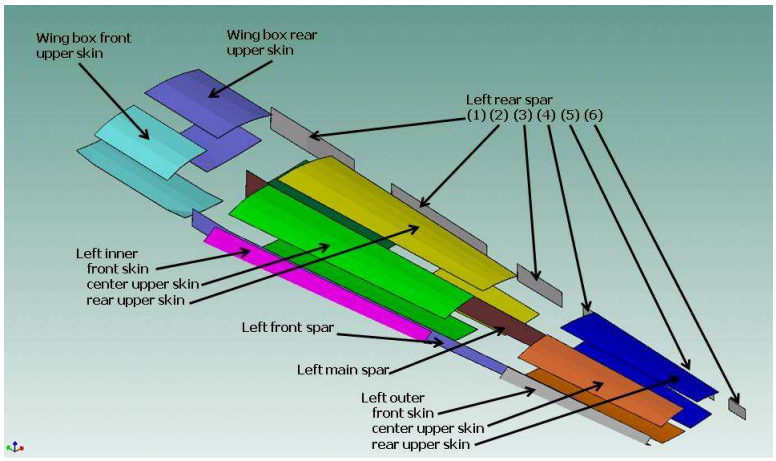

Figure 4.1.15. Subsystems of the wing and wing box.

The modal densities of wing inner and outer skins, spars and wing box and landing gear door structures are shown in Figure 4.1.16, Figure 4.1.17, Figure 4.1.18 and Figure 4.1.19, respectively.

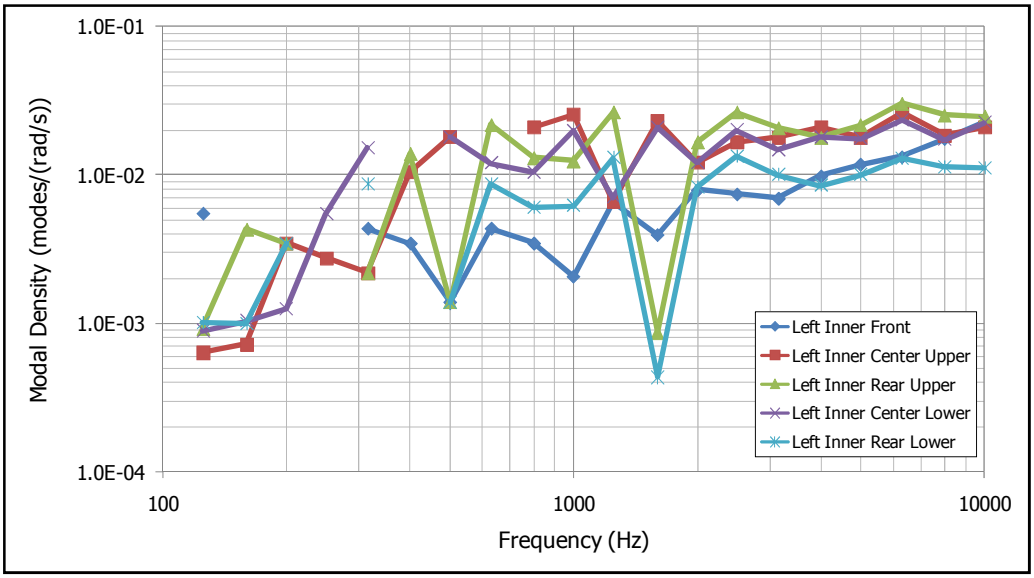

Figure 4.1.16. Modal densities of wing inner skin subsystems.

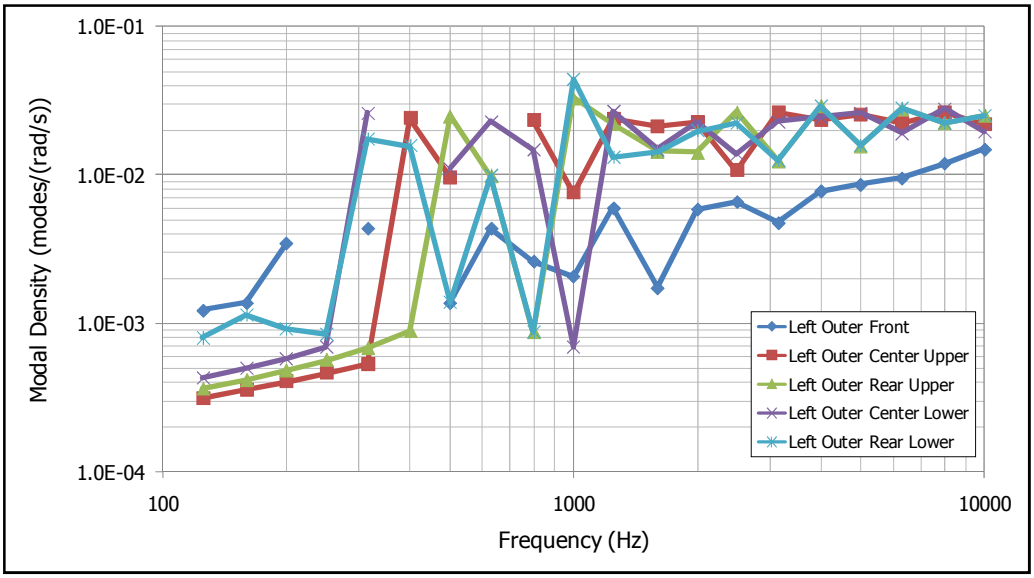

Figure 4.1.17. Modal densities of wing outer skin subsystems.

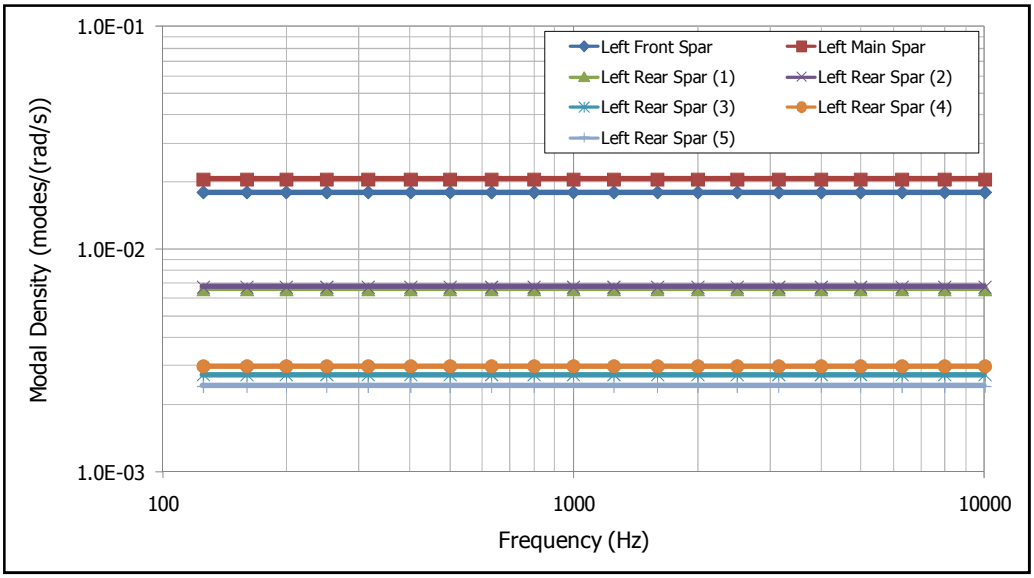

Figure 4.1.18. Modal densities wing spar subsystems.

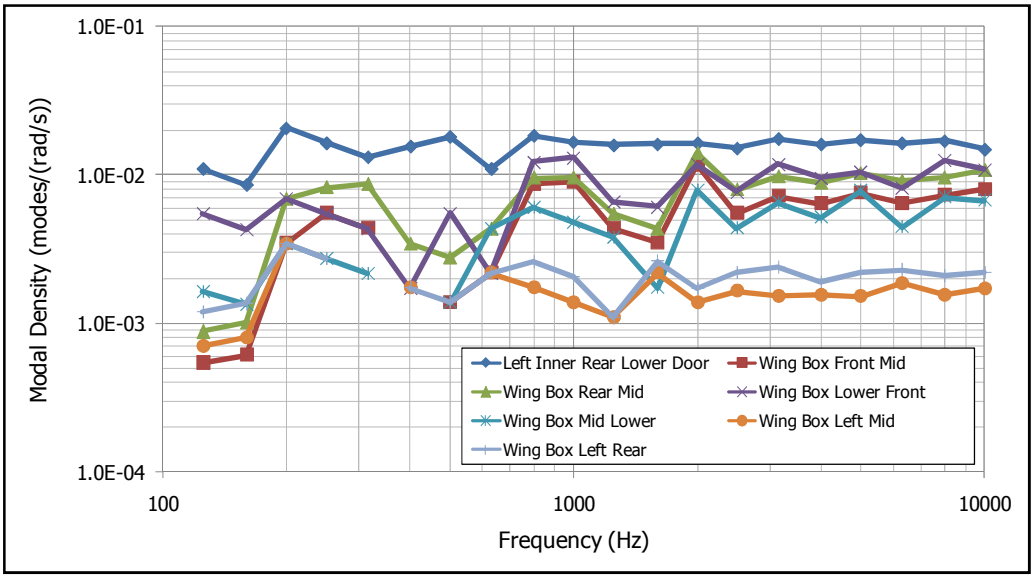

Figure 4.1.19. Modal densities of wing box and landing gear door subsystems.

The cross section dimensions of the stringers and ribs are not given. Instead of the dimensions, the cross sectional properties used in the SEA model are given in Table 4.1.4, Table 4.1.5 and Table 4.1.6.

Table 4.1.4. Inner wing ribs.

Property	**Inner Center Wing Ribs**	**Inner Rear Wing Ribs**
I_{xx} (mm^4)	420061	441152
I_{yy} (mm^4)	8701	8723
Q (mm^4)	691.4	701.8
J (mm^4)	428762	449875
Area (mm^2)	331.9	336.9
Perimeter (mm)	270.5	274.5

Table 4.1.5. Outer wing ribs.

Property	**Outer Center Wing Ribs**	**Outer Rear Wing Ribs**
I_{xx} (mm^4)	185231	207491
I_{yy} (mm^4)	8317	8374
Q (mm^4)	541.7	560
J (mm^4)	193548	215865
Area (mm^2)	260	268.8
Perimeter (mm)	213	220

Table 4.1.6. Wing box ribs and stringers.

Property	Wing Box Front Ribs	Wing Box Rear Ribs	Stringers
I_{xx} (mm^4)	716108	958852	8249
I_{yy} (mm^4)	8922	9036	6820
Q (mm^4)	815.1	893.2	45.5
J (mm^4)	725030	967888	15069
Area (mm^2)	391.3	428.8	83.4
Perimeter (mm)	318	348	134

The empennage structures composed of flat panels. Actually, they are ribbed structures; however, since they are away from the region to be analyzed, they are modeled in order to have a complete aircraft model. To compensate the neglected ribs, the spar thicknesses and the skin thicknesses are increased such that the system has the same mass with the original one. The empennage model is shown in Figure 4.1.20.

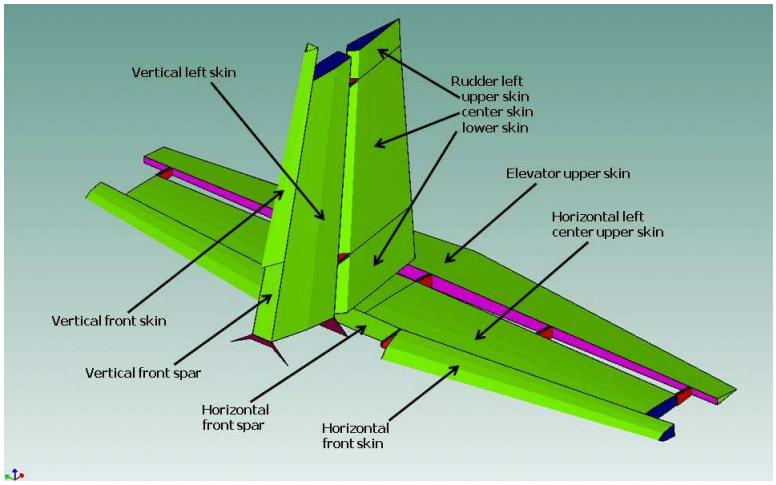

Figure 4.1.20. Subsystems of empennage.

The modal densities of the horizontal and vertical stabilizer, and elevator and rudder are given in Figure 4.1.21 and Figure 4.1.22, respectively. Only the modal densities of the primary structures (skin, spar) are given.

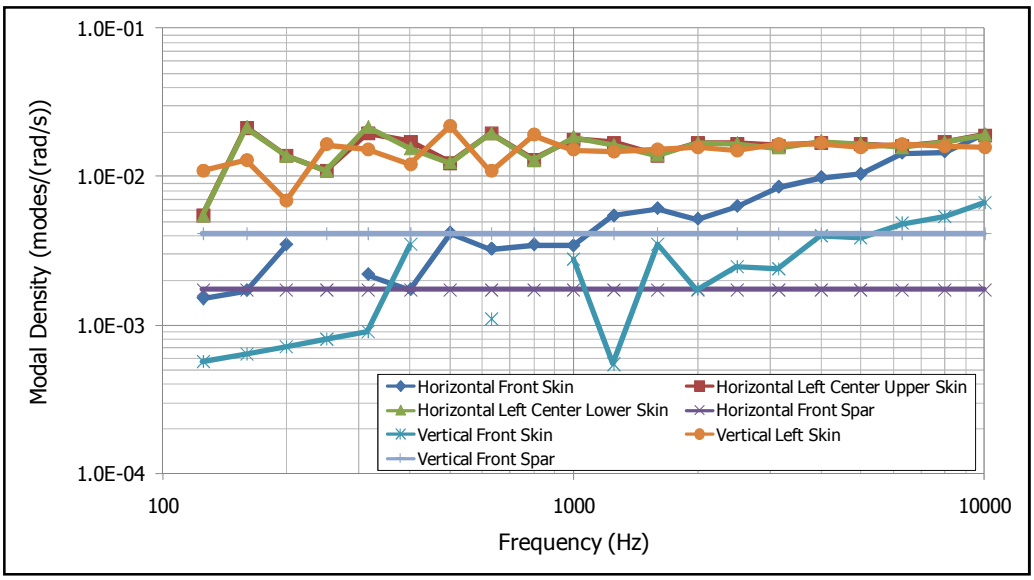

Figure 4.1.21. Modal densities of horizontal and vertical stabilizer subsystems.

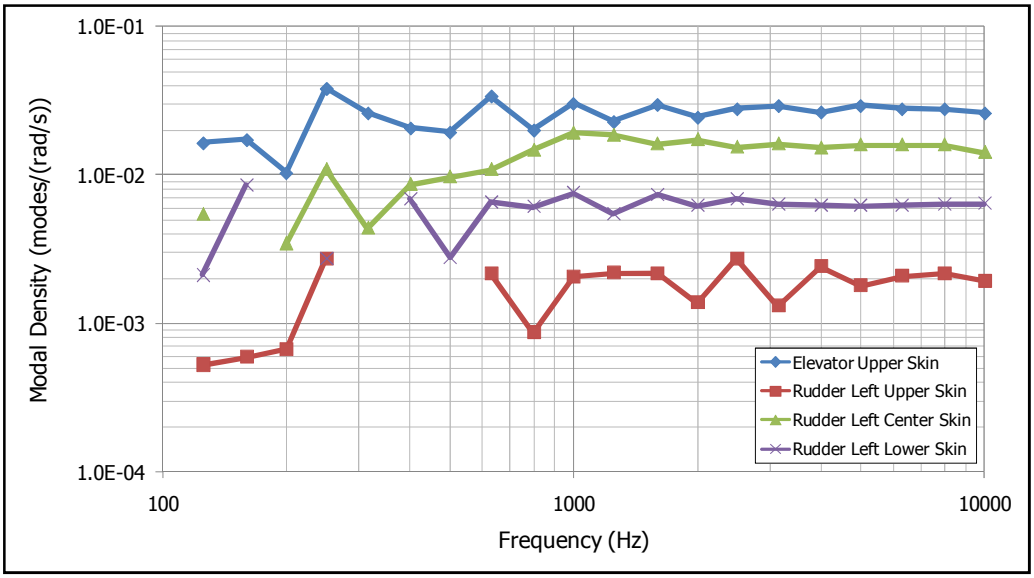

Figure 4.1.22. Modal densities of elevator and rudder subsystems.

When the modal densities of the structural subsystems are examined, it is observed that in some frequency bands, some of the subsystems do not have modes (or SEA method could not locate any mode) therefore do not store energy at that frequency bands, especially at low frequencies. This affects the other properties of the structure like radiation efficiency, and response of the structure and hence the stress levels. Although this is not appropriate for the theory of SEA, the model can still give good results at higher frequencies, above 250 Hz, because the main structures that are excited are modeled in accordance with the SEA theory above this frequency.

All these structural subsystems are connected to each other via line and point junctions. These line and point junctions are shown in Figure 4.1.23.

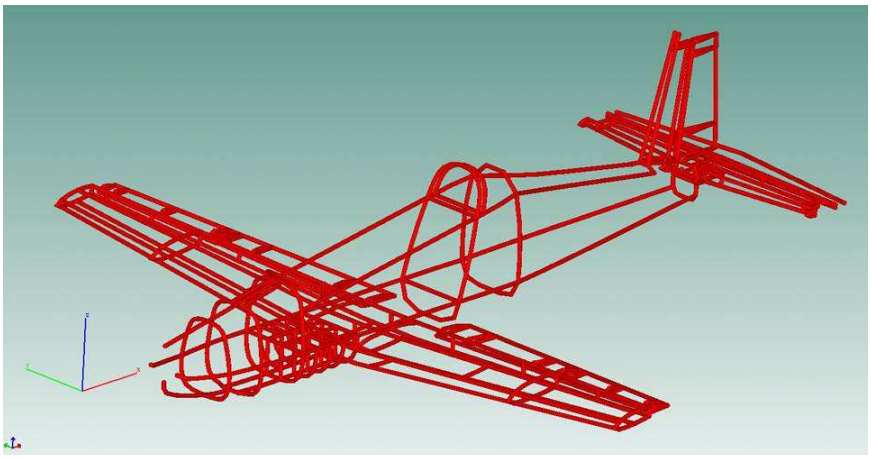

Figure 4.1.23. Point and line junctions connecting the structural subsystems.

The model contains one interior acoustic cavity for the pilot cabin. It is created by using the center fuselage structural subsystems that are surrounding the pilot cabin. The cavity geometry is shown in Figure 4.1.24.

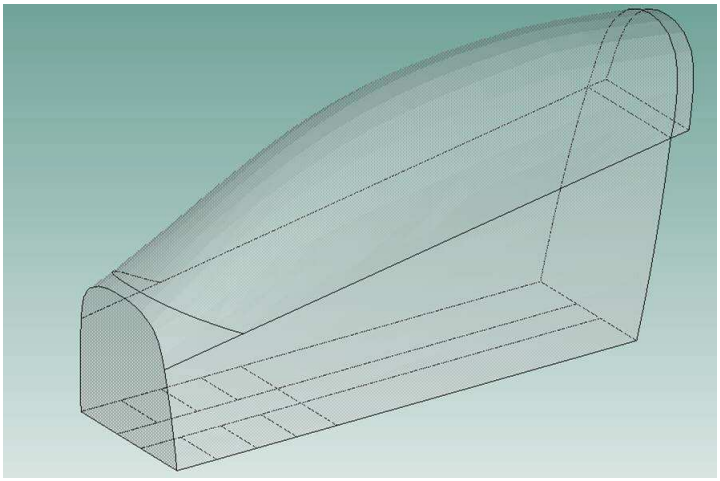

Figure 4.1.24. Pilot cabin cavity geometry.

The model also contains external acoustic field which is also modeled as a group of acoustic cavities. These cavities are connected to each other via area junctions. This model is used to determine the propeller noise around the aircraft. The model is shown in Figure 4.1.25.

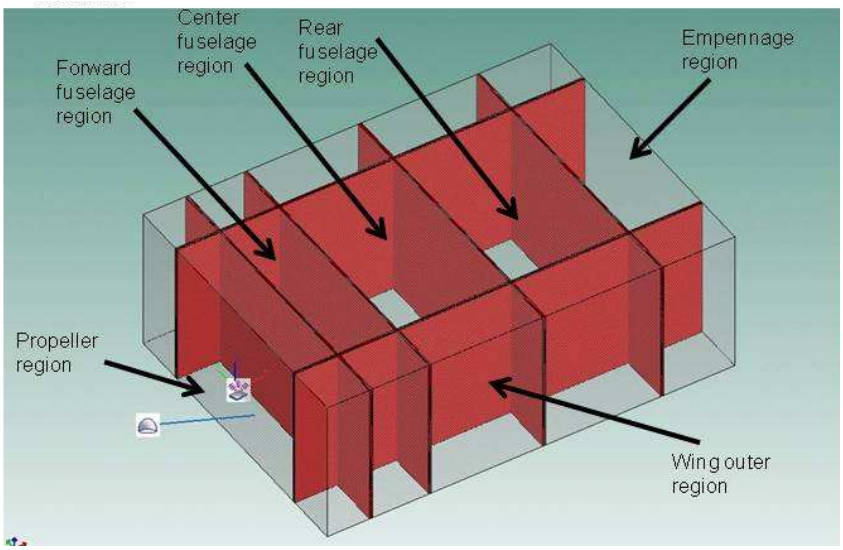

Figure 4.1.25. External acoustic fields around the aircraft and their junctions.

The damping loss factor for the metallic structural subsystems is taken from VA One™. It is taken as the bolted/riveted flexure damping spectrum. For composite structures, the internal loss factor is taken as bonded composite flexure damping spectrum. Both spectrums are shown in Figure 4.1.26.

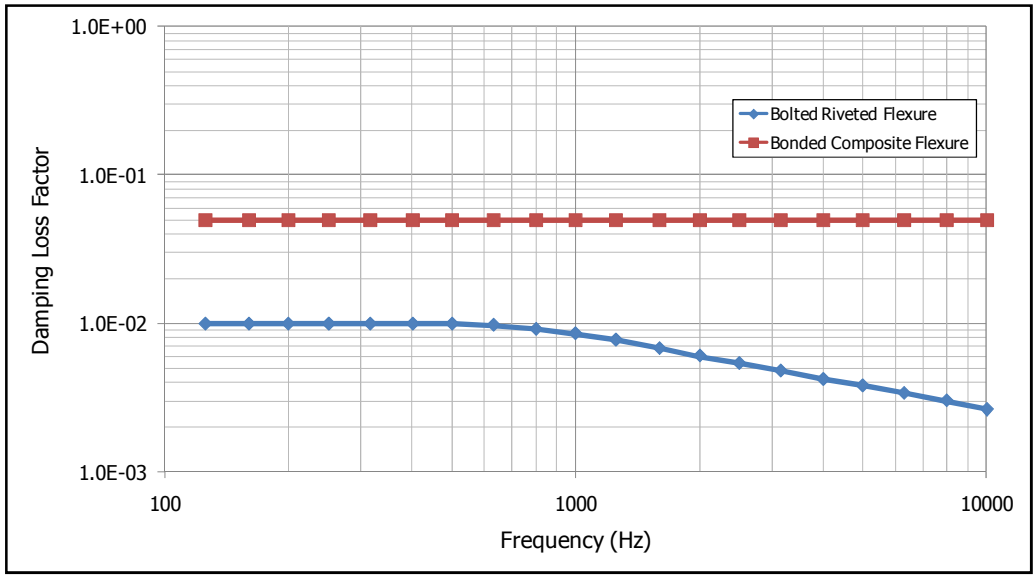

Figure 4.1.26. Damping loss factor spectrums used in the model.

4.2. APPLIED LOADS

Experience on many different aerospace vehicles showed that high frequency low amplitude pressure fluctuations associated with random acoustic loading can cause structural fatigue [34]. It is also found that the failures occur on the structure close to the jet flux, intake of fan engines, close to propeller tips. The sources for the acoustic and aerodynamic excitations that may cause acoustic fatigue are given in reference [34] in detail. The most ones which are the main sources of excitation in this study are explained below:

1. Turbulent boundary layer is one of the important sources of excitations for acoustic fatigue. TBL effect may be smaller than the effect of jet noise due to its correlation characteristics. However, high excitation levels can also be generated by the sharp profile changes in a high velocity flow.

2. Propeller noise is another important source of excitation. The propellers can produce high sound pressure levels affecting the structure approximately in line with the propeller disc.

Under the conditions described above, the TBL and the propeller noise are applied to the aircraft model. The TBL load is calculated by VA One™ by taking the subsystem midpoint distance to the leading edge of the whole system, and the free stream velocity. There are two types of TBL excitation defined in VA One™, namely the attached and separated TBL fields. The difference between them is shown in Figure 4.2.1 [40].

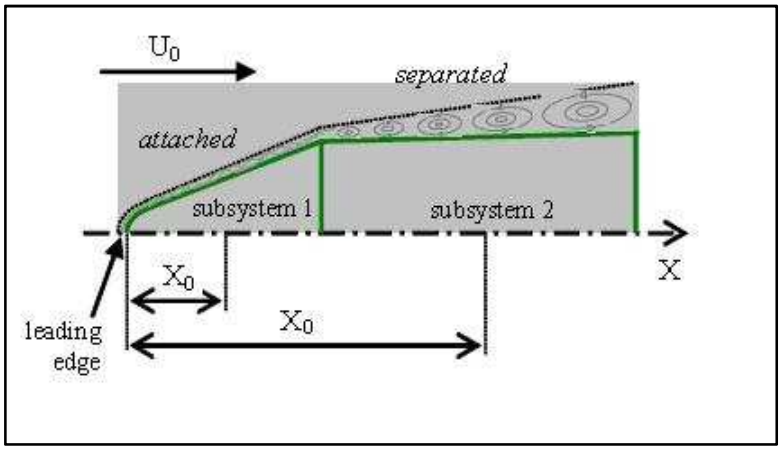

Figure 4.2.1. Attached and separated TBL.

In the figure above, U_0 denotes the free stream velocity in m/s and X_0 denotes the subsystem distance to the leading edge in m.

In order to observe the difference between the attached and the separated TBL, the excitation to one of the subsystems, mid fuselage skin panels (number 2 in figure), is plotted for both attached and separated fields. The result is shown in Figure 4.2.2.

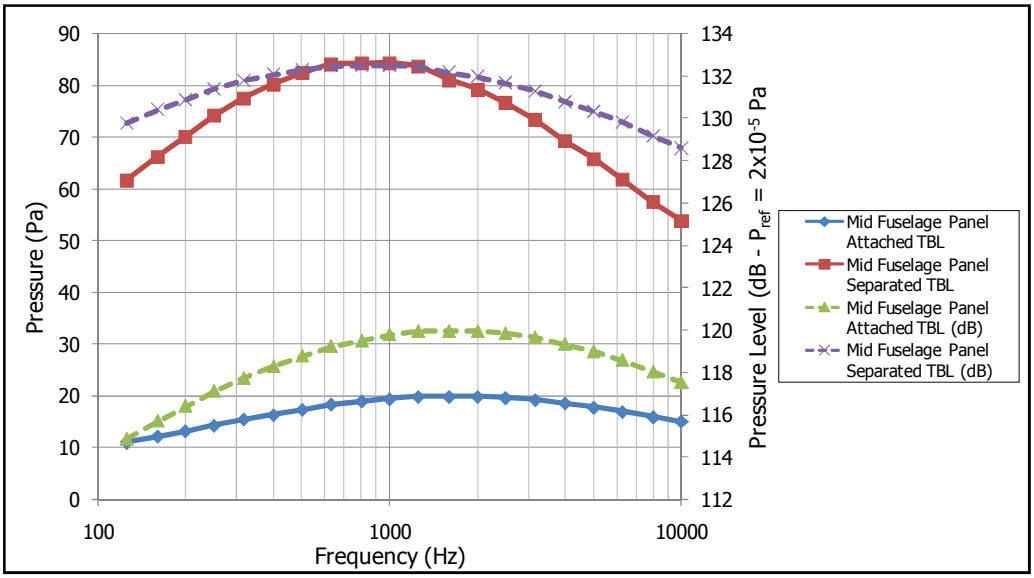

Figure 4.2.2. Attached and separated TBL load difference.

According to the Figure 4.2.2, the separated TBL field gives higher pressure spectrum than the attached one. Therefore, in the analyses, the separated TBL field is used to be conservative. The subsystem distances that are used in the calculation of TBL are shown in the Figure 4.2.3, Figure 4.2.4, Figure 4.2.5, Figure 4.2.6 and Figure 4.2.7.

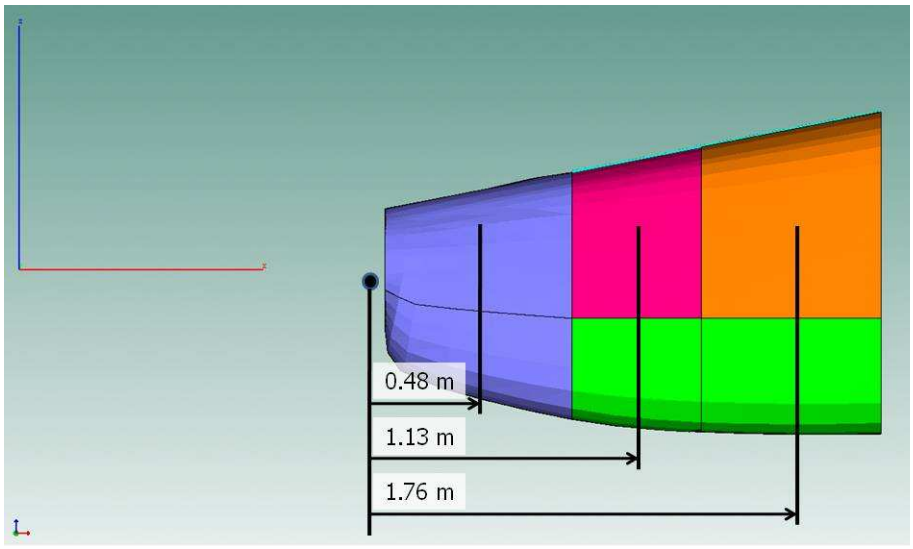

Figure 4.2.3. TBL distances for forward fuselage subsystems.

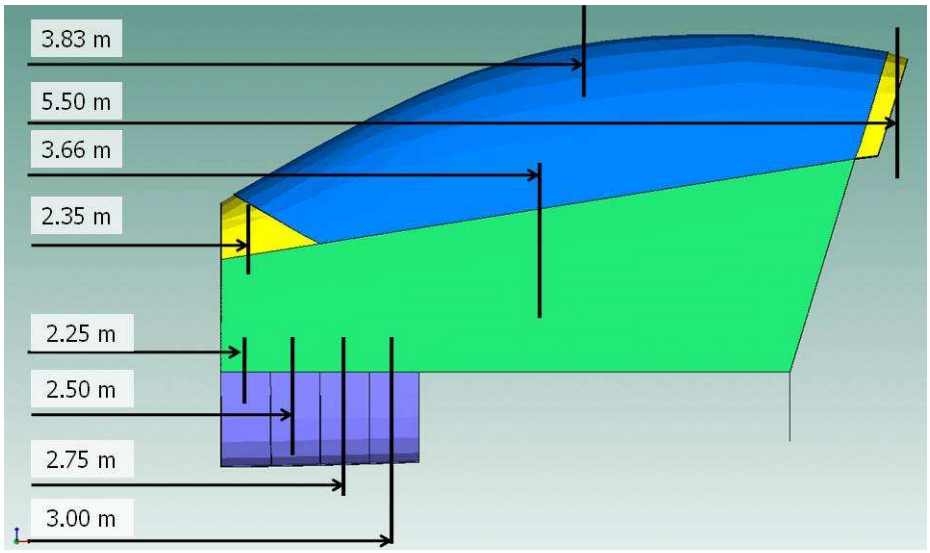

Figure 4.2.4. TBL distances for mid fuselage subsystems.

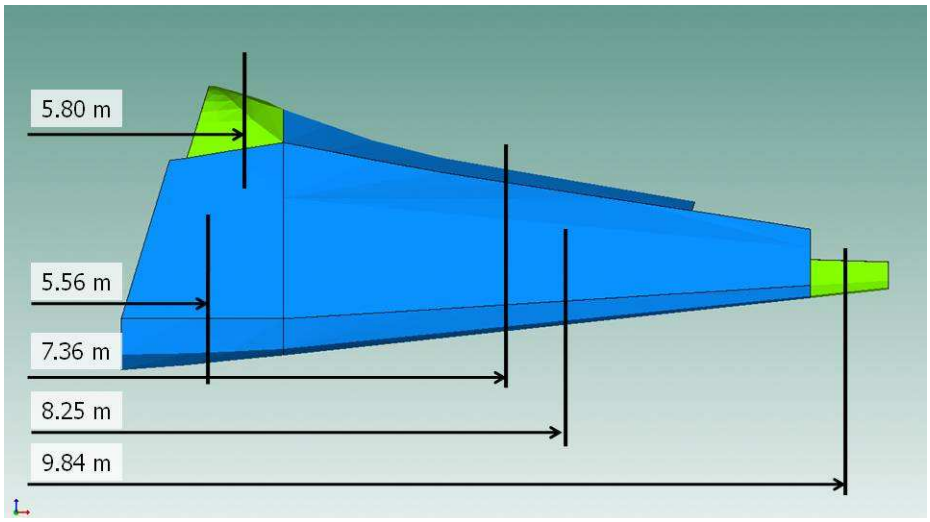

Figure 4.2.5. TBL distances for rear fuselage subsystems.

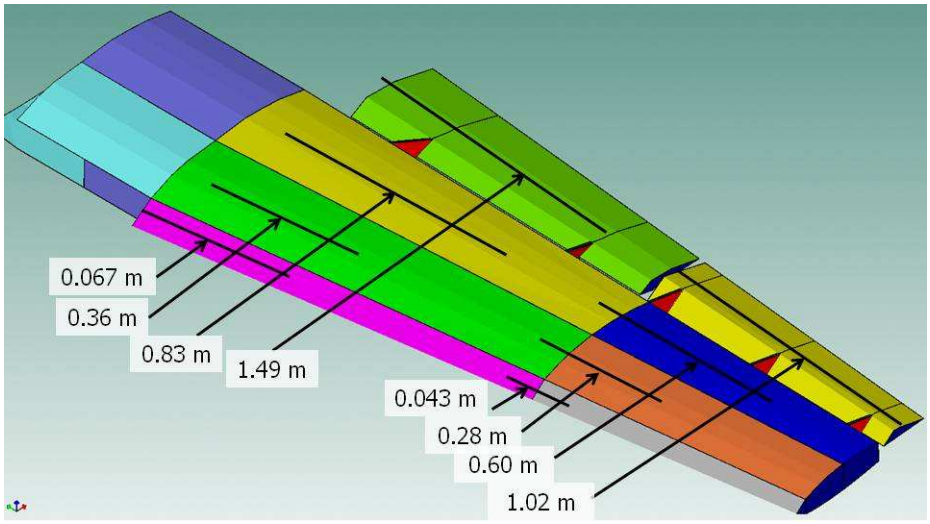

Figure 4.2.6. TBL distances for the wings.

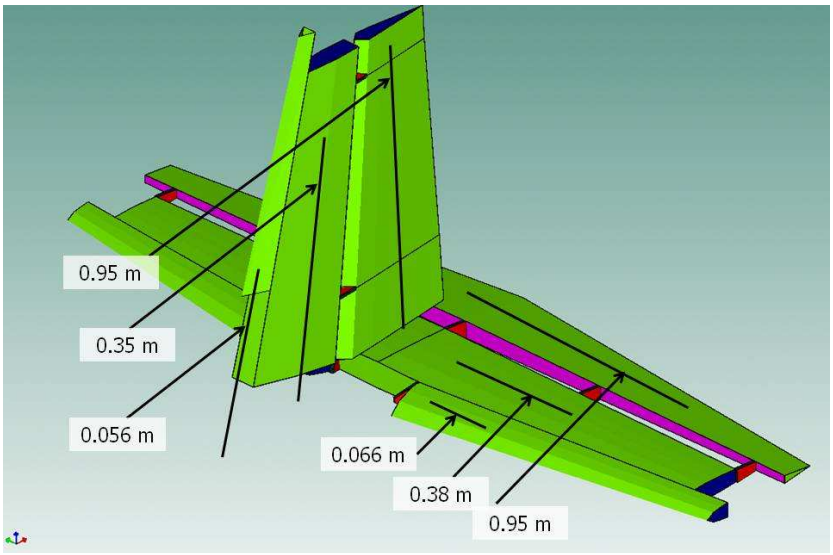

Figure 4.2.7. TBL distances for the empennage.

According to these distances, the TBL pressures and levels are calculated and they are given in figures.

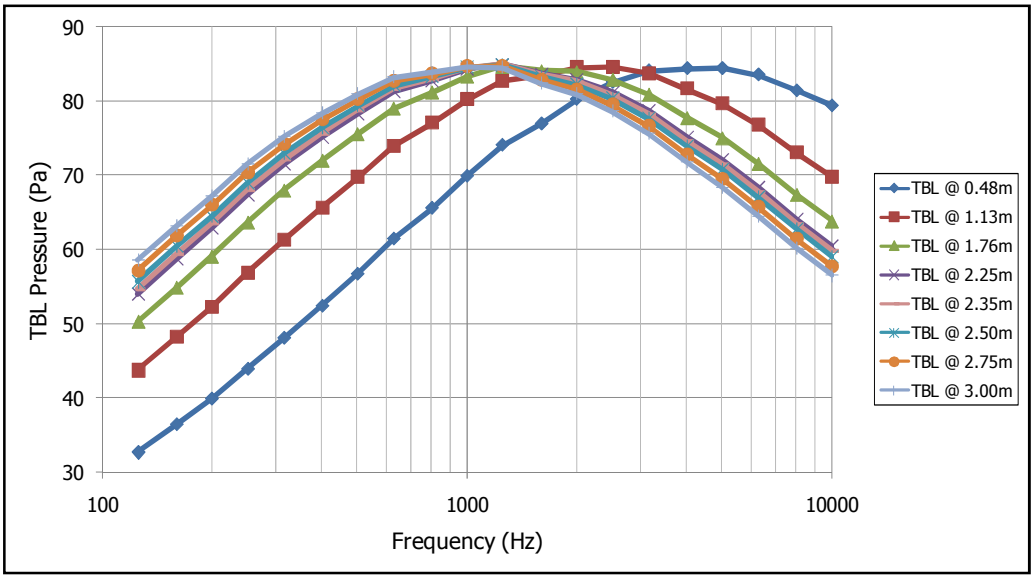

Figure 4.2.8. TBL pressures for fuselage up to subsystem distance of 3.00m.

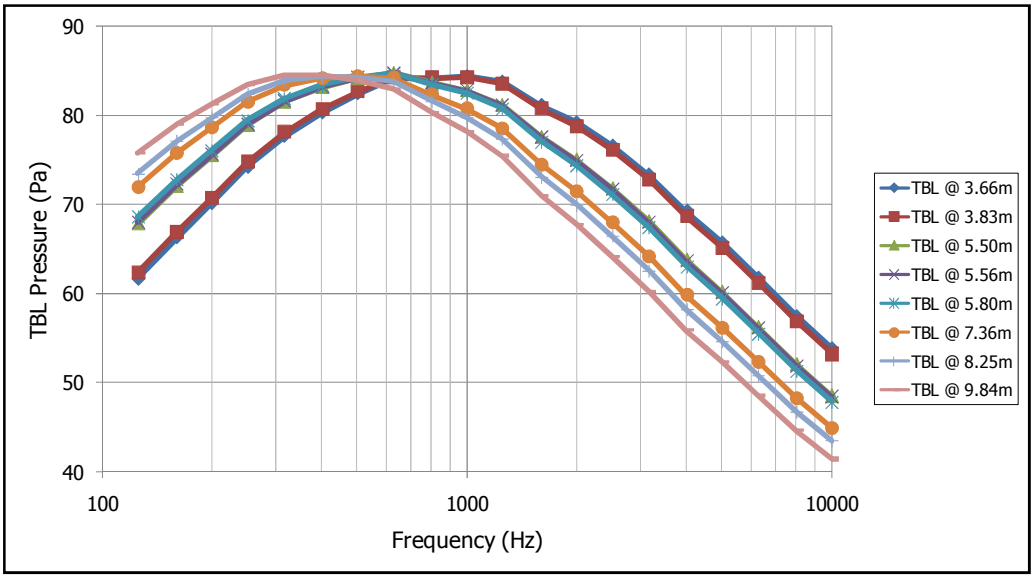

Figure 4.2.9. TBL pressures for fuselage after subsystem distance of 3.00m.

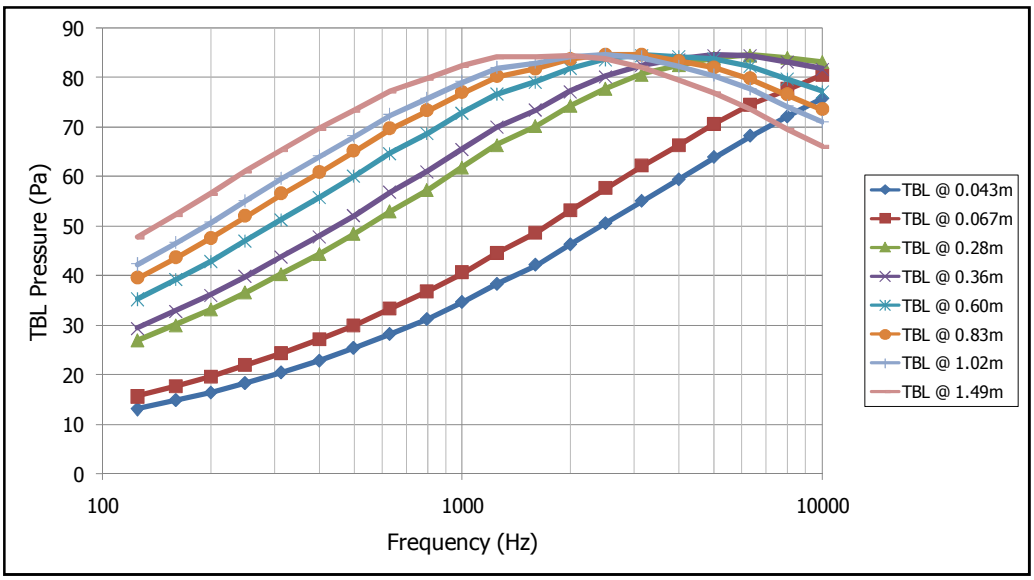

Figure 4.2.10. TBL pressures for wing subsystems.

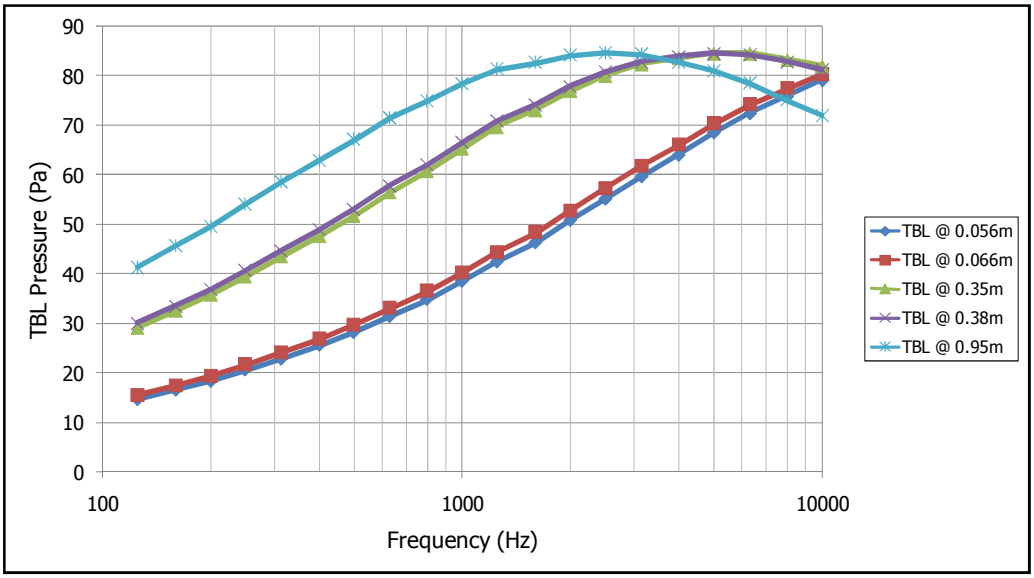

Figure 4.2.11. TBL pressures for empennage subsystems.

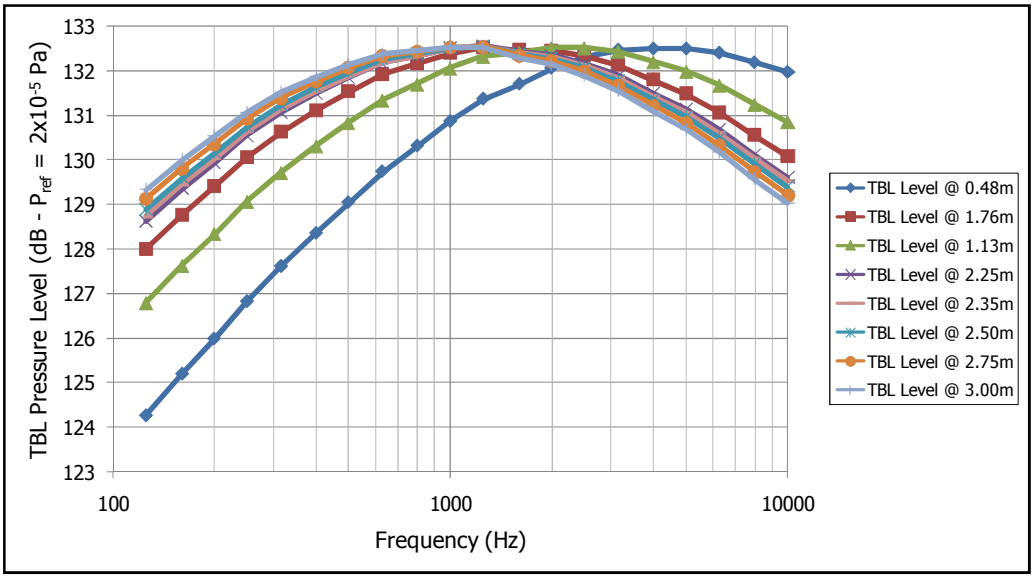

Figure 4.2.12. TBL pressure levels for fuselage up to subsystem distance of 3.00m.

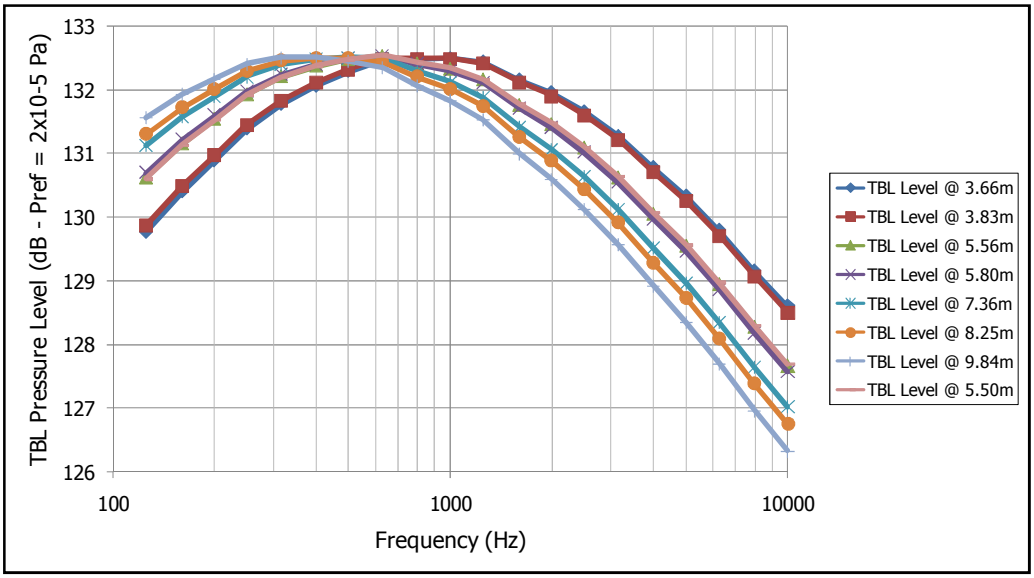

Figure 4.2.13. TBL pressure levels for fuselage after subsystem distance of 3.00m.

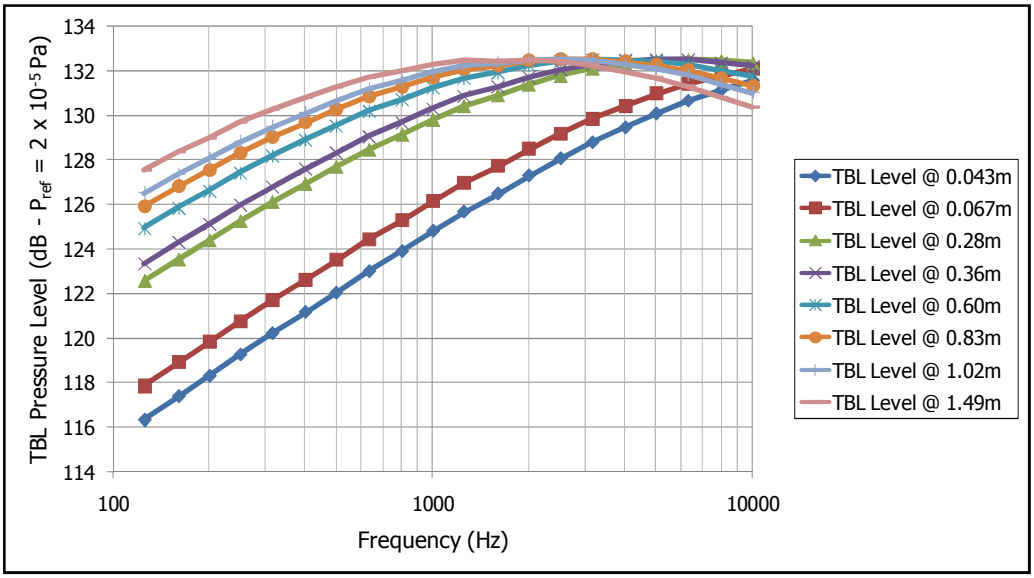

Figure 4.2.14. TBL pressure levels for wing subsystems.

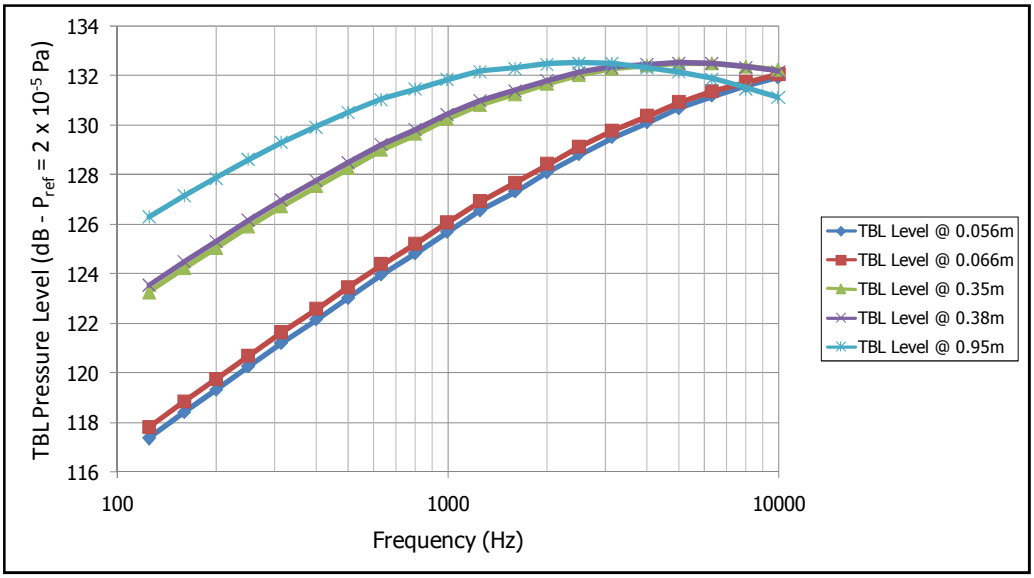

Figure 4.2.15. TBL pressure levels for empennage subsystems.

When the figures above are examined, it is observed that at closer distances to the aircraft nose region and the leading edges of the wings and empennage, the TBL levels are higher at high frequencies (above 1000 Hz). When the distances of the subsystems become larger, the TBL levels are higher at relatively low frequencies (between 200 Hz and 500 Hz).

4.2.1. DETERMINATION OF PROPELLER NOISE

It is previously mentioned that the aircraft has a propeller which composed of five blades. The properties of the propeller are given in Table 4.2.1.

Table 4.2.1. Properties of the propeller.

Manufacturer	Hartzell Propeller Inc.
Propeller Model	HC-B5MA-2
Blade Model	M9128NSK
Propeller Diameter	2.39 m (94 in)
Number of Blades	5
Blade Material	Aluminum
Hub Material	Steel
Revolutions	2000 rpm (constant)

The propeller noise is calculated using the ESDU method defined in reference [42]. The noise is calculated according to three different conditions. For each condition, the propeller noise is determined in 1/3 octave band. The results are given in the Figure 4.2.16.

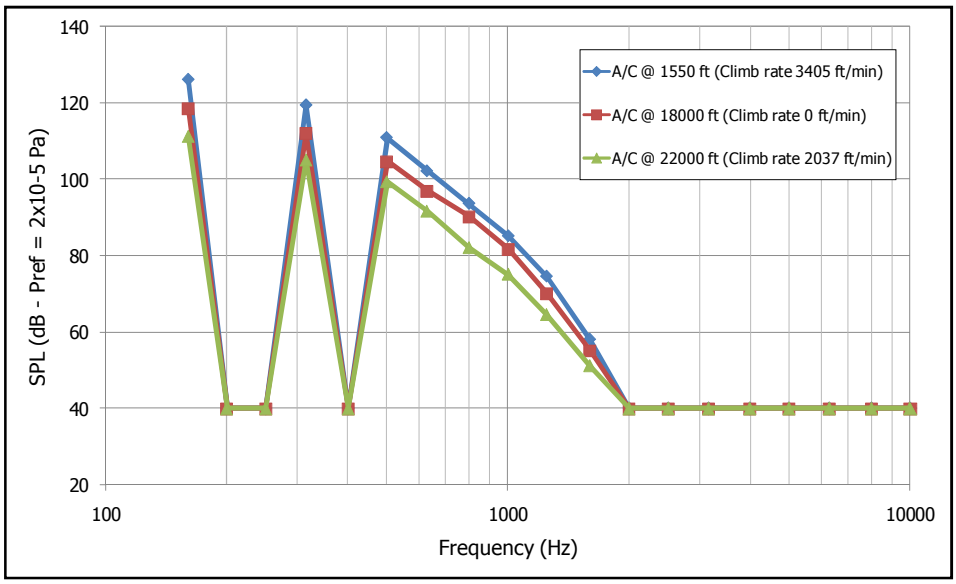

Figure 4.2.16. Propeller noise levels for different flight conditions.

When Figure 4.2.16 is examined, the effect of harmonic excitation can easily be observed. The dominant excitation frequencies are the blade passage frequency 166 Hz and its harmonics, especially the first harmonic (332 Hz, but is shown at 315 Hz in 1/3 octave band spectrum) and second harmonic (498 Hz, but is shown at 500 Hz in 1/3 octave band spectrum). Actually, these pure tones are not preferred in SEA because SEA theory requires a broadband excitation. However, when the propeller noise is combined with the TBL, the total load applied to the system does not contain these pure tones.

Among the conditions in Figure 4.2.16, although the first condition, which corresponds to the take of phase of the flight, seems to have the highest levels and therefore is the most conservative loading condition for the analyses, the second condition is used since it is the condition which the aircraft is going to be exposed in most of its service time.

The propeller noise around the aircraft is determined by using a DAF excitation in the propeller region. The sound pressure level (SPL) data are taken from each cavity. The SPL data are shown in Figure 4.2.17.

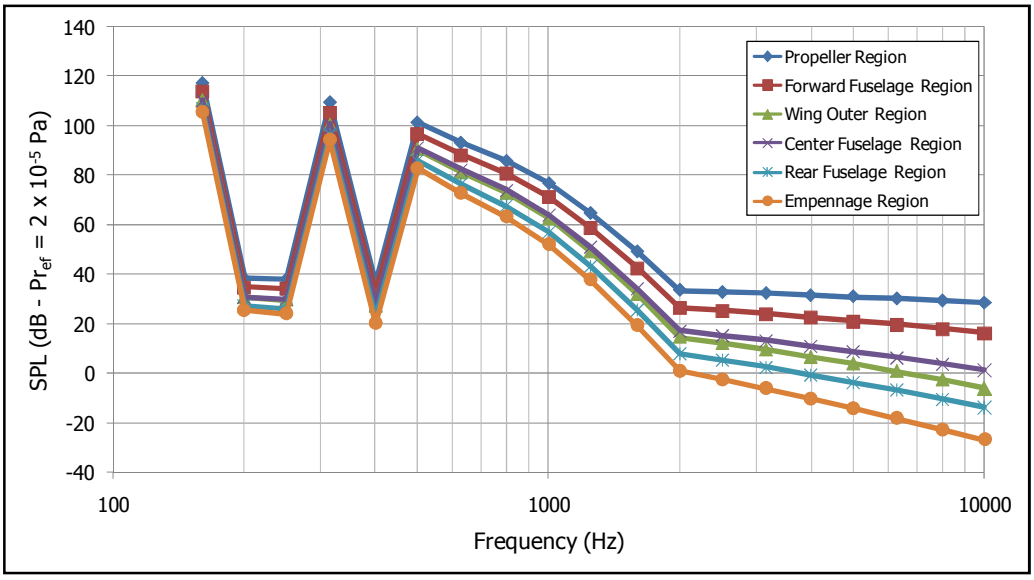

Figure 4.2.17. Sound pressure levels around the aircraft.

CHAPTER 5

ANALYSIS

5.1. ANALYSIS PROCEDURE

In order to determine the RMS stress values in the mid fuselage skin panel, SEA method is used along with formulations given by Karczub and Norton in [35,36]. In the analysis, TBL and propeller noise are modeled as the excitation sources and RMS velocity data is taken from the mid fuselage skin panels. Then, by using Equation (3.8.13) in a modified form the RMS stress values are determined. The procedure of the analysis can be summarized as follow.

1. Aircraft is modeled using SEA elements.
   a. Two different models are prepared one which is composed of only the fuselage elements, and the other is the model with the wings added.
2. The loads are applied to the model.
   a. TBL is applied to each subsystem according to the distances of them to the nose part of the aircraft for fuselage structures and to the leading edges of the wings and empennage structures.
      i TBL is assumed to be constant over the subsystem.
      ii For tapered structures, the average distance is taken.
   b. Propeller noise is applied as DAF to the face of the cavity in front of the aircraft (Figure 4.1.25), and allowed to propagate through the surrounding of the aircraft by means of the cavities.
3. RMS velocity response of the mid fuselage skin panels are taken from VA One™ and the Equation (3.8.13) is used to determine the RMS stress from strain.

Actually, the Equation (3.8.13) gives the strain value in a far field location in the panel (where the evanescent wave components do not exist). However, since SEA method gives an overall RMS velocity value for the whole subsystem, it is assumed that the RMS stress value is constant over the whole subsystem.

5.2. APPLICATION OF THE METHOD

Before applying the method defined in Section 5.1 to the actual aircraft model, a smaller model is used for trying the method. After the validation of the method, it is applied to the aircraft model.

5.2.1. GEOMETRY AND SEA MODEL DEFINITION

The structure constructed for the analysis is composed of 5 frames, 5 stringers and 16 skin panels between them. The FEM of the structure which is used for creating the SEA model is shown in Figure 5.2.1 and Figure 5.2.2.

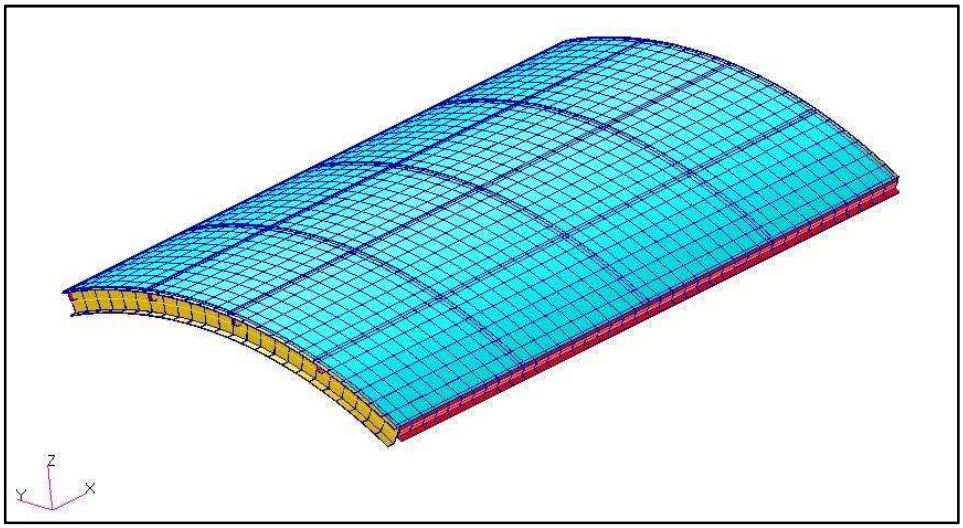

Figure 5.2.1. FEM of the curved panel structure.

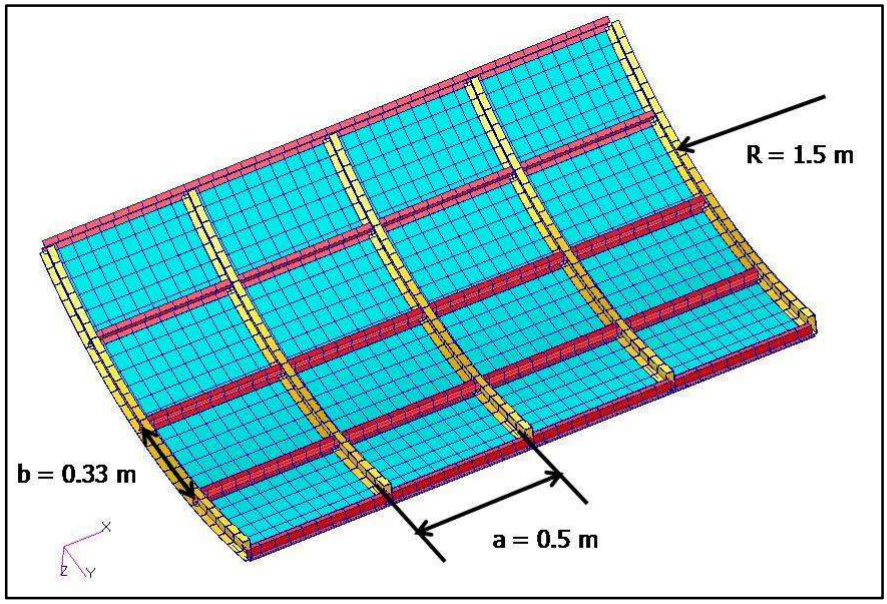

Figure 5.2.2. Dimensions of the panel.

The dimensions of the frames and stringers used in the model are given in Figure 5.2.3.

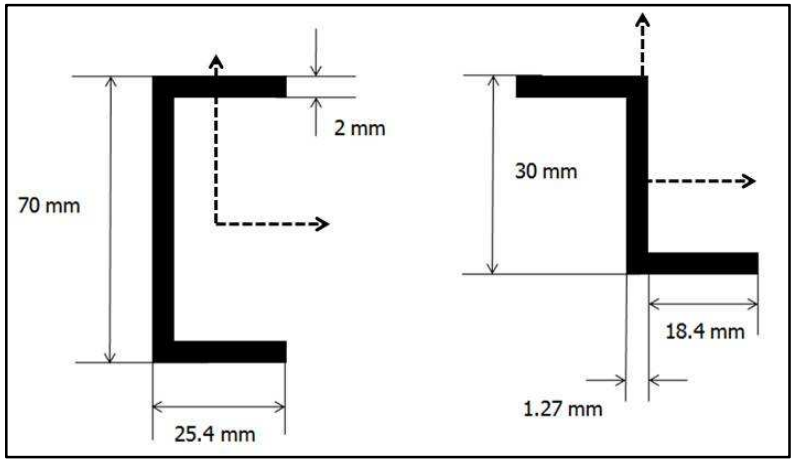

Figure 5.2.3. Sections of frames (left) and stringers (right).

The sectional properties of the stringers and frames used in SEA are given in Table 5.2.1.

Table 5.2.1. Cross section properties of stringers and frames.

Property	**Value for Stringer**	**Value for Frame**
I_{xx} (mm^4)	1.474×10^4	8.004×10^4
I_{yy} (mm^4)	7.361×10^3	4.169×10^4
Q (mm^4)	72.01	311.5
J (mm^4)	2.120×10^4	1.787×10^5
Area (mm^2)	97	233.6
Perimeter (mm)	136.1	237.6

Two different SEA models are created for the analysis. The first model is composed of a total of 26 subsystems which are 5 frames, 5 stringers and 16 skin panels between them. The second model is a much simpler one, which is composed of a single subsystem that is modeled with a ribbed plate property, and therefore the frames and the stringers are smeared into the skin panel. The two models are shown in the Figure 5.2.4 and the modal densities of the panels are shown in Figure 5.2.5. The shell elements are shown in exploded view to obtain a clear visualization.

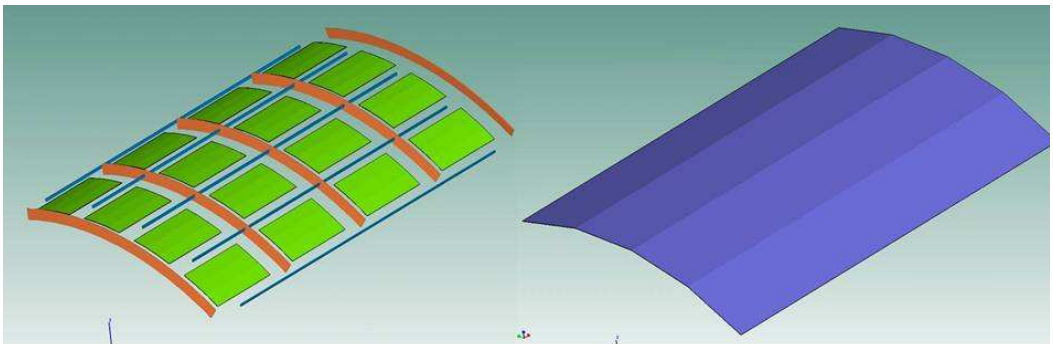

Figure 5.2.4. Two SEA models of the same panel.

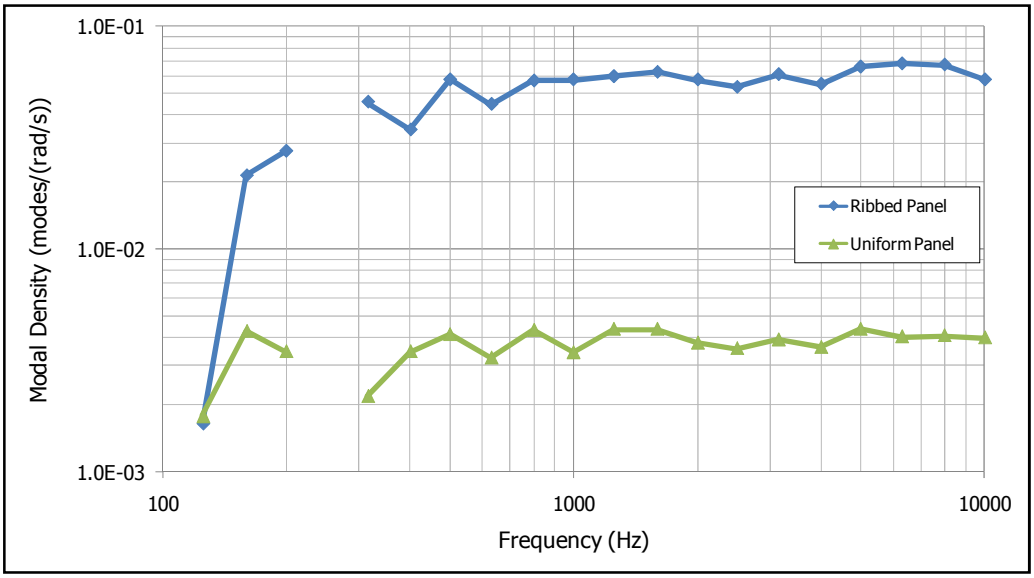

Figure 5.2.5. Modal densities of the panels.

The panels are assumed to be the section of an aircraft of length 2 m and the center of the first subsystem is 2 m away from the nose of the aircraft. Therefore, in the second model it is found that the subsystem distance is 2.75 m to the nose of the aircraft. The aircraft is assumed to be traveling at a speed of 200 m/s, and a convection constant of 0.75 is used for TBL calculation.

5.2.2. ANALYSIS

Four different cases are analyzed with two different models to see various effects on the stress levels. These cases are as follows:

1. Only TBL is applied to the model as the excitation load. Only structural vibrations are included.
2. Internal pressure is included in the analysis in addition to case 1 in order to see the stiffening effects of the internal static pressure.
3. The external fluid is modeled as semi-infinite fluid (SIF) in addition to case 2 in order to see the effect of radiations from panels to the air.
4. An internal cavity is modeled and connected to the skin panels in addition to case 3 to see the effect of loss from pressurized panels to the internal air.

5.2.2.1. CASE 1

In case 1, only the TBL excitation is used for both models. The applied loads are shown along with the models in Figure 5.2.6.

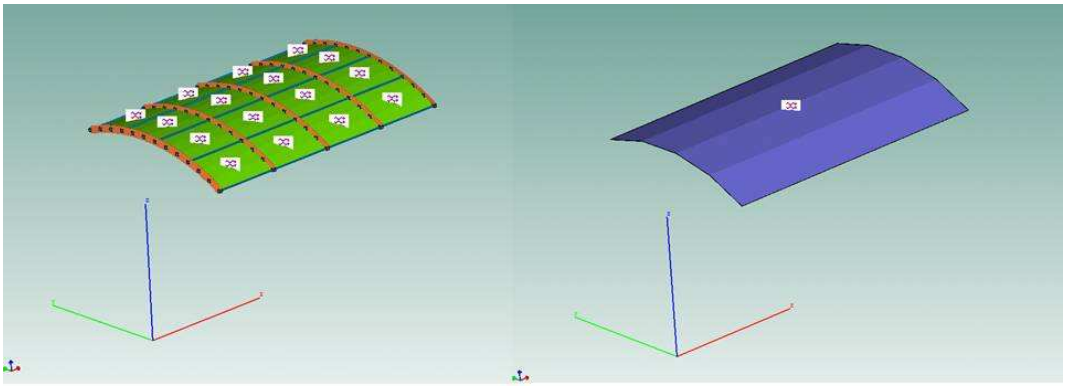

Figure 5.2.6. TBL applied to the models.

The overall RMS stress is found as 2.946 MPa for uniform panel and 2.696 MPa for ribbed panel. The 1/3 octave band frequency distribution of the panel stresses due to the TBL loading are shown in Figure 5.2.7.

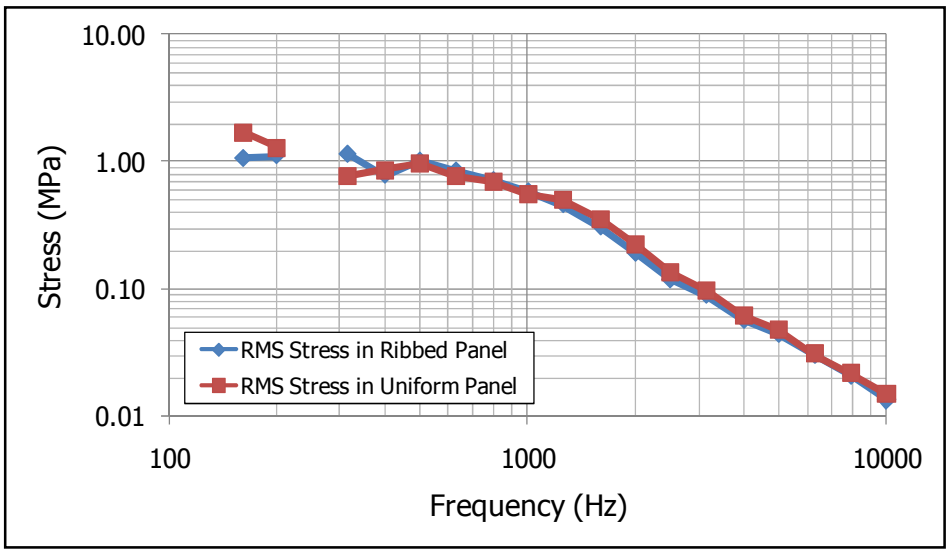

Figure 5.2.7. RMS stress distributions for case 1.

5.2.2.2. CASE 2

In case 2, in addition to the TBL in case 1, a semi-infinite fluid (SIF) is modeled to consider the effect of sound radiating from panels to the air. The models are shown in Figure 5.2.8.

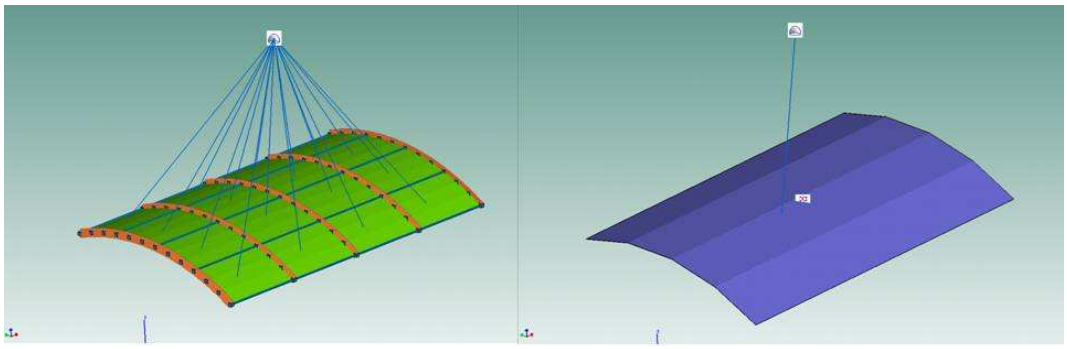

Figure 5.2.8. SIF applied along with TBL.

The overall RMS stress for the uniform panel is found as 2.830 MPa for uniform panel and 2.308 MPa for ribbed panel. The 1/3 octave band frequency distribution of the panel stresses are given in Figure 5.2.9.

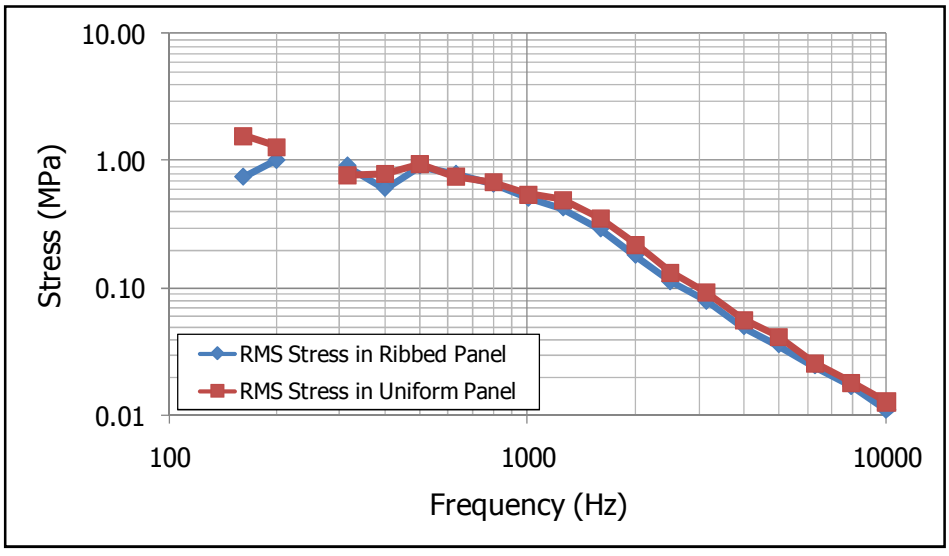

Figure 5.2.9. RMS stress distributions for case 2.

5.2.2.3. CASE 3

Generally, aircraft cabins are pressurized in order to make the passengers travel more comfortably. This pressurization makes a stiffening effect in the skin panels of the aircraft. In order to see this effect, internal pressurization (0.025 MPa) is included in case 3 in addition to case 2. After this pressurization, the modal densities of the panels are affected. The new modal densities are given in the Figure 5.2.10 along with the older ones.

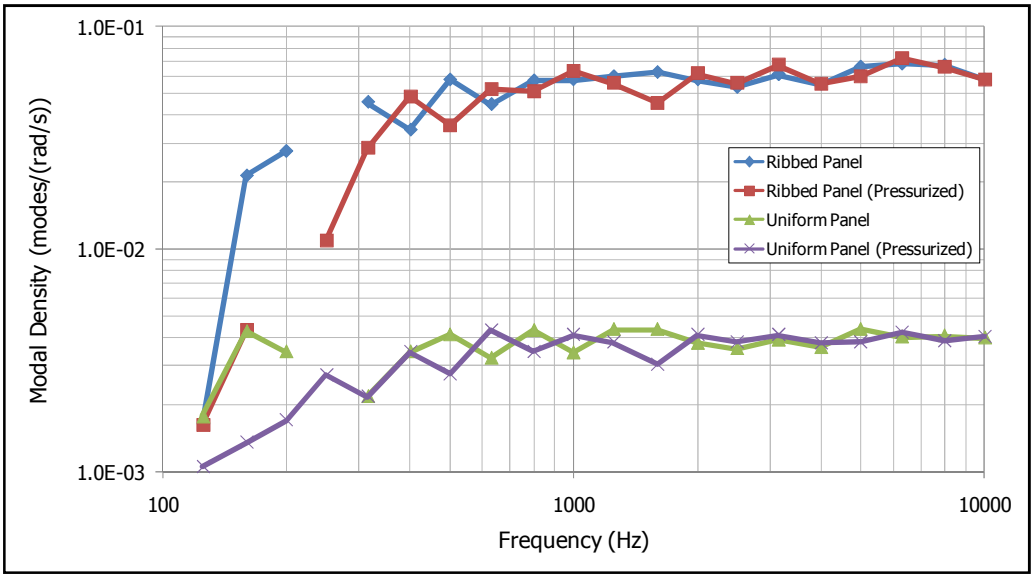

Figure 5.2.10. Comparison of modal densities of the normal and pressurized subsystems.

The overall RMS stress is found as 2.151 MPa for uniform panel and 1.842 MPa for ribbed panel. The 1/3 octave band frequency distribution of the panel stresses are shown in Figure 5.2.11.

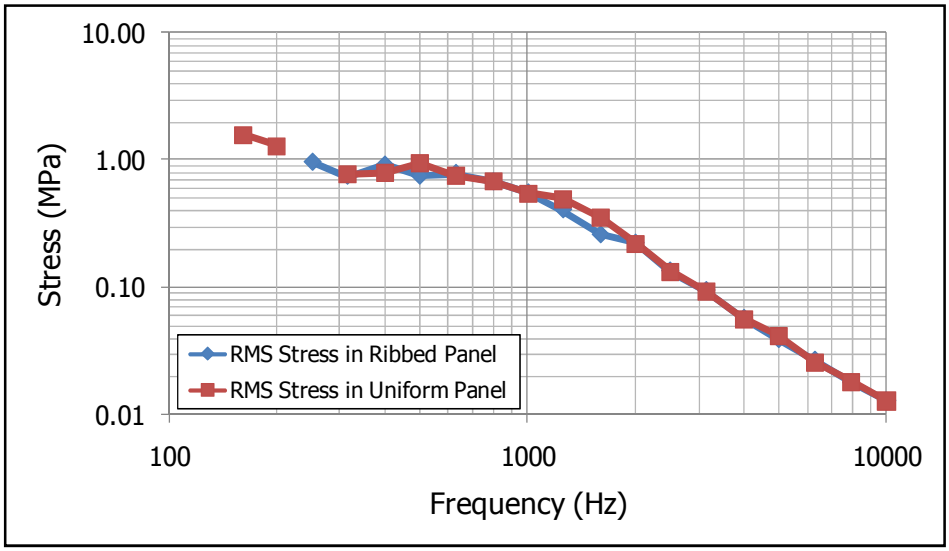

Figure 5.2.11. RMS stress distribution for case 3.

5.2.2.4. CASE 4

In addition to the case 3, the effect of radiation to the internal air is also modeled by an internal acoustic cavity. The models are shown in Figure 5.2.12 belo.

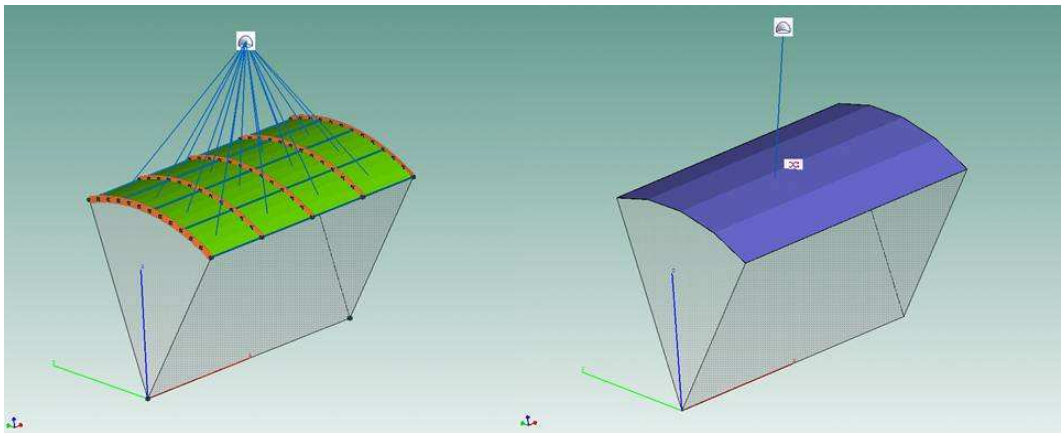

Figure 5.2.12. Cavity applied to the model.

The overall RMS stress is found as 2.085 MPa for uniform panel and 1.715 MPa for ribbed panel. The 1/3 octave band frequency distribution of the panel stresses are shown in Figure 5.2.13.

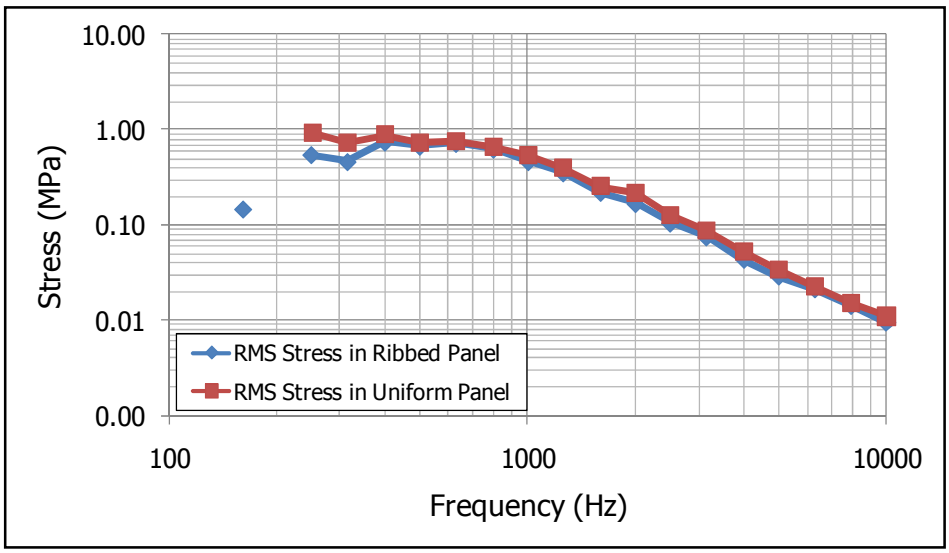

Figure 5.2.13. RMS stress distribution for case 4.

5.3. VALIDATION OF THE METHOD

The method is validated using the AGARD approach, which was first introduced by A.G.R Thomson, defined in reference [24]. By this approach, the RMS stresses in stiffened skin panels can be calculated for acoustic fatigue life prediction.

The equation used for the estimation of RMS stress is given as

$$S_{RMS} = \sqrt{\frac{\pi}{4\delta} f_n G_P(f_n) K_\delta S_0} \qquad (5.3.1)$$

where S_{RMS} is the rivet line stress due to acoustic loading, f_n is the fundamental frequency of the panel when all edges are assumed to be fixed, $G_P(f_n)$ is the spectral density of acoustic pressure at natural frequency, K_δ is the damping ratio correction factor and S_0 is the ratio of stress at rivet line in assumed mode shape to applied uniform static pressure on plate.

To understand S_0, one can check the reference [27] and see that this parameter is defined as the ratio of modal stress, $\tilde{\sigma}_i$, to the characteristic modal pressure, $\widetilde{P_{ic}}$, which is defined as

$$\widetilde{P_{ic}} = \rho h (2\pi f_i)^2 \left| \widetilde{w_i}(x_c, y_c, z_c) \right| \tag{5.3.2}$$

where $\widetilde{w_{ic}}(x_c, y_c, z_c)$ is the modal displacement of the interested point.

AGARD method has several assumptions [24]. These are listed as follows:

1. The predominant form of the skin vibration is such that each individual plate between two frame and two stringers are vibrating independently in the assumed mode. This mode is taken to be the fundamental mode of the panel when all edges are fixed.
2. The pressure on the skin is assumed to be uniform and in phase over the whole of each individual plate.
3. The pressure levels are assumed to be constant at frequencies close to the natural frequency of the panel.

Instead of using Equation (5.3.1), reference [24] gives nomographs to calculate the rivet line stress in the panel with a procedure defined in the document. According to this procedure, there are some parameters that should be calculated in order to find the stress value. These parameters are:

1. a/b where a is the distance between two frames, and b is the distance (arc length) between two stringers.
2. b/t where t is the thickness.

3. $b^2/_{Rt}$ where R is the radius of curvature of the skin panel.

4. $t/_{V_S}$ where V_S is the velocity parameter.

The velocity parameter is calculated for SI units by the formula

$$V_S = \frac{\sqrt{E/\rho}}{5080} \tag{5.3.3}$$

Among the cases in Section 5.2.2, only the TBL excitation case is validated because the AGARD method does not account for internal pressure effect and radiation from panel to air.

With the dimensions given, the necessary parameters are calculated as follows:

1. $a/_b = 1.5$
2. $b/_t = 165$
3. $b^2/_{Rt} = 36.3$
4. $t/_{V_S} = 2.00$

The AGARD method also requires the excitation level at the natural frequency of the panel between two frames and two stringers with a fixed boundary condition. For this reason, reference [43] is used to determine the fundamental mode of the interested structure. For the natural frequency, the following equation is given [43]:

$$f_n = V_S K \frac{t}{b^2} \tag{5.3.4}$$

where V_S is the velocity parameter and K is the frequency parameter. By using the appropriate figures in reference [43] and the Equation (5.3.4), the fundamental natural frequency of the panel is found as 330 Hz. The TBL excitation levels around the natural frequency of the panel are given in Table 5.3.1 for both ribbed panel and the uniform panel. The farthest uniform panel structure is used for the stress estimation.

Table 5.3.1. Excitation levels for the panels.

	200 Hz	**250 Hz**	**315 Hz**	**400 Hz**	**500 Hz**
Ribbed Panel (TBL @ 2.75 m) (dB)	134.2	134.8	135.4	135.9	136.3
Uniform Panel (TBL @ 3.5 m) (dB)	134.7	135.3	135.8	136.2	136.6

A bandwidth correction is applied to the excitation level with the formula given in reference [44] under the guidance of the procedure defined in [24]. The equation used for the level correction is

$$\Delta L = 10 \log_{10} \Delta f \tag{5.3.5}$$

where Δf is the bandwidth which is defined as $0.232 f_c$ for 1/3 octave band spectrum. After applying the bandwidth correction, the obtained excitation levels are shown in Table 5.3.2.

Table 5.3.2. Excitation levels after the bandwidth correction.

	200 Hz	**250 Hz**	**315 Hz**	**400 Hz**	**500 Hz**
Ribbed Panel Corrected (dB)	117.5	117.2	116.8	116.2	115.7
Uniform Panel Corrected (dB)	118.0	117.7	117.2	116.5	116.0

A linear interpolation between 315 Hz and 400 Hz is made in order to find the excitation level at 330 Hz which is 116.7 dB for ribbed panel and 117.1 dB for uniform panel. With these parameters, the nomograph in reference [24] gives a maximum rivet line stress of 2.6 MPa for ribbed panel excitation level and 2.7 MPa for uniform panel TBL excitation level. However, these stress values are valid for a damping ratio of 0.017. A correction factor of K_δ should be applied to the results because the damping ratio for the frequencies around the natural frequency of the panel is 0.02. This factor is also found from reference [24] as 0.92.

As a result, the final rivet line stress value is found as 2.39 MPa for ribbed panel TBL excitation and 2.48 MPa for uniform panel TBL excitation. The use of the nomograph for stress determination is explained in reference [24].

5.4. AIRCRAFT ANALYSIS

5.4.1. ASSUMPTIONS AND SIMPLIFICATIONS

In the analysis of the aircraft, the following input parameters and conditions are assumed:

1. An average cruise speed of 153 m/s is taken.
2. The convection constant is taken as 0.75 for all the subsystems.

3. A separated TBL behavior is assumed.
4. The propeller noise is given as DAF to the related subsystem in accordance with the values given in Figure 4.2.17.

Two different aircraft models are analyzed. One of them is the complete aircraft model and the other one is the simplified model with no wings and empennage structures. By the help of these two models, the effect of vibration transmission from the wings and empennage is also determined.

5.4.2. ANALYSIS RESULTS

Five different analyses are performed for the determination of stresses in center fuselage skin panels. The first analysis is performed with TBL excitation and in the following analyses; a different effect is added step by step. These effects are:

1. Propeller noise
2. Cabin pressurization
3. Radiation to the pilot cabin
4. Radiation to the external air

5.4.2.1. TBL EXCITATION

When analyzing the TBL excitation only, the subsystem representing the pilot cabin is removed from the model with the junctions connecting it to the structural center fuselage subsystems. The frequency distribution of the stress response of the center fuselage skin panels is shown in Figure 5.4.1.

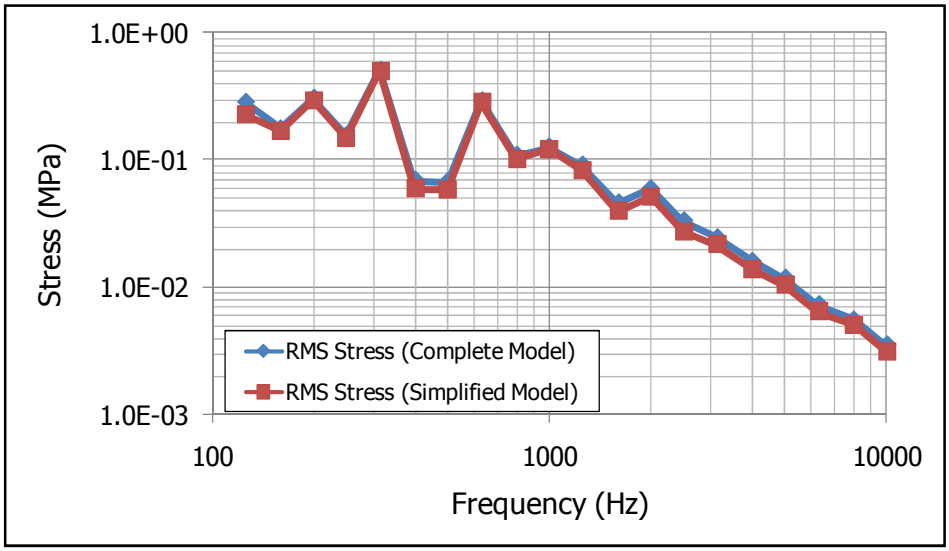

Figure 5.4.1. RMS stress distribution due to TBL excitation.

An overall RMS stress of 0.793 MPa is determined in the skin panel for the complete aircraft model and 0.749 MPa is determined for the simplified aircraft model.

5.4.2.2. PROPELLER NOISE

In addition to the TBL excitation, the propeller noise is also included in the analysis. The propeller noise levels are given in accordance with Figure 4.2.17 to the related subsystems. The RMS stress distribution with respect to frequency is shown in Figure 5.4.2.

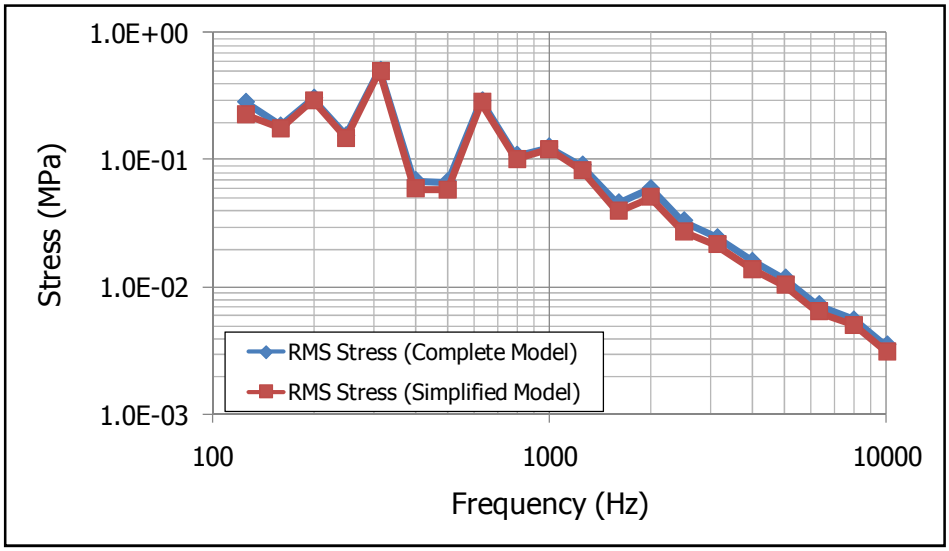

Figure 5.4.2. RMS stress distribution due to combined TBL and propeller noise.

The overall RMS stress of the panel is found as 0.795 MPa for complete aircraft model and 0.752 MPa for simplified aircraft model.

5.4.2.3. CABIN PRESSURIZATION

When the cabin is pressurized, the modal densities of the center fuselage subsystems are affected because of the stiffening. The modal densities of the original subsystems compared with the pressurized ones are shown in Figure 5.4.3.

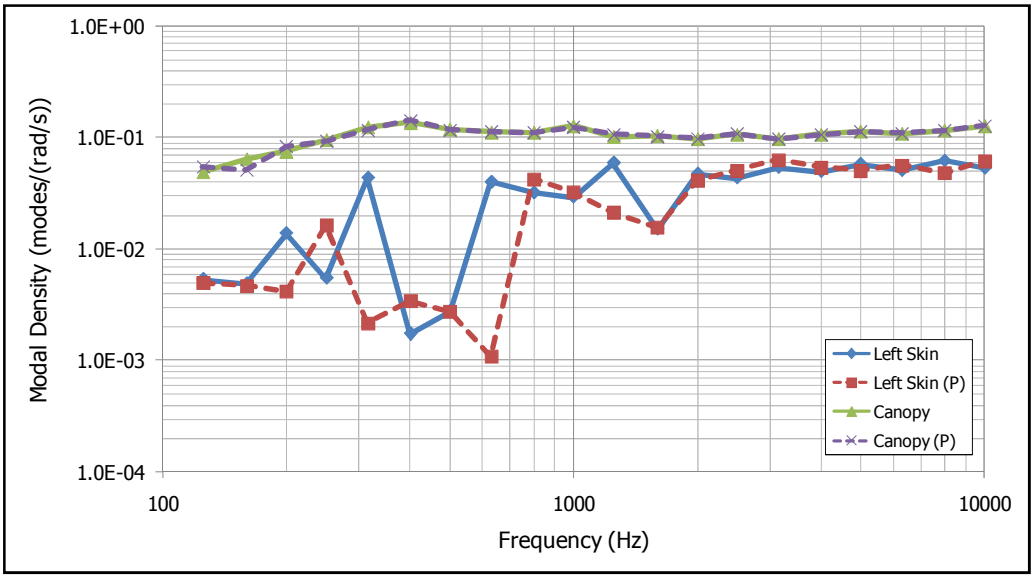

Figure 5.4.3. Comparison of modal densities of canopy and skin panel after pressurization (P).

As it can be seen from the figure above, the modal density of the canopy is not affected significantly. However, the modal density of the skin panel is affected under 2000 Hz. With the change in modal density of the pressurized subsystems, the response of the skin panels is also changed. The frequency distribution of the stress in skin panels is shown in Figure 5.4.4.

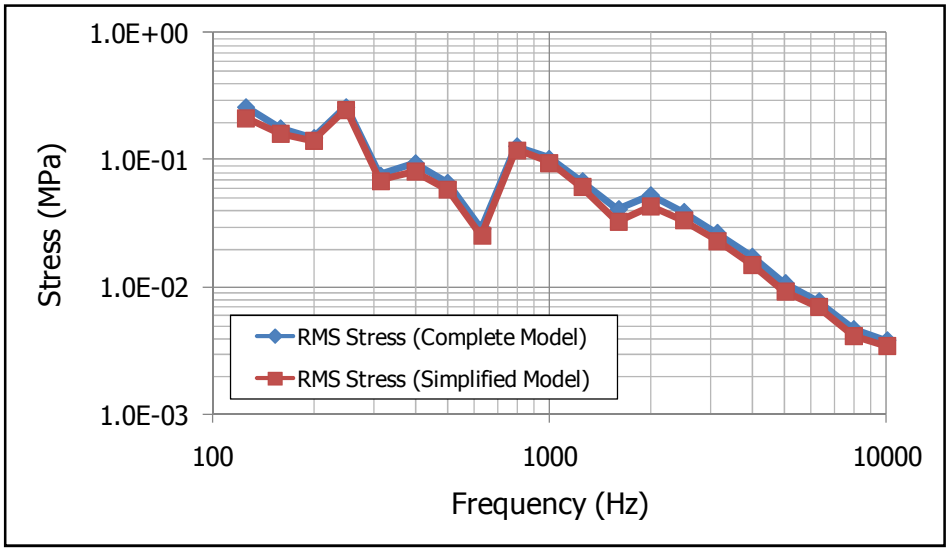

Figure 5.4.4. RMS stress distribution after the inclusion of cabin pressurization.

An overall RMS stress of 0.499 MPa is determined in the skin panel for the complete aircraft model and 0.448 MPa for the simplified aircraft model.

5.4.2.4. INTERNAL CAVITY EFFECT

When the effect of radiation from mid fuselage external elements to the pilot cabin is considered, the RMS stress distribution o the center fuselage panel is shown in Figure 5.4.5.

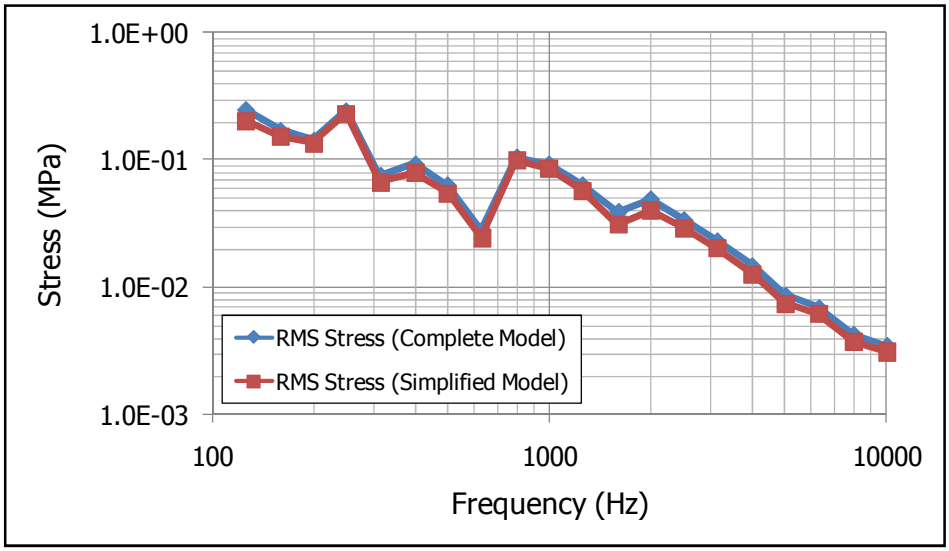

Figure 5.4.5. RMS stress distribution after the cavity effect.

An overall RMS stress of 0.467 MPa is determined in the skin panel for the complete aircraft model and 0.420 MPa for the simplified aircraft model.

5.4.2.5. RADIATION FROM AIRCRAFT PANELS

As the last case, the radiation from aircraft panels to the external air is considered. For this reason, 4 SIF locations are defined and the subsystems are connected to the nearest SIF point. The aircraft models with SIF are shown in Figure 5.4.6 and Figure 5.4.7.

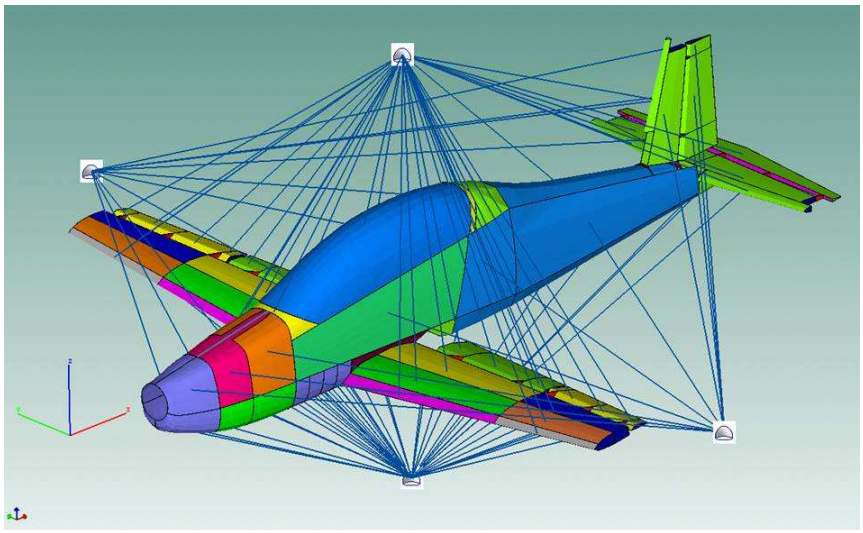

Figure 5.4.6. SIF around complete aircraft model.

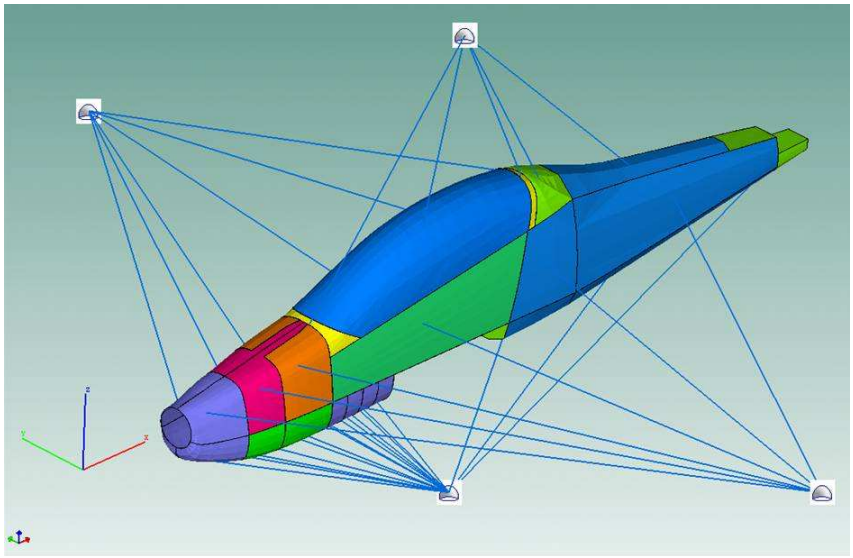

Figure 5.4.7. SIF around simplified aircraft model.

The frequency distribution of the stress in center fuselage skin panel is given in Figure 5.4.8.

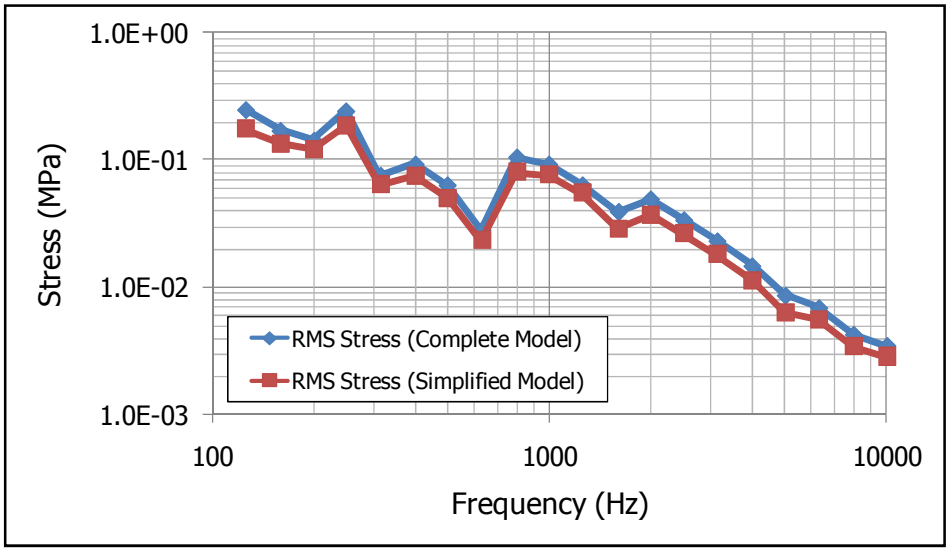

Figure 5.4.8. RMS stress distribution after radiation from panels.

An overall RMS stress of 0.392 MPa is determined in the skin panel for the complete aircraft model and 0.361 MPa for the simplified aircraft model.

5.4.3. AGARD SOLUTION

In AGARD solution, only the largest bay in the center fuselage panel is considered because the AGARD method assumes that the skin between two frames and two stringers is vibrating individually. In other words, the boundaries of the bay are fixed. The largest bay is expected to have the lowest natural frequency of the center fuselage panel and is shown in Figure 5.4.9 with the dimensions.

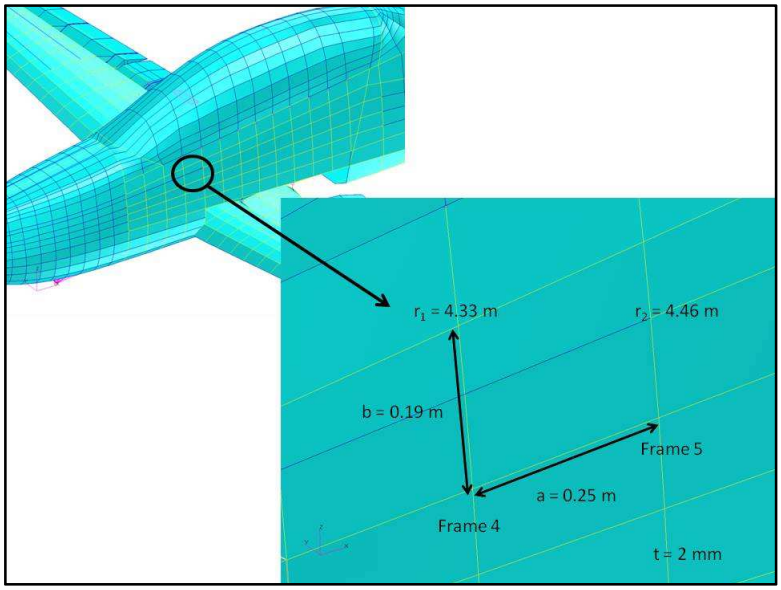

Figure 5.4.9. The dimensions of the largest bay in the skin panel.

As seen from Figure 5.4.9 above, the radius of curvature of the center fuselage panel is not constant. Moreover, since the panel is a tapered structure, the arc lengths of the skin bay corresponding to two frames are not the same. The radius at frame 4 is 4.33 m and the radius at frame 5 is 4.46 m. The same problem occurs for the arc length between two stringers. At frame 4 location the arc length is 0.196 m and in frame 5 location it is 0.204 m. To simplify the problem, the arc length and the radius of curvature are taken as the average of two extreme values, which results in an arc length of 0.2 m and a radius of 4.40 m, when calculating the parameters required for AGARD method. The parameters are calculated as follows:

1. $a/b = 1.24$
2. $b/t = 100$
3. $b^2/Rt = 4.5$
4. $t/V_S = 2.00$

The fundamental frequency of the panel is found by finite element analysis. A model is developed by using Patran 2008r1 for the considered region of interest with an element size of 5 mm. The analysis is performed with MSC.Nastran® 2005. The fundamental frequency is found as 395.7 Hz and the mode shape is shown in Figure 5.4.10.

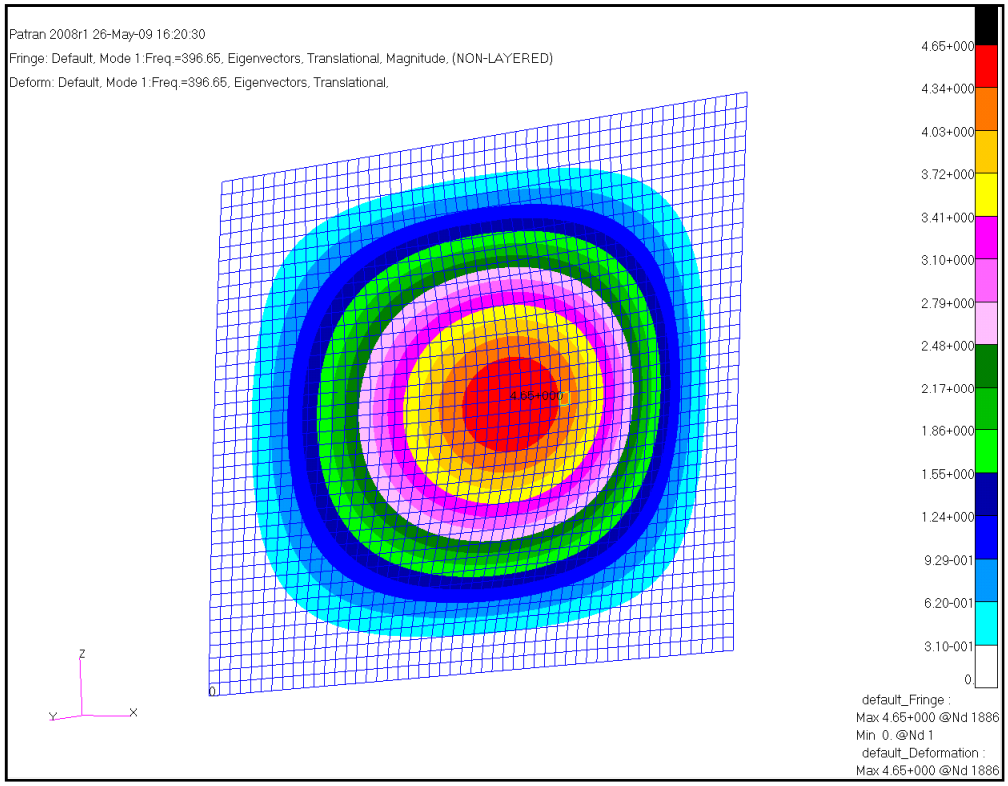

Figure 5.4.10. Mode shape of the largest panel bay in center fuselage skin.

For the AGARD solution, the excitation level around the natural frequency is determined following the same procedure in section 5.2.3. The excitation levels around 395 Hz are given in Table 5.4.1.

Table 5.4.1. Excitation levels in center fuselage skin panel.

	250 Hz	**315 Hz**	**400 Hz**	**500 Hz**	**630 Hz**
TBL Level (dB)	131.4	131.8	132.1	132.3	132.5
Correction (dB)	17.6	18.6	19.7	20.6	21.6
Corrected TBL Level (dB)	113.8	113.2	112.4	111.7	110.9

Through linear interpolation between 315 Hz and 400 Hz, the corresponding level for the natural frequency is found as 112.4 dB. When this level is entered the nomograph in reference [24] gives an RMS rivet line stress of 3.0 MPa. However, this result is valid for a damping ratio of 0.017. In the case analyzed, the damping ratio is 0.02 and therefore a damping correction should be applied. This value is found as 0.92 from reference [24] and the final result is 2.76 MPa.

CHAPTER 6

DISCUSSION AND CONCLUSION

6.1. DISCUSSION OF CASE STUDIES

In this study, the acoustically induced stress levels of center fuselage skin panels of a basic training aircraft are analyzed using SEA method. Two different models are analyzed, each of which is used for considering 5 different cases of loading. Before discussing the results of these analyses; the study carried for application and validation of the method should be examined.

The summary of the results for the application of the method is given in Table 6.1.1.

Table 6.1.1. Summary of the results of case studies.

Case	**Uniform Panel (SEA)**	**Ribbed Panel (SEA)**	**AGARD Solution**		**Difference (w.r.t. AGARD)**	
			Uniform Panel	**Ribbed Panel**	**Uniform Panel**	**Ribbed Panel**
1	2.946 MPa	2.696 MPa	2.48 MPa	2.39 MPa	18.8%	12.8%
2	2.830 MPa	2.308 MPa	N/A		N/A	N/A
3	2.151 MPa	1.842 MPa	N/A		N/A	N/A
4	2.085 MPa	1.715 MPa	N/A		N/A	N/A

When the results are examined, in case 1, the SEA method gives a stress value which is 18.8% higher for uniform panel model and 12.8% higher for ribbed panel model. The reason of the difference is that the effects of the frames and the stringers are directly included in the ribbed panel model because the properties of them are smeared into the skin panel. In uniform panel model, the frames and the stringers exist discretely in the model and the power flow from and to them affect the average velocity of the panels. Moreover, when creating the ribbed panel model, the offsets of the frame and the stringer centroid points are also included in the model, giving a better understanding of the actual physical model. In uniform panel model, since the frames and stringers are modeled separately, this offset effect does not taken into account.

The difference from the AGARD method results from several reasons. The most important one is that AGARD method assumes that the skin between frames and stringers is vibrating individually at its fundamental mode. However, the proposed method gives a stress as a function of the frequency. Higher frequencies are also taken into account although their effects are negligible.

When the radiation from panels to the external air is considered in case 2, the overall RMS stress value is decreased for both models as it is expected. There is a decrease of 3.94% in the uniform panel model and 14.4% in ribbed panel model.

Actually, when the model contains a radiation case from structural subsystems to the internal or external air, radiation from frames and stringers are also included in the default configuration of the software. Physically, when analyzing the radiation from panel to the external air, this option should be cancelled because there is no radiation to the air from the frames and stringers. When this option is removed, ribbed panel gives an RMS stress of 2.446 MPa, which gives a 9.27% decrease.

The pressurization of the cabin influences the modal density of the panels, hence affecting the stress distribution. The reason is that the pressurization makes an extra stiffening effect on the panels and changing the modal density distribution. Moreover, the ribbed panel is also modeled again such that the radiation from ribs is cancelled. The modal densities of the pressurized panels are given in Figure 5.2.10. According to this, there is a 24% decrease in the stress value for uniform panel

model and 20.2% decrease in the ribbed panel model. Again when the radiation from ribbed panel option is cancelled, the model gives an RMS stress of 1.995 MPa, which gives an 18.4% decrease with respect to the previous case when the radiation from ribs option is removed.

The last effect considered in the case studies is the radiation to the internal cavity of the aircraft. In this case, for the ribbed panel the radiation from frames and stringers is also included because it possible to have a radiation to the internal cavity. There is a 3.07% decrease in the stress value in uniform panel model and 6.89% in ribbed panel model. Like the previous two cases, when the radiation from ribs option is removed, the model gives an RMS stress of 1.908 MPa giving a decrease of 4.36% in the stress value.

The radiation from the panels to the internal cavity is examined in detail. For this reason, the radiation efficiency for each panel is found. When the radiation efficiency becomes higher, there will be more transmission to the fluid and less energy is stored in the structural subsystem, leading to lower stresses. The radiation efficiencies for the uniform panel are shown in Figure 6.1.1.

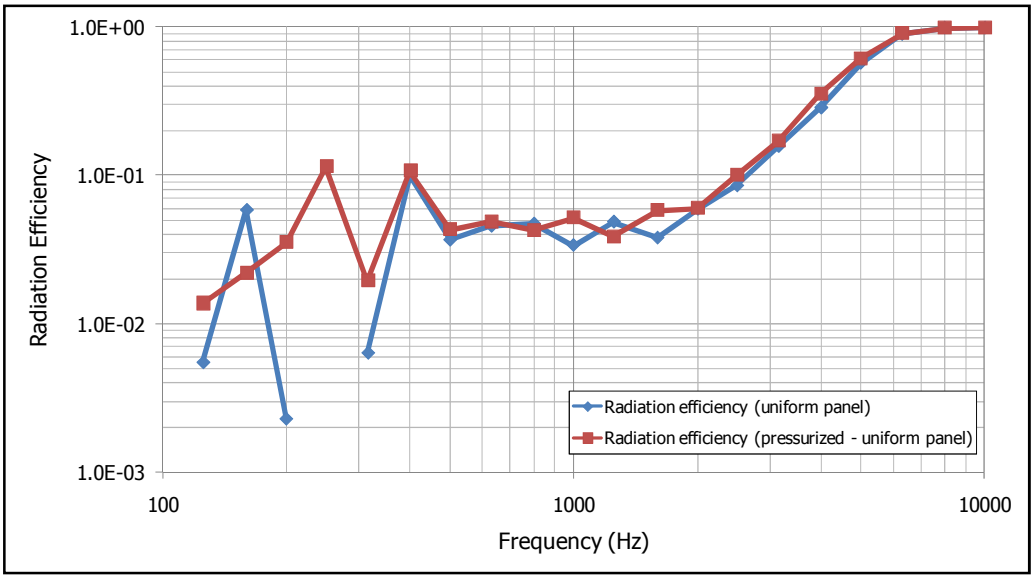

Figure 6.1.1. Radiation efficiencies of the pressurized and unpressurized uniform panel.

The radiation efficiencies for the ribbed panels are found for both unpressurized and pressurized configuration. Moreover, the effect of radiation from the frames and stringers are also examined. The radiation efficiencies for ribbed panel are shown in Figure 6.1.2.

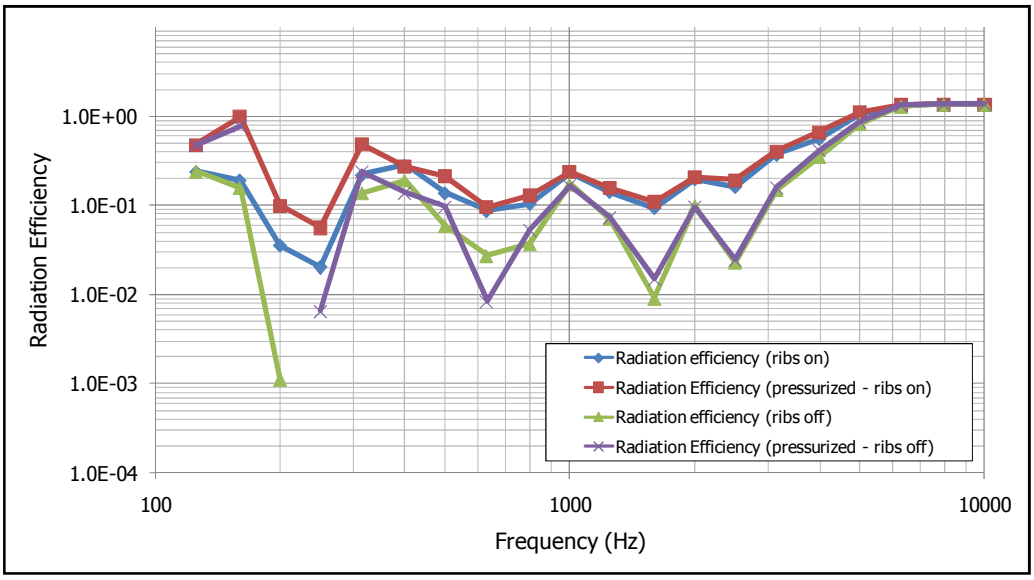

Figure 6.1.2. Radiation efficiencies of the pressurized and unpressurized ribbed panel.

When Figure 6.1.2 is examined, it is observed that when the panels are pressurized, the radiation efficiency slightly increases and hence allowing a better power flow to the connected cavity. Moreover, when figure is examined, the effect of the ribs is found to be significant in the radiation efficiency. Therefore, allowing radiation from ribs makes a better power flow as similar to the effect made by the pressurization.

One important point is that some of the frequency bands have zero stress in the response curve. There are several reasons of this situation. One of them is that if there is no mode in the subsystem at that frequency band, there is no response.

The other reason is if the net power flow for the subsystem at that frequency band is zero, then there is no response at that band.

The results of the three cases after the single TBL loading case are not compared with AGARD solution because AGARD does take radiation to internal and external environment, and pressurization effects. When the results of the first case is examined, it can be seen that without including any other effect, the proposed method gives a more conservative result for the acoustic fatigue life of the panels. The effect of the change in RMS stress to the fatigue life of several aluminum alloys can be seen in [38].

6.2. DISCUSSION OF AIRCRAFT ANALYSIS

Two models are created for the analysis of aircraft, namely the complete model and the simplified model without the wings and the empennage, as mentioned before. Five different analyses are performed for each model. These analyses are:

1. TBL excitation
2. TBL combined with propeller noise
3. Cabin pressurization in addition to case 2
4. Internal cavity effect in addition to case 3
5. Radiation from panels to external air in addition to case 4

The stress results summary for the center fuselage skin panels are given in Table 6.2.1.

Table 6.2.1. Aircraft analysis stress summary.

Case	Center Fuselage Skin Stress		Difference (w.r.t simplified model)
	Complete Model	Simplified Model	
1	0.793 MPa	0.749 MPa	5.92%
2	0.795 MPa	0.752 MPa	5.72%
3	0.499 MPa	0.448 MPa	11.4%
4	0.467 MPa	0.420 MPa	11.2%
5	0.392 MPa	0.361 MPa	8.59%

When the results of the first case are examined, it is seen that the complete model gives 5.92% higher stress than the simplified model. The reason of this difference is the total power input coming to the subsystems. The total power input to the center fuselage skin in the complete and simplified models are shown along with the power input from TBL in Figure 6.2.1.

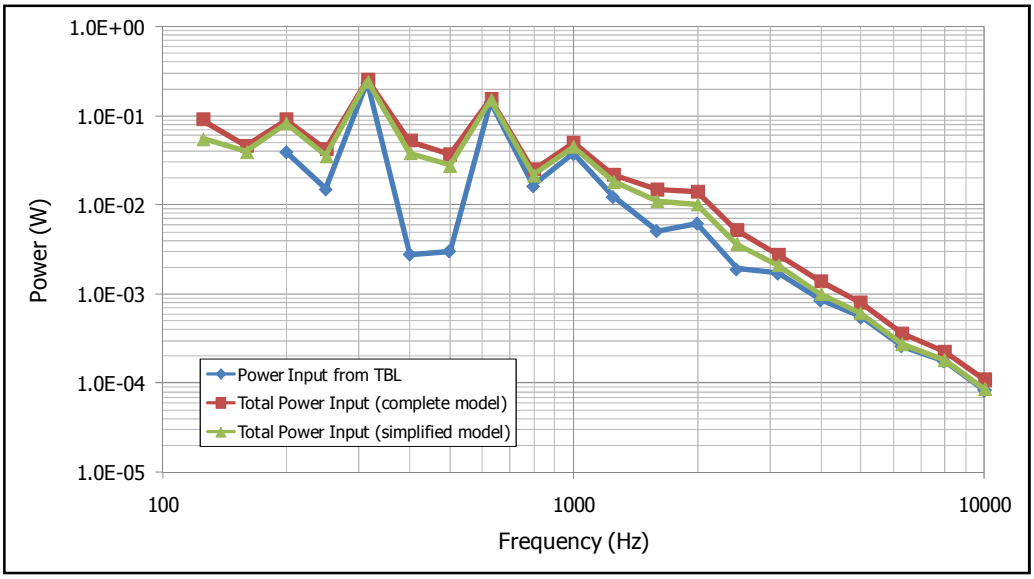

Figure 6.2.1. Comparison of the total power inputs.

As the Figure 6.2.1 is examined, it is observed that the total power input is slightly higher in the complete model. Since the TBL is the same for both models, the difference is expected to come from the wings and the empennage. Since the empennage region is far away from the center fuselage skin panels, most of the effect is due to the wings.

When the effect of the propeller noise is included, there is a 0.25% increase in the stress for complete model and 0.4% increase for simplified model with respect to the previous case. The comparison of the dB levels of the directly acting TBL and the propeller noise in the center fuselage region are given in Figure 6.2.2.

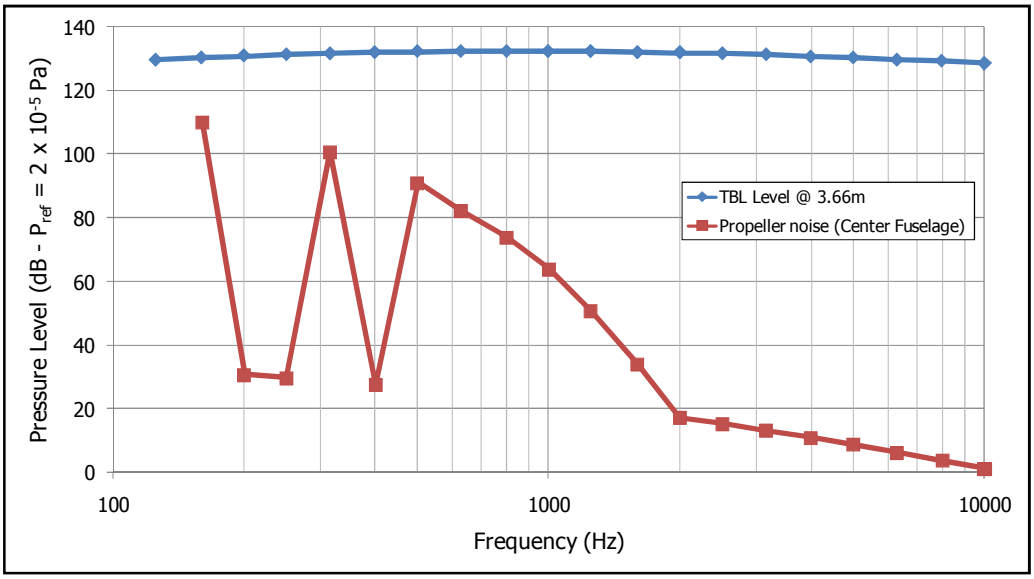

Figure 6.2.2. Comparison of the pressure levels of the TBL and propeller noise.

According to the Figure 6.2.2, the TBL has a more significant effect than the propeller noise and hence; the propeller noise can be neglected in the acoustic fatigue life analyses of the aircraft.

The cabin pressurization is included in case 3 and as expected, there is a decrease in the stress results. The complete model gives a decrease of 37% in the

stress value and the simplified model gives 40.4% decrease with respect to the previous case. The reason in the decrease can be explained by the change in modal density and hence the power flow from and to the adjacent subsystems.

In case 4, the effect of the pilot cabin is considered. Because of the radiation from panels to the internal cavity, the stress results are decreased. The complete model gives 6.4% and simplified model gives 6.25% decrease in the stress value. As it can be seen the amount of decrease is close to each other because the subsystems that have radiation to the internal cavity are identical.

At last, the radiation from the aircraft panels to the external air is included in the analysis. Complete model estimates a 16% decrease and simplified model estimates a 14% decrease in the stress value with respect to the previous case. A higher decrease in the complete model is expected because the radiation from all of the subsystems considering the wing and empennage is included. Therefore, the decrease in total power input to the center fuselage skin panel is higher in the complete model. This is illustrated in Figure 6.2.3.

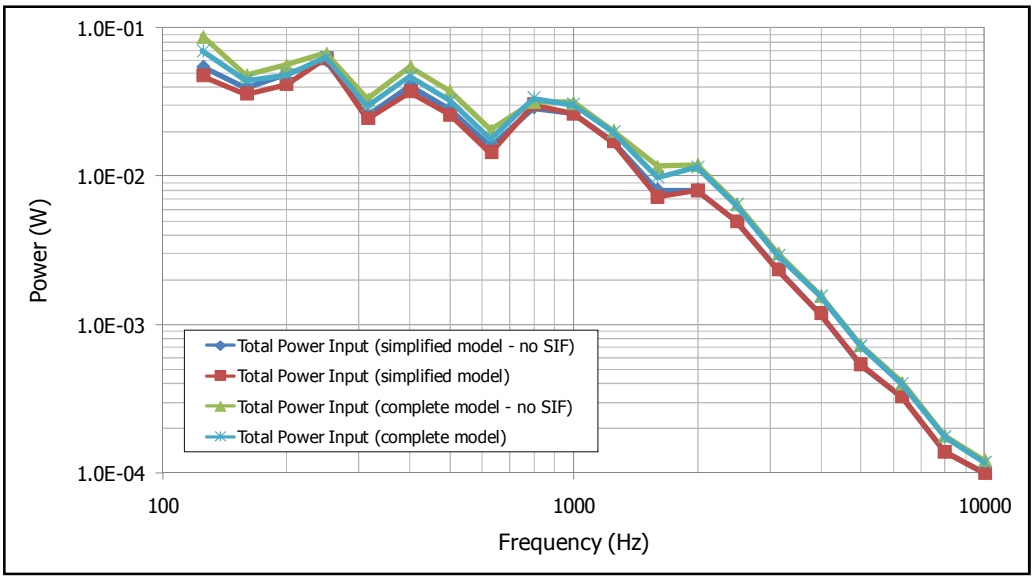

Figure 6.2.3. Total power inputs in case 4 and case 5.

An overall power input of 0.412 W is observed in the simplified model and 0.525 W in the complete model when the radiation from panels to the external air is neglected. On the other hand, 0.387 W power input is observed in the simplified model when the radiation to external air is included and 0.472 W in the complete model. Simplified model estimates a decrease of 6.1% in the power input while the full model estimates a 10.1% decrease in the power input. Therefore, complete model estimates a higher percentage of decrease in the stress value.

When the results of two models are compared, it is concluded that simplified model gives sufficiently close results to the ones obtained from the complete aircraft model. Therefore, a simplified model can be used in the initial acoustic fatigue studies of the aircraft in order to have a quick understanding of the system behavior.

For the aircraft analysis the AGARD method gives significantly higher stresses than the method proposed. The reason can be explained by the ribbed panel formulation in SEA. The ribbed panel formulation used in VA One^{TM} uses the theory introduced by Bremner [41]. This formulation assumes that ribs are orthogonally placed on the skin panel with fixed distance. However, when the structure of the center fuselage skin panel is examined, it can be seen that the frames are placed with a fixed distance but the stringers have variable distance between them due to the tapered geometry of the skin panel. The ribbed panel is modeled by taking an average value between the stringers. Therefore, a stiffer structure is introduced than the actual one. In conclusion, it can be said that for tapered structures with changing radius of curvature and ribs with variable distance, the proposed method in this study should be improved along with the modeling strategy to get reasonably accurate results to agree with the AGARD method.

6.3. RECOMMENDED FUTURE WORK

6.3.1. METHOD DEVELOPMENT

As it is seen from the results, the method proposed in the study gives sufficiently accurate results for uniform and simple geometries compared to the AGARD solution. However, for the center fuselage skin of the aircraft which is a tapered skin having a changing radius of curvature, it gives significantly lower results than the AGARD method.

AGARD method has also an inaccuracy because of the change in radius of curvature of the panel and changing stringer distances because of the taper effect. However, it is still quite a good method to estimate the stress since the curvature and stringer distance change in the analyzed region is minute.

The proposed method can be modified in terms of the formulation of the ribbed panels for tapered structures with changing radius of curvature. Since VA One^{TM} assumes that the panel is uniform and the stringer spacing is constant, the radiation behavior of the panel is significantly affected. Therefore, instead of the standard ribbed panel formulation in VA One^{TM}, a new formulation needs to be developed.

6.3.2. AIRCRAFT MODEL DEVELOPMENT

The aircraft model has some simplifications in order to be built as simple as possible. This makes the model have some problems in itself. One of them is the modal densities of the subsystems, which should be in the same order for each subsystem. This is a very difficult task to achieve because the aircraft has many local structural details that can affect the mechanical vibration and acoustical radiation characteristics of the system. Therefore, a hybrid model can be constructed for these local structural details in order to obtain a better understanding of the system.

For hybrid model generation, the primary concern is the stiffness of the subsystem, and hence the modal density. Subsystems which can be considered as "stiff" will have significantly lower modal density than the ones considered as "flexible". As an example, the frames and the stringers of the center fuselage skin panels can be modeled by finite elements and the skin elements between them can be modeled by SEA elements. One example can be seen in reference [17].

Another improvement can be the modification of connection elements of empennage and the wings to the fuselage. In order to obtain a better power transmission from these elements to the skin elements, these connections must be examined in detail. Again a hybrid model can be used for this study.

Without generating a hybrid model, FEA can still be used along with SEA. It can be used to improve the modal density of the subsystems. VA One™ uses the wave formulation in general to calculate the modal density of the subsystem. When the excitation is TBL, it uses the modal formulation but it does not perform a modal analysis as in FEA. In order to have a better understanding of the modal behavior of the subsystems, FEA can be used to override the modal density data in the analyses. However, the element size in the finite element model should be determined carefully to obtain reasonably accurate results at frequencies higher than 1000 Hz.

Another issue in the analyses is the damping loss factor used for the subsystems. As a simple assumption, the default damping loss factor spectrum for the bolted and riveted structures is taken for the flexural waves. To have a better accuracy in the analyses, the damping loss factors for flexural, extensional and torsional waves can be determined by experiments in the wind tunnel and then used in the SEA model.

The propeller noise is determined using the reference [42] as mentioned before. This method can give good approximations, however the best way to determine the propeller noise is to make experiments and get the noise data around the aircraft for different flight conditions.

REFERENCES

[1] Richard H. Lyon, "Statistical Energy Analysis of Dynamical Systems: Theory and Applications", MIT Press, 1975.

[2] B. R. Mace, 1992, Journal of Sound and Vibration, 154 (2), 321-341. The Statistics of Power Flow between Two Continuous One-Dimensional Subsystems.

[3] B. R. Mace, 2003, Journal of Sound and Vibration, 264, 391-409. Statistical Energy Analysis, Energy Distribution Models and System Modes.

[4] B. R. Mace, 2005, Journal of Sound and Vibration, 279, 141-170. Statistical Energy Analysis: Coupling Loss Factors, Indirect Coupling and System Modes.

[5] E. C. N. Wester, B. R. Mace, 1996, Journal of Sound and Vibration, 193 (4), 793-822. Statistical Energy Analysis of Two Edge-Coupled Rectangular Plates: Ensemble Averages.

[6] B. R. Mace, J. Rosenberg, 1998, Journal of Sound and Vibration, 212 (3), 395-415. The SEA of Two Coupled Plates: An Investigation into the Effects of Subsystem Irregularity.

[7] R. S. Langley, 1990, Journal of Sound and Vibration, 141 (2), 207-219. A Derivation of the Coupling Loss Factors Used in Statistical Energy Analysis.

[8] R. S. Langley, 1994, Journal of Sound and Vibration, 169 (3), 297-317. Elastic Wave Transmission Coefficients and Coupling Loss Factors for Structural Junctions between Curved Panels.

[9] R. S. Langley, J. R. D. Smith, F. J. Fahy, 1997, Journal of Sound and Vibration, 208 (3), 407-426. Statistical Energy Analysis of Periodically Stiffened Damped Plate Structures.

[10] G. Xie, D. J. Thompson, C. J. C. Jones, 2004, Journal of Sound and Vibration, 274, 621-651. Mode Count and Modal Density of Structural Systems: Relationships with Boundary Conditions.

[11] Jerome E. Manning, 1994, Philosophical Transactions: Physical Sciences and Engineering, 346, 477-488. Formulation of SEA Parameters Using Mobility Functions.

[12] C. Cacciolati, J. L. Guyader, 1994, Philosophical Transactions: Physical Sciences and Engineering, 346, 465-475. Measurement of SEA Coupling Loss Factors Using Point Mobilities.

[13] F. J. Fahy, H. M. Ruivo, 1997, Journal of Sound and Vibration, 203 (5), 736-779. Determination of Statistical Energy Analysis Loss Factors by means of an Input Power Modulation Technique.

[14] D. N. Manik, 1998, Journal of Sound and Vibration, 211 (3), 521-526. A New Method for Determining the Coupling Loss Factors for SEA.

[15] A. N. Thite, B. R. Mace, 2007, Journal of Sound and Vibration, 303, 814-831. Robust Estimation of Coupling Loss Factors from Finite Element Analysis.

[16] A. J. Keane, W. G. Price, Proceedings of the Royal Society of London. Series A, Mathematical and Physical Sciences, "Statistical Energy Analysis of Periodic Structures", 1989, 423, 331-360.

[17] U.Orrenius, Andrew Wareing, 2008, Internoise 2008 Proceedings. Coupled FE-SEA Analysis of the Sound Radiation from Aircraft Structures: Effect of Noise Control Treatment.

[18] K. Kuroda, T. Yamazaki, F. Kuratani, S. Ohno, 2007, Internoise 2007 Proceedings. Influence of In-plane Vibration on SEA Models for Plate Structures.

[19] K. Kuroda, T. Yamazaki, F. Kuratani, 2008, Internoise 2008 Proceedings. Structural Optimization of Subsystems to Realize Desired SEA Parameters.

[20] P. Ragnarsson, L. De Langhe, J. Betts, C. T. Musser, 2007, Internoise 2007 Proceedings. Using FE Analysis to Improve SEA at Mid-Frequencies.

[21] V. Cotoni, B. Gardner, J. P. Carneal, C. Fuller, 2007, ICSV14 Proceedings. Modeling Methods for Vibro-Acoustic Analysis of Commercial Aircrafts.

[22] V. Cotoni, R. S. Langley, 2007, ICSV14 Proceedings. Development of a General Periodic SEA Subsystem for Modeling the Vibro-Acoustic Response of Complex Structures.

[23] ESDU, 1967, Item 67028. Estimation of the RMS Stress in Skin Panels Subjected to Random Acoustic Loading.

[24] ESDU, 1972, Item 72005. The Estimation of the RMS Stress in Stiffened Skin Panels Subjected to Random Acoustic Loading.

[25] ESDU, 1974, Item 74026. Estimation of RMS Stress in Internal Plates of a Box Structure Subjected to Random Acoustic Loading.

[26] H. Climent, J. Casalengua, 1994, AGARD Conference Proceedings 549: Impact of Acoustic Loads on Aircraft Structures. Application of the PSD Technique to Acoustic Fatigue Stress Calculations in Complex Structures.

[27] R. D. Blevins, 1989, Journal of Sound and Vibration, 129(1), 51-71. An Approximate Method for Sonic Fatigue Analysis of Plates and Shells.

[28] S. T. Choi, R. Vaicaitis, 1989, Probabilistic Engineering Mechanics, 4 (3). Nonlinear Response and Fatigue of Stiffened Panels.

[29] B. Benchekchou, R. G. White, 1997, Composite Structures, 37 (3), 299-309. Acoustic Fatigue and Damping Technology in FRP Composites.

[30] J. Q. Sun, R. N. Miles, 1991, Journal of Sound and Vibration, 150 (3), 531-535. Acoustic Fatigue Life Prediction for Nonlinear Structures.

[31] ESDU, 1999, Item 99009. An Introduction to Statistical Energy Analysis.

[32] L. Cremer, M. Heckl, "Structure-Borne Sound", Springer-Verlag Berlin, Second Edition, 1988.

[33] N. Lalor, "An Introduction to Automotive NVH Seminar Notes", İstanbul, November 1998.

[34] ESDU, 1989, Item 74037. Introduction and Guide to ESDU Data on Acoustic Fatigue.

[35] D. G. Karczub, M. P. Norton, 1999, Journal of Sound and Vibration, 226 (4), 645-674. Correlations between Dynamic Stress and Velocity in Randomly Excited Beams.

[36] D. G. Karczub, M. P. Norton, 2000, Journal of Sound and Vibration, 230 (5), 1069-1101. Correlations between Dynamic Strain and Velocity in Randomly Excited Plates and Cylindrical Shells with Clamped Boundaries.

[37] ESDU, 2006, Item 06009. Fatigue Damage Life under Random Loading.

[38] ESDU, 1972, Item 72015. Endurance of Aluminum Alloy Structural Elements Subjected to Simulated Acoustic Loading.

[39] Robert J. M. Craik, "Sound Transmission Through Buildings Using Statistical Energy Analysis", Gower Publishing Limited, 1996.

[40] VA One™ 2007.5 User's Guide, ESI Software, 2007.

[41] P. G. Bremner, 1994, NoiseCon94 Proceedings. Vibro-Acoustics of Ribbed Structures: A Compact Modal Formulation for SEA Models.

[42] ESDU, 1996, Item 95029. Prediction of Near-Field and Far-Field Harmonic Noise from Subsonic Propellers with Non-Axial Inflow.

[43] ESDU, 1987, Item 87002. Natural Frequencies of Rectangular Singly Curved Plates.

[44] ESDU, 1978, Item 66016. Bandwidth Correction.

[45] C. Yılmazel, 2004, "Analysis of High Frequency Behavior of Plate and Beam Structures Using Statistical Energy Analysis Method", Ph. D. Thesis.